Section

~~CONFIDENTIAL~~ UNCLASSIFIED

NASA TECHNICAL MEMORANDUM

NASA TM X-996

NASA TM X-996

CLASSIFICATION CHANGE
TO UNCLASSIFIED
By Authority of NASA CCN 211 in CSTAR v 8, no 24 dtd 12/31/70
Changed by [illegible] Date 7/31/90

AERODYNAMIC INVESTIGATION OF A LARGE WINGED VERTICAL-TAKE-OFF REUSABLE ORBITAL LAUNCH VEHICLE AT MACH 0.4 TO 2.1

by P. Kenneth Pierpont

Langley Research Center
Langley Station, Hampton, Va.

NATIONAL AERONAUTICS AND SPACE ADMINISTRATION • WASHINGTON, D. C. • AUGUST 1964

~~CONFIDENTIAL~~ UNCLASSIFIED

~~CONFIDENTIAL~~

UNCLASSIFIED

AERODYNAMIC INVESTIGATION OF A LARGE WINGED VERTICAL-TAKE-OFF REUSABLE ORBITAL LAUNCH VEHICLE AT MACH 0.4 TO 2.1

By P. Kenneth Pierpont

Langley Research Center
Langley Station, Hampton, Va.

NATIONAL AERONAUTICS AND SPACE ADMINISTRATION

UNCLASSIFIED

~~CONFIDENTIAL~~

AERODYNAMIC INVESTIGATION OF A LARGE WINGED VERTICAL-TAKE-OFF REUSABLE ORBITAL LAUNCH VEHICLE AT MACH 0.4 TO 2.1*

By P. Kenneth Pierpont
Langley Research Center

SUMMARY

Several configurations of a winged first-stage reusable booster have been investigated to determine effects of various components on the drag and stability characteristics. Effects of forebody shape, base flare shape, simulated rocket engines and shrouds, and an arbitrary afterbody fairing were investigated on a fineness-ratio-4 body to provide a basis for evaluating drag characteristics and to indicate methods for improvement. The reusable vehicle consisted of the body with appropriate components and an attachable recovery package, which was constituted of the wing, vertical tails, necessary wing-body fairing and flyback propulsion-system nacelles. Two wing planforms were employed - a 55° clipped delta and a 65° swept trapezoidal wing - for which the wing area, aspect ratio, taper ratio, and airfoil section were identical. Effects on both longitudinal and lateral-directional aerodynamic characteristics of the various components, as well as some modifications, were evaluated. The investigation was conducted largely in the Langley 8-foot transonic pressure tunnel at Mach numbers from 0.4 to 1.2 over an angle-of-attack range at 0° and 5° sideslip. Selected configurations were tested at moderate supersonic speeds in the Langley Unitary Plan wind tunnel at Mach numbers from 1.6 to 2.1. Test Reynolds numbers varied from 2×10^6 to 4×10^6.

The results indicated that the drag of a low-fineness-ratio body, whose base is distorted by the presence of conical rocket-engine shrouding, is excessive; however, shroud and body shaping demonstrated that significant base-drag reduction could be achieved. A hemispherical forebody was shown to be the shortest nose consistent with low subsonic drag and stability. Employment of highly swept trapezoidal-wing planforms will be required to obtain positive longitudinal stability for reusable boosters having centers of gravity close to the rear of the body. Large wing-tip-mounted vertical tails are required to provide adequate directional stability. Maximum lift-drag ratios for reusable boosters of the type considered of greater than 6.0 can be obtained and some further small increases appear to be possible.

---

*Title, Unclassified.

INTRODUCTION

Early evaluations of winged reusable orbital launch vehicle systems were based largely on possible economic advantages of reusable compared with expendable systems. However, the rapid growth in mission reliability and safety, potentially obtainable through reuse, are currently considered of greater importance than economic factors alone. The latter generally require assumptions which are at present indeterminant to show significant advantage over expendable vehicles. Reliability and safety are of special interest for manned missions as well as for those in which supply and timing may be critical. The improvements in these factors due to reuse may be expected to accrue product improvement as a result of postflight inspection, redesign, and rework where required.

The adequate development of winged reusable orbital launch-vehicle systems will involve consideration of aerodynamic efficiency, stability, and control over a wider range of the aerodynamic spectrum than heretofore investigated for wing-body arrangements and proportions which are appreciably different than those previously considered. Furthermore, the two fundamentally different launch modes, which consist of vertical and horizontal take-off, impose significantly diverse criteria on the individual stages of the orbital launch vehicle The Langley Research Center has therefore initiated a program to ascertain the nature and magnitude of the aerodynamic problems associated with both horizonta and vertical-take-off launch-vehicle systems with fixed wings on at least the first stage. Results of investigations of initial concepts of vehicles representing both types and which employed large-fineness-ratio propellant tankage, characteristic of early rocket launch vehicle technology, have been reported in references 1 to 4.

Two factors have contributed to a major change in design philosophy for propellant tankage for vertically launched vehicles and which now result in the employment of low-fineness-ratio propellant tankage. These are the structural weight penalties associated with high-fineness-ratio stages with their accompanying large transverse bending moments, together with the structurally adverse effects resulting from the dynamic behavior of long slender bodies. Therefore, designs for most advanced liquid-propellant vertical-launch vehicles tend to employ stage fineness ratios of about 4 or less. Wing-body configurations for winged reusable launch vehicle stages of this type therefore assume proportions not heretofore considered in aerodynamic investigations of conventional aircraft. For example, the ratio of the wing span to body diameter tends to become small and would therefore be expected to contribute to adverse longitudinal and lateral stability characteristics. In addition, the larger body base, generally associated with low-fineness-ratio bodies, may be expected to cause increased degradation of the lift-drag characteristics during the recovery-flight mode because of the body base pressures. Finally, the large masses associated with the rocket engines and thrust structure will result in center-of-gravity locations during the return flight and landing which are clo to the rear end of the body. Ability to achieve wing-body designs which posse adequate longitudinal and directional stability margins may consequently prove to be difficult.

The purpose of the present investigation therefore was to examine the longitudinal and lateral-directional stability together with aerodynamic efficiency characteristics of wing-body-tail configurations which might be representative of advanced concepts of liquid rocket-propelled vertical-take-off winged reusable orbital launch vehicles. The present investigation was limited to ascertaining the aerodynamic characteristics of the first stage, and primary emphasis was placed on the subsonic flight mode for the recovery and return flight (flyback) portion of the mission. Some of the effects of forebody shape, engine shrouding at the base, and afterbody shape on the drag characteristics of the basic body were examined. These coupled with some effects of wing planform geometry, vertical-tail arrangement, and flyback engine provision were then examined to ascertain the basic aerodynamic characteristics of a complete reusable first stage and to indicate the primary problems requiring additional research.

The investigation was conducted largely in the Langley 8-foot transonic pressure tunnel; however, selected configurations were also tested in the Langley Unitary Plan wind tunnel. The Mach number ranges were from 0.4 to 1.2 and 1.6 to 2.1, respectively. Data to derive longitudinal and lateral stability characteristics were obtained over an angle-of-attack range at 0° and 5° sideslip. Reynolds number based on the length of the body varied from about 2×10^6 to 4×10^6.

SYMBOLS

The aerodynamic data have been reduced to standard coefficient form. Body-alone and all lateral-directional data have been referred to the body axes whereas longitudinal data for the wing-body configurations have been referred to the stability axes. The moment reference for all data was selected to be 1.25 body diameters forward of the body reference station, which is the model base. All coefficients have been referred to the body base area and body diameter.

C_N normal-force coefficient, $\dfrac{\text{Normal force}}{q_o S_{ref}}$

C_A axial-force coefficient, $\dfrac{\text{Total axial force}}{q_o S_{ref}}$

C_L lift coefficient, $\dfrac{\text{Lift}}{q_o S_{ref}}$

C_D drag coefficient, $\dfrac{\text{Total drag}}{q_o S_{ref}}$

$C_{D,i}$ internal drag coefficient, $\dfrac{\text{Internal drag}}{q_o S_{ref}}$

C_m pitching-moment coefficient, $\frac{\text{Pitching moment}}{q_o S_{ref} D}$

C_l rolling-moment coefficient, $\frac{\text{Rolling moment}}{q_o S_{ref} D}$

C_n yawing-moment coefficient, $\frac{\text{Yawing moment}}{q_o S_{ref} D}$

C_Y side-force coefficient, $\frac{\text{Side force}}{q_o S_{ref}}$

C_{N_α} normal-force-curve slope, $\frac{\partial C_N}{\partial \alpha}$, per deg

C_{L_α} lift-curve slope, $\frac{\partial C_L}{\partial \alpha}$, per deg

C_{m_α} longitudinal stability parameter (body axes), $\frac{\partial C_m}{\partial \alpha}$

$C_{m_{C_L}}$ longitudinal stability parameter (stability axes), $\frac{\partial C_m}{\partial C_L}$

C_{l_β} effective dihedral parameter, $\frac{\Delta C_l}{\Delta \beta}$, per deg

C_{n_β} directional-stability parameter, $\frac{\Delta C_n}{\Delta \beta}$, per deg

C_{Y_β} side-force parameter, $\frac{\Delta C_Y}{\Delta \beta}$, per deg

L/D lift-drag ratio

C_p pressure coefficient, $\frac{p - p_o}{q_o}$

c local chord, ft

$\bar{c}$ mean aerodynamic chord of wing, ft

D body diameter, ft

M free-stream Mach number

p static pressure, lb/sq ft

p_o free-stream static pressure, lb/sq ft

q_o free-stream dynamic pressure, lb/sq ft

R	Reynolds number
S_{ref}	model reference area, $\frac{\pi D^2}{4}$, sq ft
t	local thickness, ft
x	model distance measured from base reference station, ft
x_{ac}	distance from body base reference station to aerodynamic center, ft
α	angle of attack, deg
β	angle of sideslip, deg

Subscripts:

0	conditions at zero angle of attack or zero lift
max	maximum
b	body base
c	balance chamber
f	flare base
r	rocket engine base
s	shroud base

DESIGN APPROACH

Design Philosophy

The possible development of a large expendable vertical-take-off launch vehicle into a fixed-wing reusable vehicle suggests that the finally evolved system should have the capability of two modes of operation. One mode should permit the body of the first stage to be employed in an expendable system to exploit the maximum payload thereby achievable. The other mode should permit the first stage of the otherwise expendable version to be mated with appropriate wings, flyback engines, and other gear necessary to provide recoverability and hence reuse. If all the physical features for recovery are contained as a unit, then it is possible to conceive of its use as a ferry vehicle for empty first-stage units, upper stages, or for some other useful mission. It is also conceivable that the recovery system, since it is independent of the booster, would undergo a normal airplane flight-test program prior to being flown with the booster. Therefore many details and problems could be solved before actually flying it in a vertical launch mode. An additional possible advantage of

this approach lies in the fact that phasing of the expendable system into the reusable system could be accomplished with a minimum interference with the development and operation of a programed expendable system. The philosophy of a separate recovery system package therefore was adopted in the design of models for the present investigation.

Design Requirements

During the postseparation portion of the flight of the first-stage reusable vehicle, the trajectory involves an atmospheric exit, reentry, supersonic glide, and a subsonic powered cruise back (referred to as flyback) to the launch site. For the exit, reentry, and supersonic glide, the principal aerodynamic requirement is that the vehicle must be controllable within the atmosphere and should employ shapes conducive to low local temperatures. During the subsonic flyback portion, the principal requirements are for good inherent stability, high lift-drag ratios for efficient powered flight, and usable landing characteristics. It is considered that for a vehicle of this type that an L/D of about 6 would provide adequate handling and landing characteristics. Superimposed on the aerodynamic requirements is the fundamental necessity for minimum weight for the entire recovery system in order to obtain the maximum payload. Furthermore, it would be desirable to minimize modifications to the launch stand for the expendable system to permit employment of the reusable vehicle system on the same launch facility.

Selected System

Adoption of the two mode of operation design philosophy limited the selection of wing-body configurations to either high- or low-wing arrangements. A low wing was selected from two considerations; the landing gear must be retracted into the wing and be as light as possible, and the recovery system should provide heat protection to the main-stage tank structure and components during reentry. The wing was therefore placed so that the body was tangent to the chord plane of the wing on the premise that intertank structure would carry some of the wing bending moments.

Preliminary estimates of the probable flyback center of gravity indicated it would be only about 1.25 body diameters forward of the body base, but since these component weights were probably somewhat optimistic, any weight increases would tend to shift the center of gravity more rearward. Wing planforms of moderate leading-edge sweep would therefore be necessary to obtain subsonic aerodynamic-center locations in close proximity to the center of gravity for suitable longitudinal stability. As a first approximation, the quarter chord of the mean aerodynamic chord of the exposed wing planform was located at the estimated center of gravity. To provide reasonable reentry from suborbital velocities of about 6,500 feet per second and suitable landing characteristics, the wing was sized to provide a wing loading of about 50 pounds per square foot of total wing planform area. To minimize the total wing weight, a moderately thick symmetrical wing section was selected with a wing planform having both a low aspect ratio and taper ratio. Wing sections with large leading-edge radii were selected to provide a good subsonic lift-curve slope and a low drag due to

lift factor, while simultaneously keeping local surface temperatures during exit and reentry low. The symmetrical section would minimize drift in the direction normal to the wing plane during the launch phase.

Two wing planforms were selected which had identical geometric characteristics except for leading- and trailing-edge sweep angles. The first was constrained to a straight trailing edge which would not extend rearward of the rocket nozzle exit plane in order to avoid the intense pressure fluctuations caused by the rocket engines during launch and to minimize ground launch-stand modifications. For this case a wing leading-edge sweep angle of 55° approximately satisfied all the requirements. The trailing edge at the center was notched to provide for the rocket nozzles. The resultant planform was therefore a modified clipped delta. Vertical fins, which were mounted inboard from the tip, on this wing would have relatively short moment arms; hence, directional stability problems were anticipated.

A second planform, without the trailing-edge constraints of the first wing, was selected to have a 65° leading-edge sweep. Although it was recognized that the higher leading-edge sweep might compromise the maximum lift-drag ratios available at subsonic speeds, the larger contribution of the outboard wing sections to the longitudinal stability coupled with an appreciably longer vertical tail moment arm to achieve directional stability were important considerations in this selection.

For each of the two wing planforms, twin vertical tails were employed, which had a planform corresponding to the outboard 20 percent of each wing-panel area. Each fin was mounted initially at the spanwise location for which its root chord was identical to the local wing chord.

For the subsonic flyback, turbojet or turbofan engines would be required. These engines should be sized to provide both engine-out cruise back and/or take-off of the flyback vehicle. The engine-out requirement dictated the engine size and number. Two nacelles were located at the wing-body juncture on the upper surface to permit six turbojet engines to be mounted therein. This location appeared to be compatible with good heat protection during reentry and the nacelles could have removable fairings ahead of the inlet and rearward of the tailpipe for launch.

With respect to the body nose shape, a strong tradeoff exists between the aerodynamic characteristics desired and the weight of the interstage structure between the first and second stages. A spherical forebody was tentatively selected as the best compromise of these two factors; however, alternate shapes were considered.

Inasmuch as the vehicle employs a vertical take-off, a rocket-propulsion system consisting of four engines near the periphery of the body base and one center engine was employed. To avoid excessive aerodynamic loads on the rocket nozzles, which would lead to excessively heavy engine gimballing hardware, shrouds for the outboard engines were provided on the rear of the basic booster body. Several alternate arrangements of shroud shapes, annular flares, and base venting were employed to investigate the anticipated base-drag problem

area. In addition, to ascertain the probable upper limit for the lift-drag ratio, an afterbody shape was designed which would fair in the shrouds and body base to a fully closed shape.

DESCRIPTION OF MODELS

The models employed in this investigation consisted of an axisymmetric cylindrical body 4.0 diameters long to which were added various forebody and base component parts, and a wing-body-tail model which was obtained by the addition of an assembly consisting of the wing, and vertical tails with the further addition of air-breathing engine nacelles for some cases. Model general arrangements are shown in figure 1 and component details in figure 2. Photographs of two representative configurations of the basic booster and reusable booster are shown in figure 3 and pertinent dimensions are given in table I.

Basic Booster

The basic booster is considered to consist of the cylindrical body with an appropriate forebody and either annular flares or shrouds at the base.

Body.- The basic body was cylindrical and had a length-diameter ratio of 4.0. Three interchangeable forebodies were constructed, consisting of a 1:1 ellipse (hemisphere), a blunt 1:4 ellipse, and a long 4:1 ellipse, and are shown in detail in figure 2(a).

Annular flares.- Two annular base flare shapes were designed to provide enclosure of the assumed engine gimbal strut and pylon supports. The length of the cone flare was 0.79 diameter and the flare angle was 15°. A short extension, about 0.16 body diameter long, was provided to turn the local surface angle to 0° and this extension had a circular-arc longitudinal shape as shown in figure 2(a). Provision for venting the base was made by cutting four longitudinal slots, having peripheral lengths of 60° arc at the body surface and located 90° apart so that the air would bleed into the base region between the rocket engines. The combined vent area was about 7 percent of the total base area. Details are shown in figure 2(a).

A second flare shape, having the same length and base diameter as the 15° flare, was designed to have a longitudinal shape consisting of a parabola constrained to have zero slope at the base. Details of this flare shape are given in figure 2(a). No venting was provided on this flare shape.

Rocket engine and shrouds.- Provision was made to mount four simulated rocket engines and corresponding shrouds either on top of the body and 90° apart around the base or displaced 45° from the initial location. Details of the simulated rocket engines are shown in figure 2(b), where it is indicated that provision was made to mount the engines canted toward the center line 12°. This angle corresponded to that which would result if the outboard engine nozzl just touched the center engine nozzle.

Two sets of individual engine shrouds were designed. The first consisted of 15° half conical shrouds, approximately the same length as the annular flares. The individual shrouds were designed not to exceed the diameter of the conical flare. (See fig. 1(a).) The second set of shrouds were more complex in shape but of the same overall length. They were designed to provide the minimum cross-sectional area needed to just enclose the assumed engine gimbal struts and pylons and to provide as much boattailing at their base as practicable. The selected cross-sectional shape was a half ellipse with a ratio of major to minor axes of 1.39. Forward of the maximum cross-sectional station, the longitudinal shape consisted of a parabola constrained to the same leading-edge station and length as the conical shrouds and having zero slope at the maximum area. Rearward from this station, a second parabola constrained to zero slope at the maximum area station and having a slope at the shroud base such that a tangent would just intersect the outer extremity of the corresponding rocket nozzle when the latter was canted inward 12°. The resulting shape minimized the shroud base area. Details of these shrouds are given in figure 2(b).

For the initial tests, the base of the model and shrouds coincided; however, when the shrouds and rocket nozzles were tested simultaneously, a short portion of the model base (0.412, see fig. 1(a)) was removed to evaluate the effect of shroud overhang. In one case the body length between the shrouds was restored but was boattailed to a shape similar to the rear end of the parabolic shrouds. (See figs. 1(c) and 3(b).)

Afterbody.- A complex afterbody, to fair in the body base, considered to consist of the basic body and 15° shroud assembly, was constructed as shown in figure 2(b). Before cutting off the base to permit installation of the model support sting, it was 3.0 diameters long. The longitudinal shapes were parabolas designed to fair smoothly to the local angles at the base of the basic model. Details of the shape are given in the table on the figure.

Winged Reusable Booster

General arrangement of the complete winged reusable booster configurations are shown in figures 1(b) and 1(c). In each configuration arrangement, the reference model is considered to consist of the cylindrical body with spherical forebody together with the wing and vertical tail assembly. All principal geometric characteristics are referred to the exposed wing area and the body diameter. Various combinations of the forebodies, shrouds, rocket engines, and afterbody already described were employed with the wing and tail assemblies shown in figures 2(c) and 2(d).

55° clipped delta-wing model.- The 55° clipped delta wing was mounted on the basic booster (fig. 1(b)) so that the quarter chord of the exposed planform coincided with the assumed center of gravity which was 1.25 diameters forward of the engine gimbal station (nominally the model base). The exposed planform area, the small vee-notch at the inboard trailing edge being neglected, was $7.5D^2$, the exposed span-to-body-diameter ratio was 3.75 diameters, and the taper ratio was 0.20. The corresponding panel aspect ratio was 1.87. The airfoil consisted of a symmetrical 10-percent-thick circular arc in the streamwise direction. The leading-edge radius was $t_{max}/6$ and the trailing edge was blunt

and equal in thickness to the leading-edge diameter. The wing had 0° geometric dihedral and was mounted so that the chord plane was tangent to the body diameter. Details of the wing are shown in figure 2(c) and in table I. Vertical-slab fairings from the body diameter to the wing surface were installed to form the wing-body juncture. At the wing leading edge, the juncture was hand faired to the body to provide a gentle upward sloped lower surface as indicated in figures 1(b) and 2(c).

The vertical-tail planform corresponded to the outer 20 percent of the wing-panel area. Each of the outboard mounted vertical tails was located at the spanwise station so that the root chord of the tail coincided with the local chord of the wing. A toe-in angle of 3° was provided by rotating the vertical fin about its midchord, because of anticipated directional stability problems of hypersonic speeds; no cant was employed.

The flyback engine nacelles shown in figure 2(c) consisted of a simple quadrant of a circle in cross section and were located at the wing-body juncture on the upper surface so that the engines would be situated at the assumed center of gravity. Three turbojet engines were assumed to be housed in the nacelle in a one-over-two arrangement. Subsonic inlets, and appropriate internal ducting, sized for a mass flow ratio of about 0.6 at $M = 0.6$ were employed. The engine tailpipes were considered to be extended approximately to the wing trailing edge. The external fairing was arbitrary but nearly parabolic in longitudinal shape.

For this model, the complete cylindrical basic booster was used; and the shroud base therefore coincided with the body base. No rocket engines were tested on this configuration and only the 15° conical shrouds were employed.

65° swept trapezoidal-wing model.- The 65° swept trapezoidal wing (figs. 1(b) and 2(d)) was mounted identically to the clipped delta wing in that the $0.25\bar{c}$ of the exposed planform coincided with the assumed center of gravity. Except for the basic geometry change of the leading- and trailing-edge sweep angles of the wing and vertical tails, all other details and dimensions were generally the same as those for the 55° clipped delta wing.

Modified 65° swept trapezoidal-wing model.- The modified 65° swept trapezoidal wing model (fig. 1(c)) was derived from the previously described configuration. The wing was shifted rearward 0.19 diameter, the vertical tails were relocated at the wing tip with 10° outboard cant and the toe-in angle was increased to 5°. Trailing-edge closure extensions on the wing amounting to about 8 percent of the local chord and consisting of simple wedge profiles were provided. A small portion of the body (0.412 inch) was removed to simulate the engine shroud overhang, and simulated rocket engines were installed together with the parabolic shrouds. They were oriented 45° from the vertical plane of symmetry; thus, only the two upper shrouds would be needed since the wing base and wing-body fairing would take the place of the two lower shrouds. The flyback engine nacelles were not tested on this configuration. In addition, special boattailed fairing was added between the engine shrouds and an extension with boattailing was added to the wing-body fairing. (See figs. 1(c) and 3(b) for modified configuration.)

APPARATUS AND TESTS

Most of the tests were conducted in the Langley 8-foot transonic pressure tunnel over a Mach number range from 0.4 to 1.2 and angles of attack up to 12° and at 0° and 5° sideslip. Selected configurations of the modified 65° wing configuration were tested in the Langley Unitary Plan wind tunnel at Mach numbers of 1.6, 1.9, and 2.1 for angles of attack up to 28° and at 0° and 5° sideslip. In all cases, artificial transition, consisting of a 0.1-inch-wide strip of No. 80 carborundum grains, was installed on all forebodies, and at the 0.10c station of both surfaces of the wings and vertical tails. Test Reynolds numbers based on body length varied from approximately 2.2×10^6 to 4.4×10^6 in the Langley 8-foot transonic pressure tunnel and from 1.9×10^6 to 2.0×10^6 in the Langley Unitary Plan wind tunnel as shown in figure 4.

Static aerodynamic force and moment data were measured with a six-component internally mounted strain-gage balance. Angles of attack and sideslip were corrected for balance and sting deflections under load. All drag data have been presented with no base-pressure corrections applied, including those configurations with airflow nacelles. The internal drag of the ducts was measured with a rake of 6 total-pressure and 2 static-pressure tubes. Pressure measurements were made in the balance chamber, on the model base, and on various components at the model base for some of the tests. (See fig. 1(b).) All forces and moments have been reduced to coefficient form and referred to the area of the base of the cylindrical body and its diameter in order that comparisons of the contributions of the various components can be readily made. The moment reference station was located 1.25 diameters forward of the model base. (See fig. 1.)

PRESENTATION OF RESULTS

The results of this investigation have been divided into four primary parts. The first consists of data applicable to the several configurations of the body alone or the basic booster; whereas, the remaining three parts contain the data for the wing-body configurations of the reusable booster. For the body alone, longitudinal data, referenced to body axes, are presented in figures 5 to 8. Figures 9 to 13 include basic and summary data for the 55° clipped delta-wing configuration. Figures 14 to 18 include basic and summary data for the 65° swept trapezoidal-wing configuration. Finally, figures 19 to 24 present basic and summary data for the modified booster-wing configuration using the 65° swept trapezoidal wing. Because of the diversity of configurations examined, all force and moment data are referred to common areas and dimensions consisting of the body base area and the body diameter. All moments have been referred to an assumed center of gravity which was 1.25 diameters forward of the engine gimbal station, which is essentially the model base.

DISCUSSION OF RESULTS

The importance of the subsonic flyback portion of the reusable booster mission has been indicated previously; therefore, the discussion will concentrate on the subsonic problem areas related to stability and aerodynamic efficiency together with subareas contributing to these factors.

Basic Booster

The reference configuration of the basic booster consisted of the plain cylindrical body with the spherical forebody. The total axial-force coefficient at 0° angle of attack for a Mach number of 0.6 is shown in figures 5 and 8 to be about 0.16 and the corresponding base-pressure coefficient was about -0.13.

Effect of axisymmetric flares.- The booster with the 15° conical flare is shown in figure 8(a) to have resulted in a total axial-force coefficient at $\alpha = 0^\circ$ of 0.63 at $M = 0.6$, an increase by nearly a factor of 4 over the reference configuration. This increase was caused by a decrease in the base-pressure coefficient by a factor of 2 coupled with an increase in the base area by a factor of 2.03. Addition of the short-flare extension decreased the axial-force coefficient about 12 percent despite a base-area increase of nearly 6 percent. The turning of the local surface angle to 0° by means of the extension increased the base-pressure coefficient about 15 percent, from -0.26 to -0.22. If a longer more gradually turning extension could have been provided, the base-pressure coefficient would have been expected to increase toward the value for the plain cylindrical body of -0.13.

Venting of the base has been shown by a number of investigations (for example, ref. 5) to be useful in reducing the level of the base drag. Figure 6 shows results of providing a base venting area of about 7 percent of the total base area for the 15° annular flare equipped with the extension. Figure 8(a) shows a comparison between the nonvented and vented configurations at an angle of attack of 0°. Two factors probably contributed to the increase in axial-force coefficient shown for the vented configuration. It was indicated in reference 5 that the amount of base-drag reduction was highly sensitive to the amount of venting. Since each geometric configuration would require considerable investigation to ascertain the optimum, it may be concluded that the present case is merely not the optimum and individual tailoring would be required. Secondly, good venting and pressure relief, together with overall drag reduction require that the vented air have high pressure recovery. In the present case, the vent inlet was located at the forward end of the flare; and aside from simple rounding of the inlet lips, no attempt was made to design an efficient inlet and duct.

Figure 8(a) shows that installing the parabolic flare shape decreased the axial-force coefficient at $M = 0.6$ to 0.46 compared with 0.63 for the conical flare or 0.55 for the extended conical flare. For the parabolic flare the total turning angle amounted to about 28° (see fig. 2(a)), which is considerably

greater than the 15° flare and occurred because of the large initial slope of the parabola at its forward end. Despite the favorable improvements, the total axial-force coefficient is still about 3 times that for the cylindrical body and the base-pressure drag contribution is greater by a factor of 1.6. It is concluded that despite the greater turning required by a convex shape, the factor affecting the base drag is primarily the ability to restore completely the flow to a direction at least parallel to the free stream provided no local flow separation occurs. These results also suggest that some boattailing at the end of the parabolic flare would be beneficial.

Effect of individual engine shrouds.- Figures 7 and 8(b) show that installation of the individual 15° conical engine shrouds increased the total axial-force coefficient at $M = 0.6$ from 0.16 for the "no shroud" case to 0.51. This increase is nearly as great as that for the 15° conical flare extended with its associated much larger base area. Comparison of the base pressures in figures 5 and 7 shows that magnitude of the average base-pressure coefficient increased 27 percent for the individual 15° shrouds compared with the 15° flare. This increase in magnitude (a decrease in base-pressure coefficient) can be explained as a base pumping action. The flow near the body surface between the shrouds must have behaved much as the flow through a venturi; that is, a significant acceleration occurred along the body as the net flow area decreased on approach to the base. (See fig. 1(a).) Figure 7 shows, for example, that for the extended shrouds, the body base-pressure coefficient is lower (more negative) than for the shroud base and thereby substantiates the pumping theory described.

Installation of the parabolic shrouds is shown in figure 8(b) to have reduced the total axial-force coefficient about 50 percent compared with the conical shrouds. Some of the reduction is attributable to about a 9-percent reduction in base area; however, the magnitude of the base-pressure coefficient decreased nearly 47 percent. In fact, the base-pressure coefficient is more negative by only 0.04 than that for the plain cylinder. In addition, figure 7 shows that the shroud base-pressure coefficient is about the same as that for the body; thus, little or no pumping occurred between the shrouds on the surface of the body. It is of significance to observe that the total axial-force coefficient for the model with parabolic shrouds is only about 60 percent greater than that for the reference body with no shrouds as compared with 230 percent for the 15° conical shroud case. It is concluded that careful tailoring of the shrouds and body in the vicinity of the base is required. Some boattailing on the body in the region of the shrouds could be expected to provide some further improvements.

Effect of rocket engines.- Figure 7 shows that some additional pressure recovery, compared with the body base, occurred on the base of the rocket engines. Since a pressure differential exists therefore between the external foreportion of the rocket engines and the base of the engine, some additional reduction in total axial-force coefficient could be anticipated. Figures 7 and 8(b) show that a small decrease of about 0.01 did indeed occur. However, because the model support sting essentially replaced the region which would be occupied by the center engine, it is not yet clear what the true axial-force and base-pressure characteristics would be. Additional investigation is needed to ascertain the effect of the sting and the fifth engine.

Effect of afterbody fairing.- The afterbody fairing, which faired in both the body base and the 15° conical shrouds is shown in figure 8(b) to have decreased the total axial-force coefficient to a value of only 31 percent of that for the reference model at $M = 0.6$ despite the large increase in wetted area. Although it is probably not practical to provide such an afterbody fairing, even if made of collapsible materials and then inflated when required, this result clearly emphasizes the seriousness of the base-drag problem.

55° Clipped Delta-Wing Reusable Booster

Longitudinal stability.- Principal effects of shrouds, nacelles, and afterbody fairing on the longitudinal stability have been summarized in figure 12. All configurations were unstable at most subsonic test conditions. In fact, the aerodynamic center is nearly 0.2 diameter forward of the assumed center of gravity for the reference configuration, which consisted of the cylindrical body, spherical forebody, and the wing-tail assembly. Progressively additional adverse increases in the aerodynamic-center shift with Mach number resulted from the addition of the several components. Should a more rearward center-of-gravity location result from a more accurate weight and center-of-gravity estimate for the actual vehicle, the magnitude of the instability would, of course, be greater. An appreciable rearward shift of the wing would be required to attain a longitudinally stable configuration subsonically. Such a shift would place large regions of the wing in the intense noise field of the rocket engine during launch and would also require extensive launch-stand modifications. Therefore, the potential advantages of this planform seem to have been removed.

Lift-drag characteristics.- The lift-drag characteristics shown in figure 12 indicate that the reference configuration achieved an $(L/D)_{max}$ of approximately 5.8 at $M = 0.6$. Addition of the shrouds caused a 30-percent reduction to a value only a little more than 4.0. Fairing in the entire back end with the afterbody not only removed the shroud penalty but increased $(L/D)_{max}$ even further to about 6.5. This value is considered the upper limit for this configuration and could not be achieved in a practical manner. It is concluded that the aerodynamic efficiency is inadequate.

Lateral-directional stability.- Figure 13 shows that the effective dihedral was negative (C_{l_β} positive), which was not unexpected in view of the low wing configuration with a large body together with the fact that no geometric dihedral was incorporated in the wing. Directional instability, as expected, was very large, $C_{n_\beta} > -0.05$.

Evaluation.- Since the clipped delta wing resulted in severe longitudinal and lateral directional stability problems coupled with an inadequate lift-drag ratio, the type of modification which would be required to rectify the deficiencies would reduce the potential advantages of this configuration. Therefore, further analysis and investigation of this configuration was curtailed, and the investigation concentrated on the second wing planform arrangement.

65° Swept Trapezoidal-Wing Reusable Booster

Longitudinal stability.- Figure 17 summarizes the effects of the addition of the various components to the reference configuration consisting of the body, spherical nose, and wing-tail assembly. All configurations were longitudinally unstable at $M = 0.6$; however, when compared with the 55° clipped delta wing (fig. 1(a)), the amount of instability has decreased markedly. For the reference configurations, for example, the negative static margin is only 6 percent for the present wing compared with 20 percent for the former wing arrangement. The improved longitudinal stability is the result of the high loading of the outboard wing panel, characteristic of swept trapezoidal wings with sweptback trailing edges. Furthermore, comparison of figures 17 and 12 shows that the aerodynamic-center variation with Mach number in the transonic range was only two thirds as great for the 65° wing compared with the 55° wing.

Figures 14 and 9 indicate that the positive $C_{m,0}$ for the 65° wing was appreciably greater than that for the 55° wing; this positive $C_{m,0}$ is desirable to reduce the level-flight trim requirements. The increased $C_{m,0}$ is at least in part associated with the positively sloped lower wing surface at the wing leading edge in the wing-body juncture (see fig. 1(b)), which for the 65° wing was considerably farther ahead of the center of gravity than was the case for the 55° wing. The sensitivity of $C_{m,0}$ to the addition of the various corresponding components was considerably less for the 65° wing than for the 55° wing. Although satisfactory stability was not achieved, it is concluded that the configuration employing the 65° wing offers considerably greater potential for achieving usable longitudinal characteristics than the 55° clipped delta wing.

Zero-lift drag and lift-drag ratio.- Figures 17 and 12 show that the zero-lift drag coefficient at $M = 0.6$ for the reference configuration was somewhat less for the 65° wing than for the 55° wing-body configuration. However, when the shrouds and engine nacelles were added, any differences were inconsequential. The addition of the shrouds and engine nacelles approximately doubled the drag coefficient of the reference configuration, the shrouds contributing about 90 percent of the increase. It can be seen from the magnitude of the measured internal drag that it is so small that it has no appreciable effect on either the zero-lift drag coefficient or the lift-drag ratio values.

The effect of changing the forebody shape from the blunt 1:4 ellipse to the 1:1 ellipse (hemisphere) and finally to the 4:1 ellipse is shown in figure 14. The 4:1 ellipse produced no discernible change in zero-lift drag coefficient, but, in addition, produced sizable destabilizing increments. Installing the 1:4 blunt ellipse increased the drag coefficient more than 50 percent at $M = 0.6$ compared with the reference configuration which employed the 1:1 elliptical forebody. Comparison of these results with those of references 6, 7, and 8 indicated excellent agreement on the effects of forebody bluntness. The conclusion from this comparison is that essentially no increase in forebody bluntness can be tolerated beyond that for a hemisphere without attendant large drag coefficient increases. It is concluded therefore that the 1:1 ellipse (hemisphere) used for most of the present investigation is

nearly the optimum compromise between interstage weight and aerodynamic shape for this vehicle application. The observation is made, however, that most of the data were obtained at Reynolds numbers and surface conditions for which most of the boundary layer on the forebody would be laminar. Uncertainty therefore exists as to the validity of the trends for large Reynolds numbers and practical construction surfaces in which case turbulent flow would probably be established on the forebody. The advantage of blunter forebody shapes lies in significant reductions in interstage weight and hence larger payloads.

Figure 14 also shows the effects of rotating the shrouds 45° from their initial position. For this position, the two lower engines are protected from aerodynamic loads during launch by the wing base; hence only two shrouds are required. Nearly 25 percent of the initial shroud increment drag has been recovered; however, only one of the original three shrouds and a small portion of the fourth have been removed. It is probable that some of the pumping action, described earlier, occurred in the space on the side of the vehicle between the shroud and the upper wing surface; however, this pumping would be less severe than that for adjacent shrouds.

The maximum lift-drag ratio is shown in figure 17 to be about 6.1 at $M = 0.6$ for the reference configuration; but this value decreased to 4.2 with the addition of the shrouds and flyback engine nacelles. The results of figure 14(c) show that rotating the shrouds 45° would increase this value to about 4.5. A measure of the probable upper limit for the configuration is indicated by the maximum lift-drag ratio of 7.1 when the faired afterbody was installed, which was about 10 percent higher than that for the 55° wing. It is concluded that the 65° swept trapezoidal-wing configuration has greater potential for lift-drag-ratio improvement than the 55° clipped delta wing configuration and that the 45° shroud position is preferred over the originally selected orientation.

Lateral-directional stability.- Figure 18 shows that both effective dihedral and directional stability are unsatisfactory. Although the vertical tail for the present configuration was located farther rearward than for the previous 55° wing because of the increased leading-edge sweep, its effectiveness has not significantly improved. It is probable that the effect of the longer tail moment arm has been canceled by the reduced lift-curve slope of the more highly sweptback vertical tail (65° compared with 55°). Reducing the fin leading-edge sweep, moving it to the wing tip to obtain a longer moment arm, together with increasing the fin area may be necessary to provide positive directional stability. The effective dihedral, now negative, can probably be corrected by incorporating some geometric dihedral and, if the vertical fin is relocated at the wing tip, by canting the fin outboard.

Evaluation.- The results of this part of the investigation indicate that although significant deficiencies in both stability and aerodynamic efficiency exist, they are considerably less severe than those for the 55° clipped delta-wing configuration. Therefore further detailed investigation was considered desirable, and the pertinent results of the changes incorporated are discussed in the next section.

Modified 65° Swept Trapezoidal Wing Reusable Booster

Comparison of the model description and the recommendations of the previous sections indicates that practical changes could be made without a complete redesign of the configuration to improve both the stability and the aerodynamic efficiency parameters.

Longitudinal stability.- Figure 23 shows that a subsonic static margin at $M = 0.6$ of 25 percent of the body diameter was obtained, which corresponds to about 11 percent of the mean aerodynamic chord of the exposed wing planform. At the maximum supersonic test Mach number, the static margin was approximately 40 percent of the body diameter. The transonic change in static margin represents about 7 percent of the mean aerodynamic chord and is not considered to be excessive. Installation of the wing trailing-edge extension, considered desirable for subsonic lift-drag ratios, caused about a 50-percent decrease in static margin at subsonic speeds but little change at supersonic speeds. The change in static margin with Mach number has increased from about 0.1 to more than 0.2 or nearly a factor of 2.

Figure 19 shows that at $M = 0.6$ the $C_{m,0}$ for the modified configuration was about 0.35 and increased nearly 100 percent by the addition of the trailing-edge extension. This shift in the pitching-moment curve is shown to have resulted in a trimmed lift coefficient of about 4.0 which is close to that which would correspond to maximum L/D. Little trim control would be needed therefore. It should also be observed, however, that the addition of the small fairings between the shrouds and at the wing-body juncture virtually eliminated all the $C_{m,0}$ change. The sensitiveness of local tailoring, of the type needed to provide high $(L/D)_{max}$, on both stability and trim requirements is clearly indicated by these results.

The effect of the wing-tip-mounted vertical fins on the longitudinal stability variation with angle of attack is shown in figure 19(d) to consist, at subsonic speeds, of the removal of most of the nonlinearity of the pitching-moment curve at low lift coefficients but to cause a severe pitchup at lift coefficients corresponding to maximum L/D. Data such as that given in reference 9 indicate that an unstable break would be expected as $C_{L,max}$ is approached for wings with this sweepback and aspect ratio, but a break at such low lift coefficients as indicated by the present data would not be foreseen. These results suggest that the usual strong spanwise flow near the wing tip was eliminated by the presence of the vertical fin. Such a change in the local flow would tend to cause the tip loads to increase with the accompanying increase in stability observed. This increased tip loading would, however, promote earlier flow separation and would therefore provide the explanation for the early pitchup observed with the vertical tails on.

Drag and lift-drag ratio characteristics.- Comparison of the zero-lift drag characteristics for the modified configuration shown in figure 23 with those for the original 65° wing arrangement with shrouds and rocket engines shown in figure 17 indicates that the drag coefficient at $M = 0.6$ has decreased from 0.76 to 0.48 or about 37 percent. This reduction is attributed

to employment of the parabolic shrouds discussed earlier and rotation of the position of the shrouds 45°. Installation of the wing trailing-edge extensions and rocket engines further decreased the drag coefficient to 0.40. Finally, the addition of the small body boattail fairing between the shrouds and at the wing fuselage juncture reduced the level of $C_{D,0}$ to 0.35. The total drag coefficient for the complete reusable booster has been reduced to less than that of the basic expendable booster with the 15° shrouds and rocket engines which was 0.53. This drag level also compares favorably with that for the expendable booster with parabolic shrouds and rocket engines with $C_{D,0} = 0.25$. Comparison of the base-pressure coefficients on the various components (figs. 7 and 23) shows that considerable improvement has been achieved. On the basis of the present data and the trends shown, it is believed that some further improvements can be obtained, possibly by further detailed shaping or other means.

From figure 19(d) the drag-due-to-lift factors at $M = 0.6$ were calculated to lie between 0.018 and 0.019. Full leading-edge suction would indicate values of 0.017 when both lift and drag coefficient are referred to the body base area as in this investigation. Nearly full leading-edge suction appears to have been obtained. To verify this result further, reference 10 indicates that nearly full leading-edge suction would be expected when the Reynolds number, based on the leading-edge radius is as great as 3×10^4 to 4×10^4. For the present tests the leading-edge Reynolds number was almost 3×10^4; hence, little further improvement could be expected.

For the initial configuration of the modified 65° wing model the maximum L/D is shown in figure 23 to be 5.5 at $M = 0.6$; and that for the best configuration, this value increased to nearly 6.1. These values are comparable to 4.5 for the best previous configuration. Comparison of figures 23 and 17, however, show that $(L/D)_{max}$ has become more sensitive to Mach number. No measurable improvement is shown at transonic speeds for the modified configuration, and the level of $(L/D)_{max}$ at moderate supersonic speeds is shown to be about 2.0. Special tailoring to improve subsonic L/D for the return flight will probably have to be examined at higher Mach numbers to insure that some other adverse effects do not simultaneously occur, although small decreases in $(L/D)_{max}$ are probably not too important at high Mach numbers for this type of vehicle. It is concluded that significant improvements in the maximum lift-drag ratio can be obtained and some further improvements may be possible if sufficient effort is expended.

Lateral-directional stability.- The outboard mounted vertical tail coupled with its outboard cant is shown in figure 24 to have produced a reduction of 25 percent in the negative effective dihedral measured on the original 65° wing configuration. Differences at supersonic speeds between the two tail arrangements however appear to be negligible. The strong influence on the effective dihedral of angle of attack is illustrated by the results shown for 0° and 12°.

Marked improvements in the directional stability for the modified 65° wing model are indicated by comparing figures 24 and 18. For the tail-on case, some directional stability is shown for nearly all Mach number conditions; however,

deterioration with increasing supersonic Mach number should be noted. The increase in the tail moment arm of 86 percent for the modified configuration coupled with an increased toe-in from 3° to 5° resulted in an increase in vertical-tail effectiveness of about 100 percent compared with the original inboard location. The effects of both Mach number and angle of attack also are significantly less than those for the inboard location.

Evaluation.- The results of the modified configuration indicated that reasonable values of $(L/D)_{max}$ are attainable and that positive longitudinal stability about the assumed center of gravity was obtained. Furthermore, marked improvement in the directional stability was also shown. However, a re-evaluation of the location of the center of gravity for the modified configuration indicated that it would move significantly rearward. Employment of a more detailed weight analysis with more realistic unit weights than employed initially showed that the center of gravity might be as far back as 0.9 diameter forward of the base rather than the value of 1.25 diameters initially calculated and used in this investigation. To cope with a more rearward center of gravity, an increase in the wing taper ratio coupled with some rearward shift of the wing would provide a substantial increase in longitudinal stability and would allow an improved vertical-tail installation. A lower leading-edge sweep of the vertical tail coupled with an increase in the area would also be needed. Incorporation of some or all of these changes would have some adverse effects on the $(L/D)_{max}$ available.

CONCLUDING REMARKS

An investigation has been conducted in the Langley 8-foot transonic pressure tunnel and the Langley Unitary Plan wind tunnel to ascertain some of the aerodynamic characteristics of bodies and wing-body-tail configurations representative of large payload vertical-take-off reusable orbital launch vehicles. Test data were obtained from Mach numbers of 0.4 to 1.2 and for selected configurations from Mach numbers of 1.6 to 2.1 over a range of angles of attack and at sideslip angles of 0° and 5°. Test Reynolds number varied from 2×10^6 to 4×10^6. The results indicate the following remarks are appropriate:

1. Pertinent characteristics of the flow in the base region of a low-fineness-ratio body whose base region is distorted by the presence of rocket engines and accompanying shrouding have led to methods of shaping the shrouds and body base boattailing to provide significant reduction in the base drag.

2. Employment of highly swept trapezoidal wing planforms will be required to obtain positive subsonic longitudinal stability for reusable boosters which have centers of gravity close to the rear of the body.

3. Wing-tip-mounted vertical fins having large (20 percent or greater) ratios of fin area to wing area and which employ both outboard cant and toe-in have been shown to be effective in providing positive subsonic and supersonic directional stability for vehicle systems which have large blunt bodies relative to the wing span.

4. A spherical forebody shape for large low-fineness-ratio bodies is nearly optimum from zero-lift drag and longitudinal stability considerations.

5. Maximum lift-drag ratios for reusable boosters of the type considered of more than 6.0 can be obtained, and some further increases appear to be possible.

Langley Research Center,
National Aeronautics and Space Administration,
Langley Station, Hampton, Va., April 18, 1964.

REFERENCES

1. Pierpont, P. Kenneth: Transonic Stability of a Preliminary Vertical-Take-Off Launch Configuration With a Horizontal-Landing Recoverable Booster. NASA TM X-689, 1962.

2. Clark, Larry R., and Pierpont, P. Kenneth: Hypersonic Aerodynamic Characteristics of Preliminary Vertical-Take-Off Launch Configurations With a Horizontal-Landing Reusable Booster. NASA TM X-887, 1963.

3. Pierpont, P. Kenneth: Transonic Aerodynamic Characteristics of a Horizontal-Take-Off-and-Horizontal-Landing Recoverable-Booster Concept With Upper Stages Arranged in Parallel. NASA TM X-696, 1962.

4. Clark, Larry R., and Pierpont, P. Kenneth: Spacecraft and Stage-Geometry Effects on the Hypersonic Characteristics of a Horizontal-Take-Off Reusable Booster. NASA TM X-900, 1963.

5. Henry, Beverly Z., Jr., and Cahn, Maurice S.: Additional Results of an Investigation at Transonic Speeds To Determine the Effects of a Heated Propulsive Jet on the Drag Characteristics of a Series of Related Afterbodies. NACA RM L56G12, 1956.

6. Cleary, Joseph W.: The Effects of Nose Bluntness on the Flow Separation and Longitudinal Characteristics of Ellipsoidal-Nosed Cylinder-Flare Models at Transonic Speeds. NASA TM X-370, 1960.

7. Judd, Joseph H., and Woodbury, Gerard E.: Free-Flight Measurements of the Transonic Drag Characteristics of Low-Fineness-Ratio Cylinders Including Stabilizing Plates and Flares and Varying Nose Bluntness. NASA TN D-361, 1960.

8. Stanbrook, A.: A Correlation of the Forebody Drag of Cylinders With Plane and Hemispherical Noses at Mach Numbers From Zero to 2.5. Tech. Note No. Aero. 2875, British R.A.E., Feb. 1963.

9. Shortal, Joseph A., and Maggin, Bernard: Effect of Sweepback and Aspect Ratio on Longitudinal Stability Characteristics of Wings at Low Speeds. NACA TN 1093, 1946.

10. Osborne, Robert S., and Kelly, Thomas C.: A Note on the Drag Due to Lift of Delta Wings at Mach Numbers Up to 2.0. NASA TN D-545, 1960. (Supersedes NACA RM L53A16a.)

TABLE I.- GEOMETRIC CHARACTERISTICS

[All dimensions are in inches]

(a) Basic booster

Body:	
Overall length	14.25
Diameter	3.17
Base area	7.88
Length/diameter, cylindrical body	4.0
Moment reference from base	3.96
Flares:	
Length	2.51
Annular base area -	
15° cone	8.10
Parabolic	8.10
Extension	9.02
Vent area	1.14
Shrouds:	
Length, 15° and parabolic	2.51
Base area (total 4 shrouds) -	
15°	3.72
Parabolic	2.72
Afterbody:	
Length	6.68
Base area	3.27

TABLE I.- GEOMETRIC CHARACTERISTICS - Continued

(b) Reusable booster with 55° clipped delta wing

Body:	
Overall length	14.25
Diameter	3.17
Base area	7.88
Length/diameter, cylindrical body	4.0
Moment reference from base	3.96
Wing:	
Total area	104.93
Exposed area (approximately $7.5D^2$)	73.13
Root chord at fuselage juncture	10.58
Tip chord	2.12
Span (total)(4.75D)	15.04
Span (exposed)(3.75D)	11.87
Leading-edge sweep, deg	55
$(t/c)_{max}$	0.10
Leading-edge radius	$t_{max}/6$
Trailing-edge thickness	$t_{max}/3$
Airfoil section	Circular arc
$\bar{c}$, based on exposed area	7.28
Moment reference	$0.25\bar{c}$
Moment reference, distance from body base	3.96
Aspect ratio (not including trailing-edge notch)	1.87
Vertical tail:	
Area, each	7.56
Root chord	5.09
Tip chord	2.17
Height	2.10
Leading-edge sweep, deg	55
$(t/c)_{max}$	0.10
Leading-edge radius	$t_{max}/6$
Trailing-edge thickness	$t_{max}/3$
Airfoil section	Circular arc
Toe-in, deg	3
Cant, deg	0
Tail moment arm, center of gravity to $(\bar{c}/4)$ tail	2.61

TABLE I.- GEOMETRIC CHARACTERISTICS - Concluded

(c) Reusable booster with 65° swept trapezoidal wing

Body:	
Overall length	14.25
Diameter	3.17
Base area	7.88
Length/diameter, cylindrical body	4.0
Moment reference from base	3.96
Wing:	
Total area	114.23
Exposed area (approximately $7.5D^2$)	75.40
Root chord at fuselage juncture	10.58
Tip chord	2.17
Span, total (4.75D)	15.04
Leading-edge sweep, deg	65
$(t/c)_{max}$	0.10
Leading-edge radius	$t_{max}/6$
Trailing-edge thickness	$t_{max}/3$
Airfoil section	Circular arc
$\bar{c}$ based on exposed area	7.28
$\bar{c}$ based on total area	8.76
Moment reference, original	$0.25\bar{c}$
Moment reference, modified	$0.17\bar{c}$
Moment reference, distance from base	3.96
Aspect ratio, design	1.87
Vertical tail:	
Area, each	7.23
Root chord	5.09
Tip chord	2.17
Height	2.10
Leading-edge sweep, deg	65
$(t/c)_{max}$	0.10
Leading-edge radius	$t_{max}/6$
Trailing-edge thickness	$t_{max}/3$
Airfoil section	Circular arc
Toe-in, deg -	
Original	3
Modified	5
Cant, deg -	
Original	0
Modified	10
Tail moment arm, center of gravity to $(\bar{c}/4)$ tail -	
Original	4.36
Modified	8.11

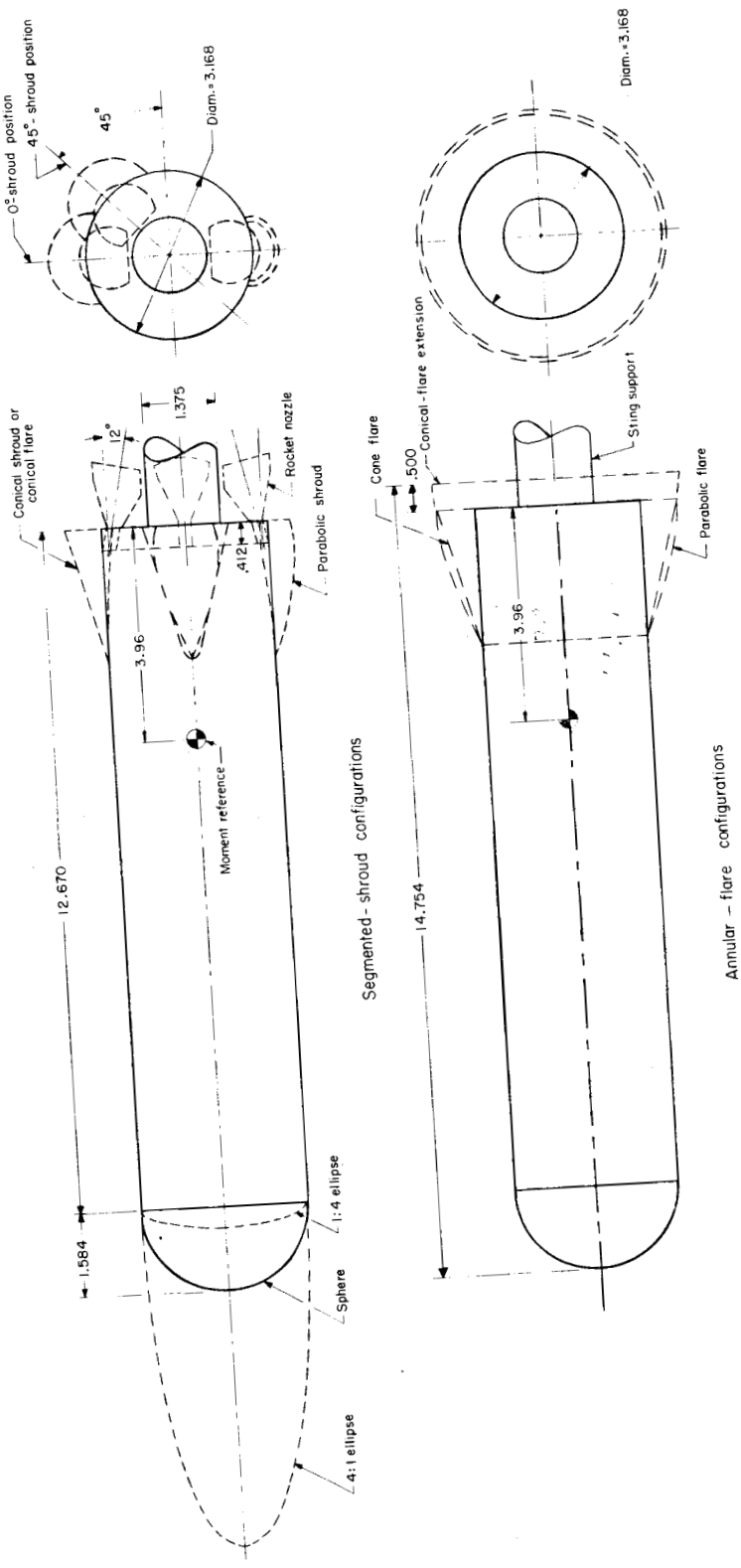

(a) Body alone.

Figure 1.- General arrangement of reusable first-stage booster. All dimensions are in inches unless otherwise noted.

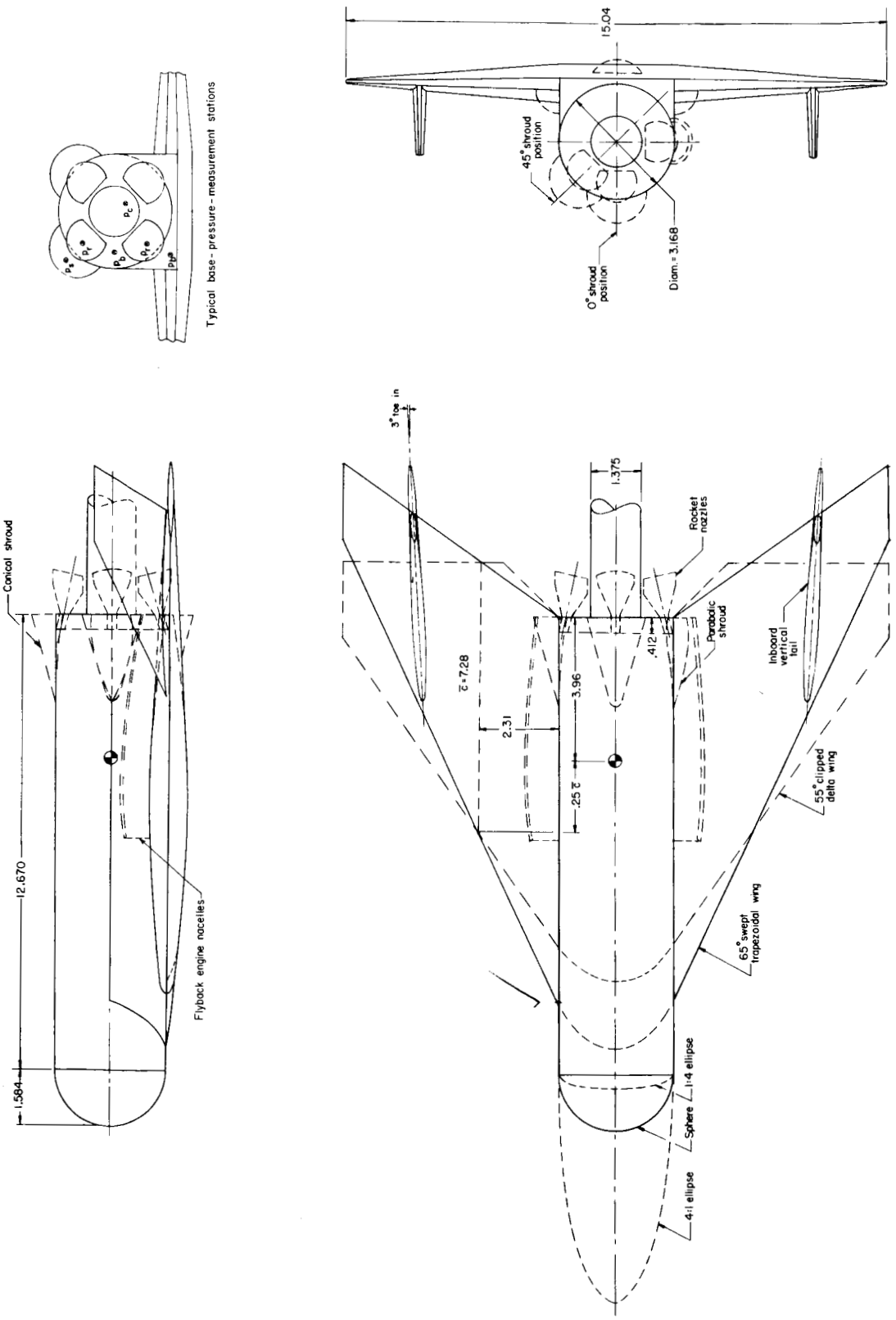

(b) Complete model.

Figure 1.- Continued.

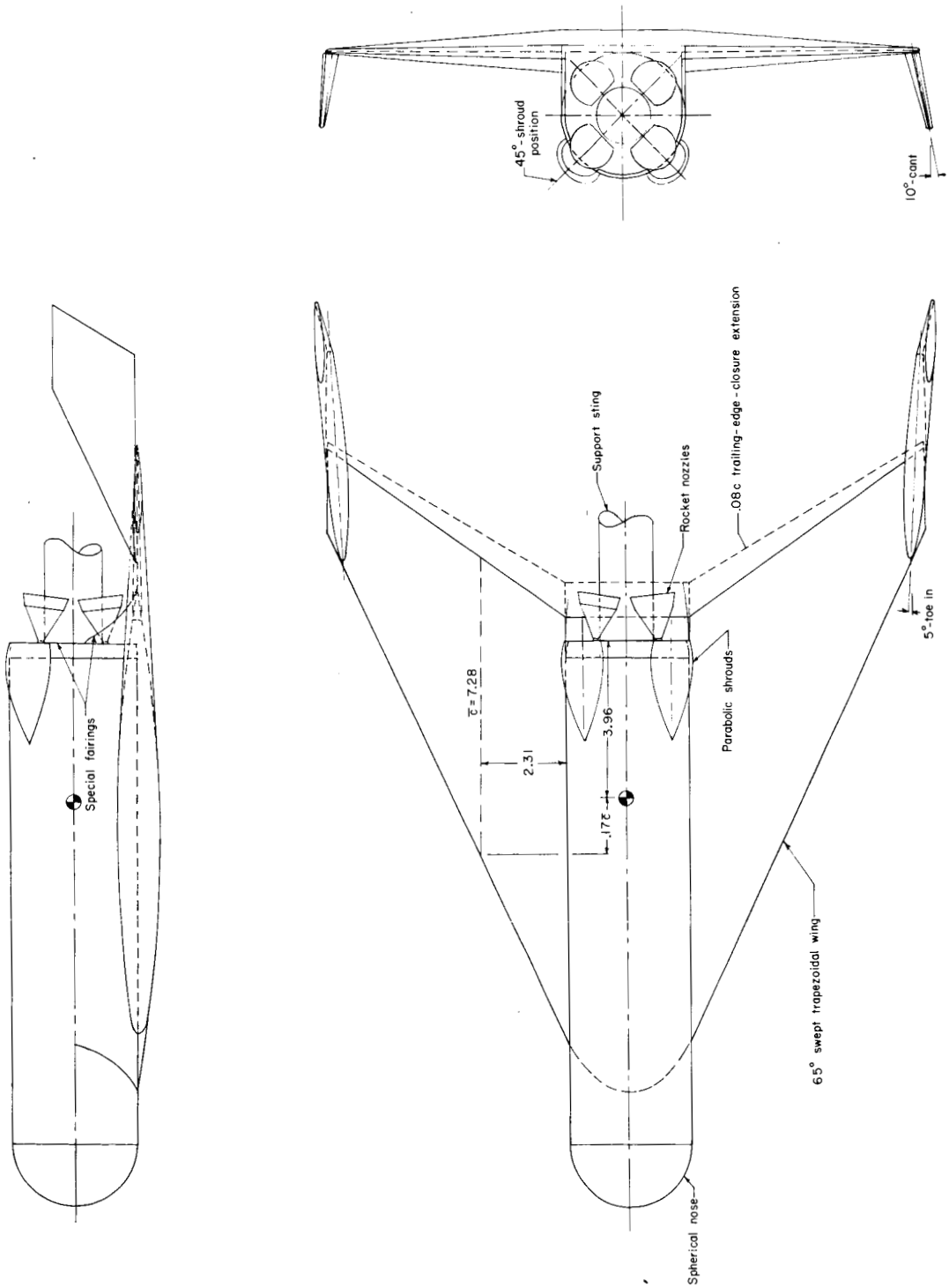

(c) Modified 65° swept trapezoidal wing model.

Figure 1.- Concluded.

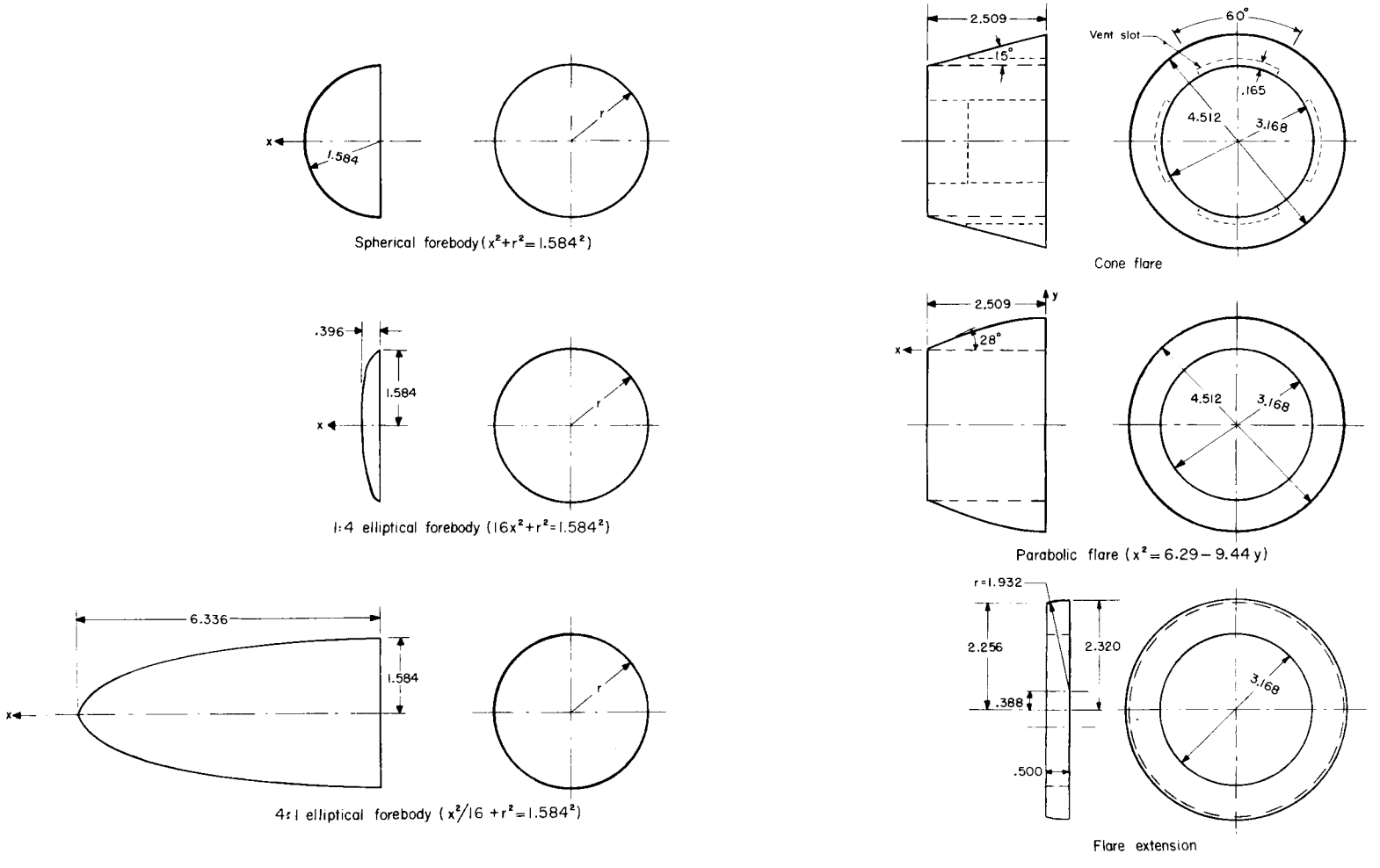

(a) Forebodies and flares.

Figure 2.- Details of model components. All dimensions are in inches unless otherwise noted.

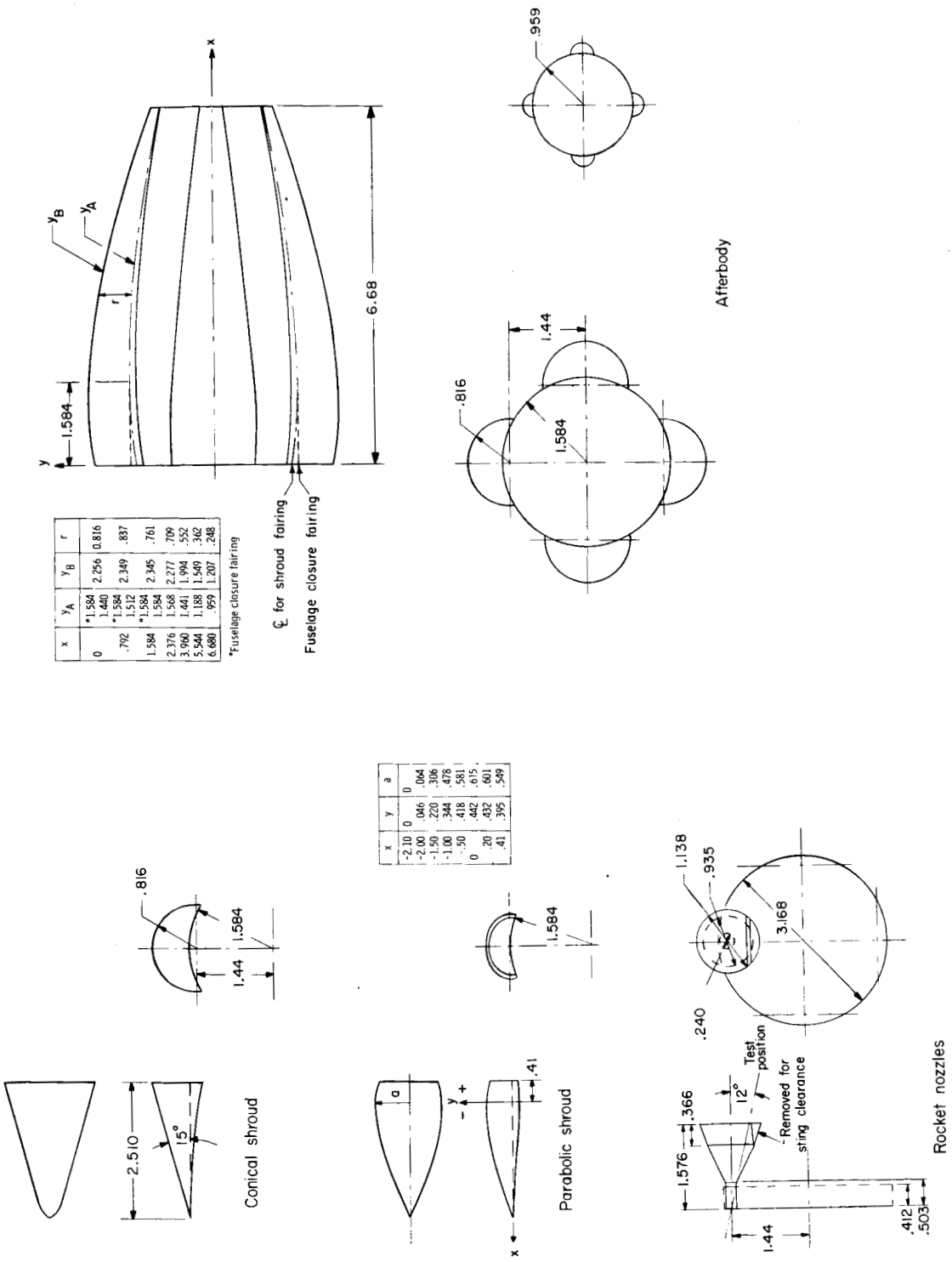

x	y_A	y_B	r
0	*1.584	2.256	0.816
	1.440		
.792	*1.584	2.349	.837
	1.512		
1.584	*1.584	2.345	.761
	1.584		
2.376	1.568	2.277	.709
3.960	1.441	1.994	.552
5.544	1.188	1.549	.362
6.680	.959	1.207	.248

x	y	a
-2.10	0	0
-2.00	.046	.064
-1.50	.220	.306
-1.00	.344	.478
-.50	.418	.581
0	.442	.615
.20	.432	.601
.41	.395	.549

(b) Shrouds, afterbody, and rocket nozzles.

Figure 2.- Continued.

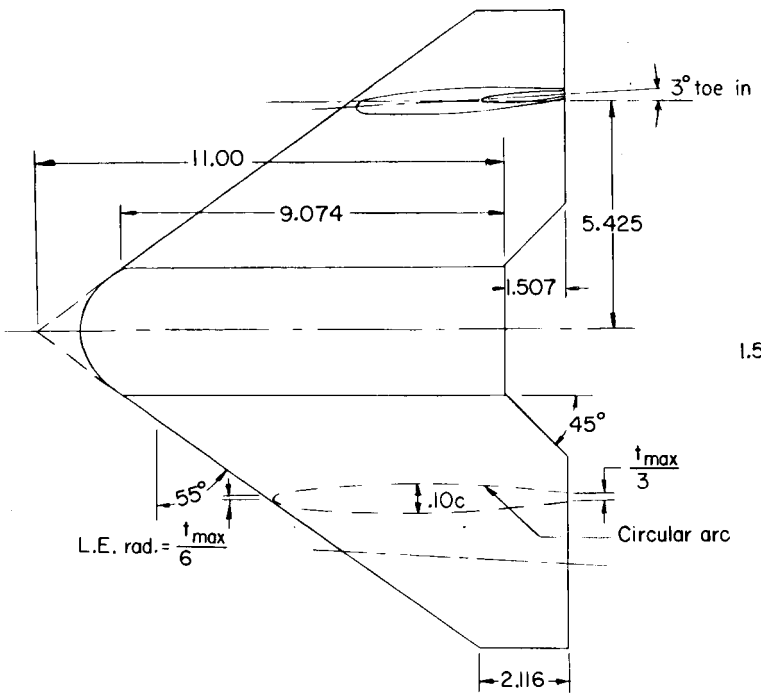

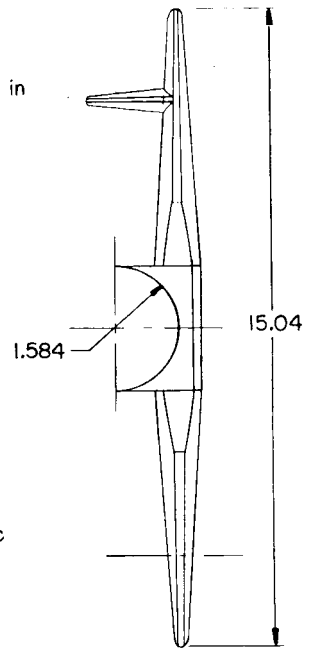

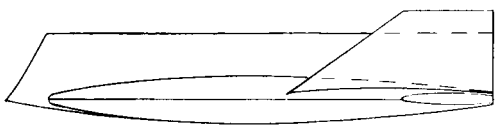

Wing

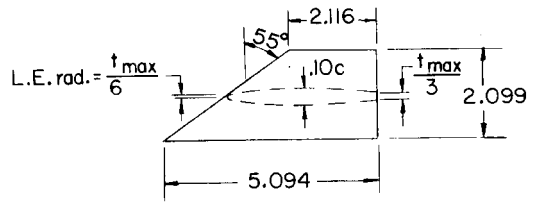

Vertical tail

Nacelle coordinates
(measured from model base)

x	y	r
0	0.547	0.654
.494	.392	.708
.994	.450	.775
1.494	.468	.807
1.994	.488	.875
2.494	.508	.911
2.994	.521	.951
3.494	.529	.946
3.784	.529	.940
3.990	.529	.950
4.074	.529	.940
4.574	.521	.940
5.074	.518	.917
5.574	.488	.891
6.074	.468	.841
6.559	.430	.789

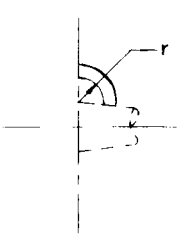

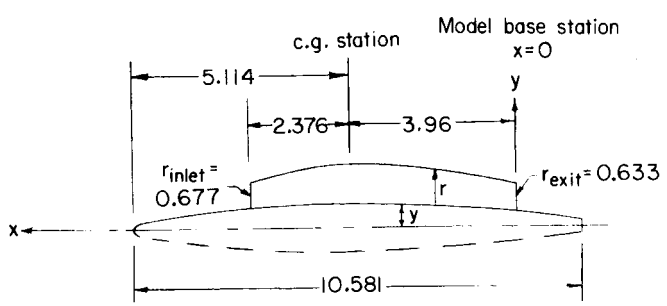

Flyback engine nacelles

(c) 55° clipped delta wing and components.

Figure 2.- Continued.

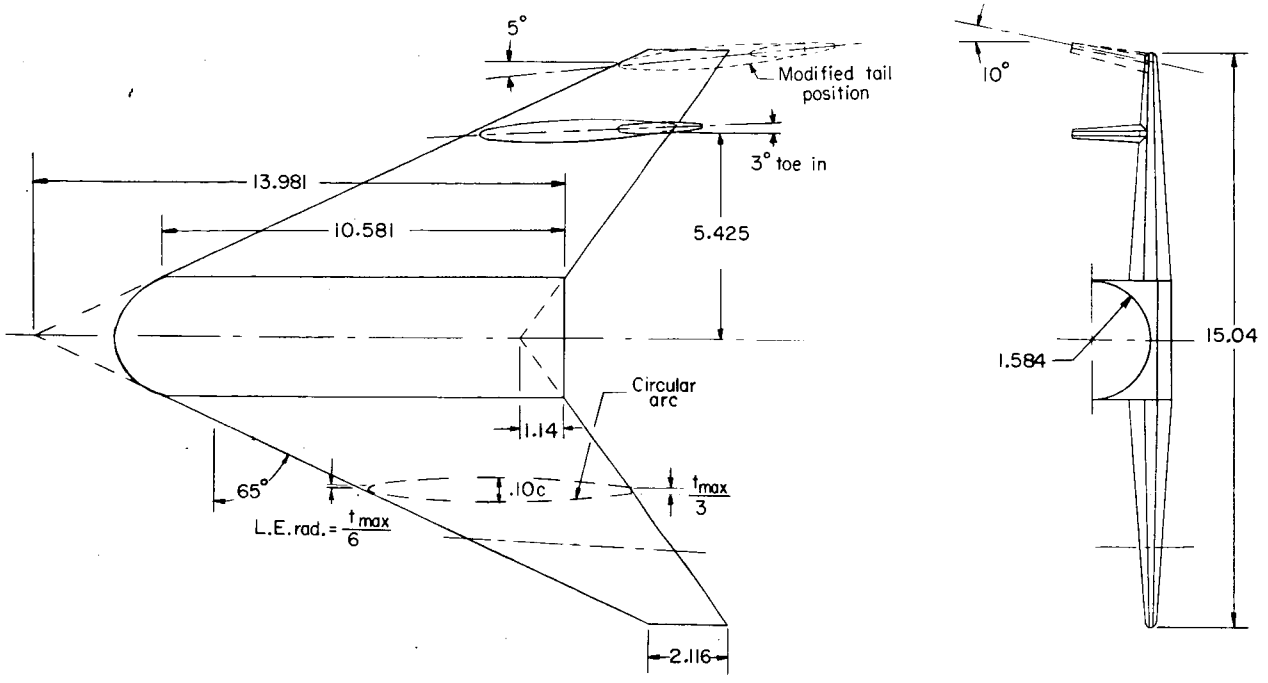

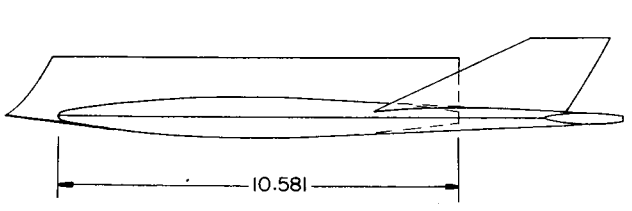

Wing

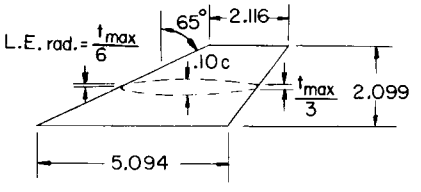

Vertical tail

Nacelle coordinates
(measured from model base)

x	y	r
0.155	0.175	0.657
.655	.238	.760
1.155	.296	.813
1.655	.347	.860
2.155	.392	.895
2.655	.430	.920
3.155	.462	.939
3.655	.488	.949
3.960	.508	.950
4.155	.508	.949
4.655	.521	.930
5.155	.528	.890
5.735	.528	.828
6.235	.521	.761
6.536	.513	.710

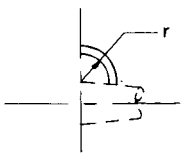

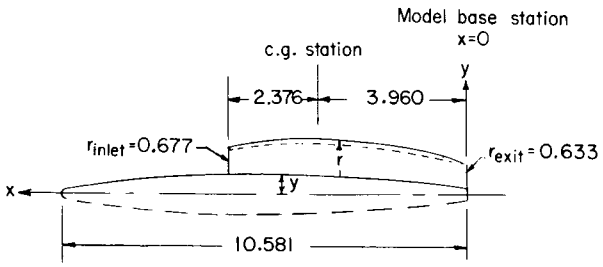

Flyback engine nacelles

(d) 65° swept trapezoidal wing and components.

Figure 2.- Concluded.

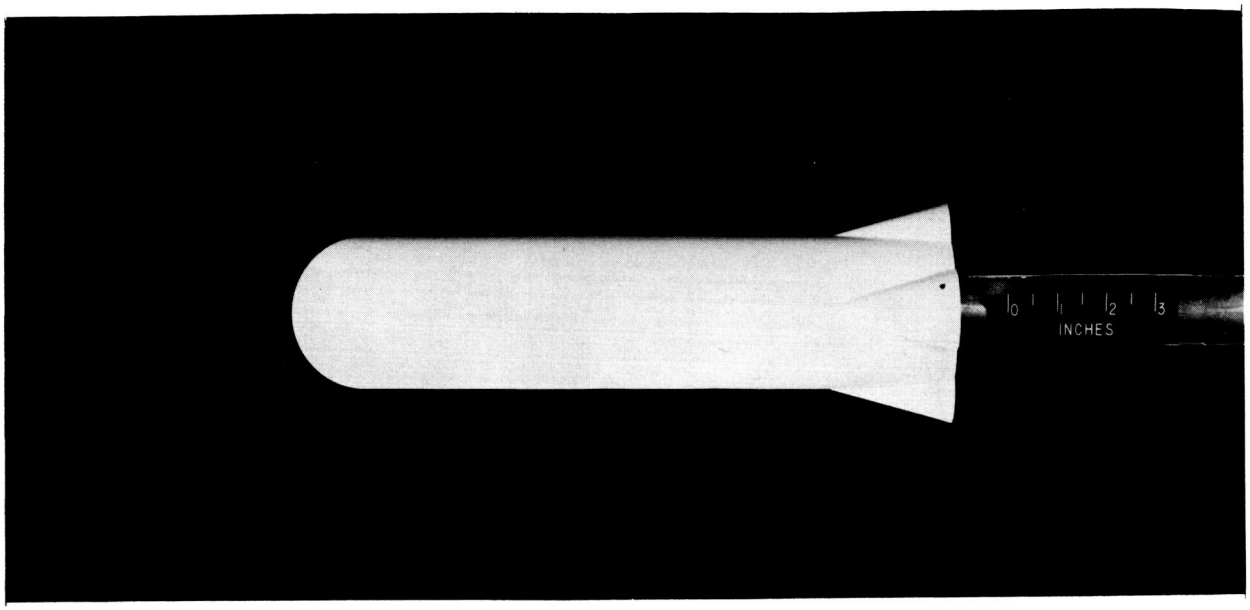

15° conical shrouds. L-63-8573

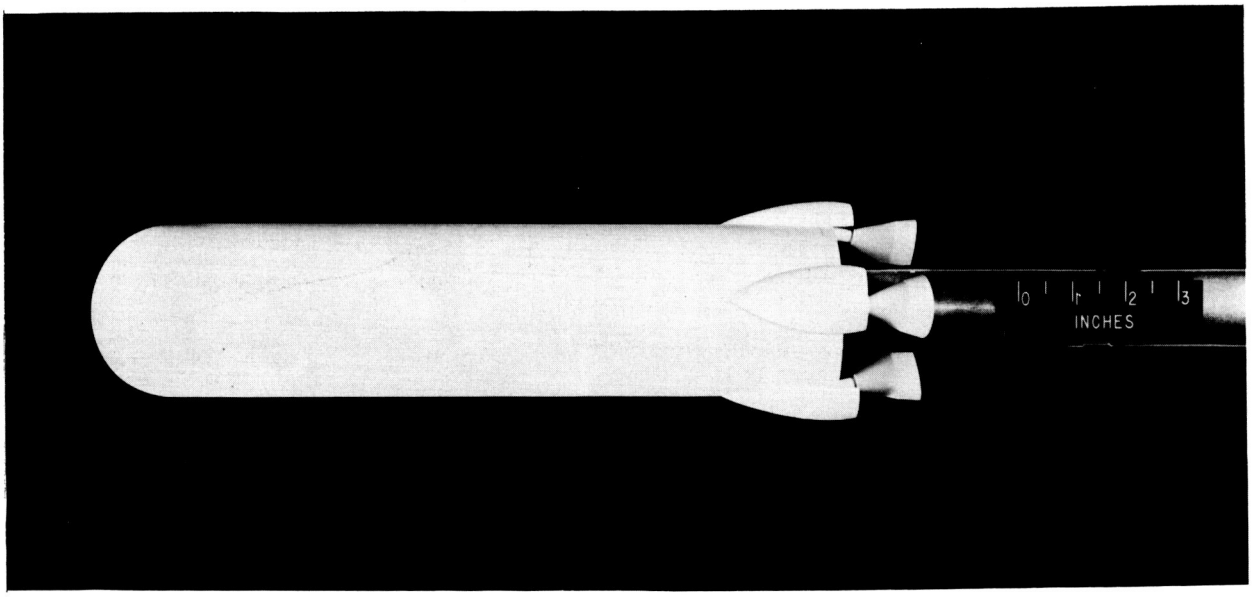

Parabolic shrouds and rocket engines. L-63-8572

(a) Basic booster (body alone); spherical nose.

Figure 3.- Representative configurations of basic booster and reusable booster.

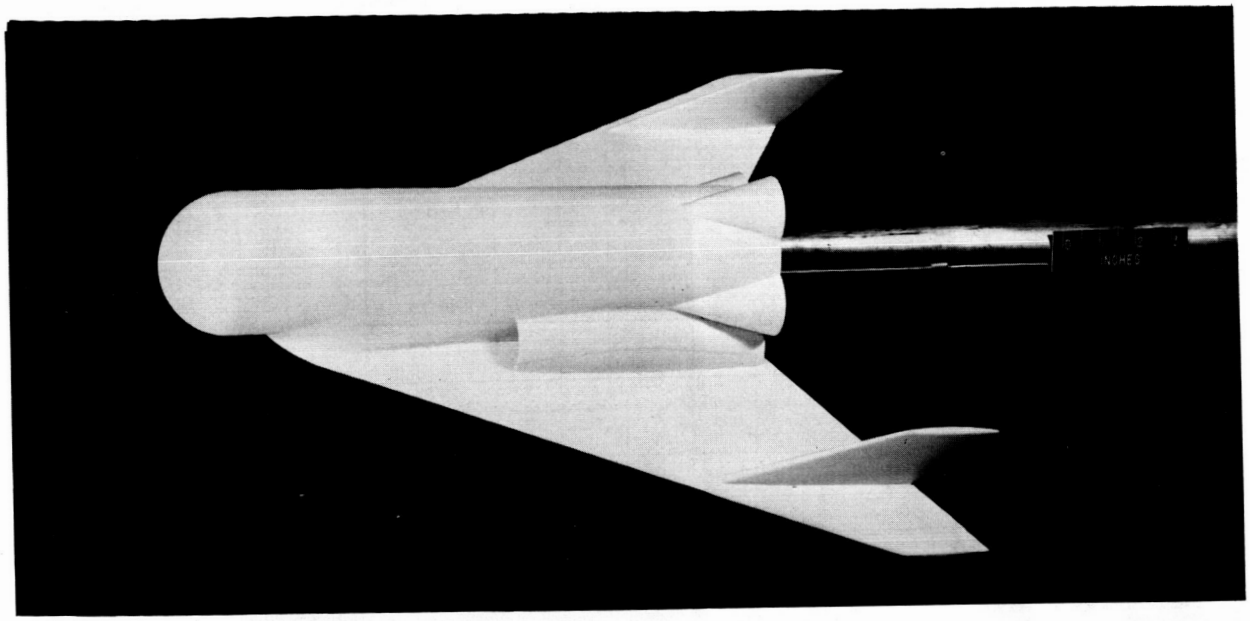

Original. L-63-8568

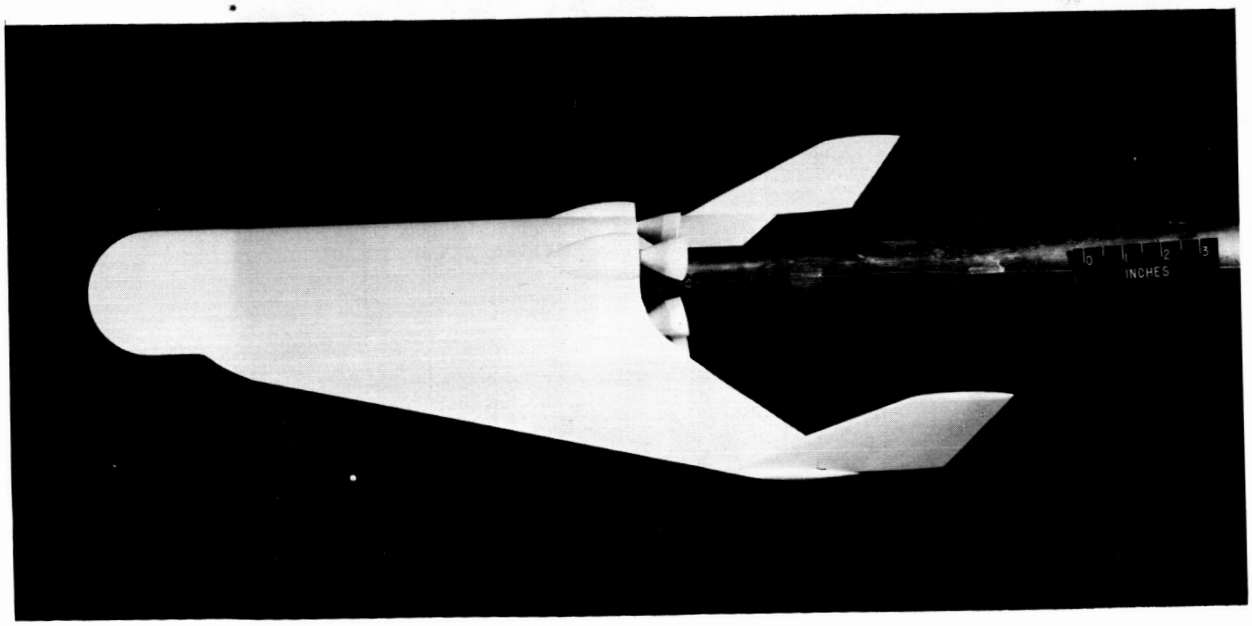

Modified. L-63-8569

(b) Reusable booster; 65° swept trapezoidal wing.

Figure 3.- Concluded.

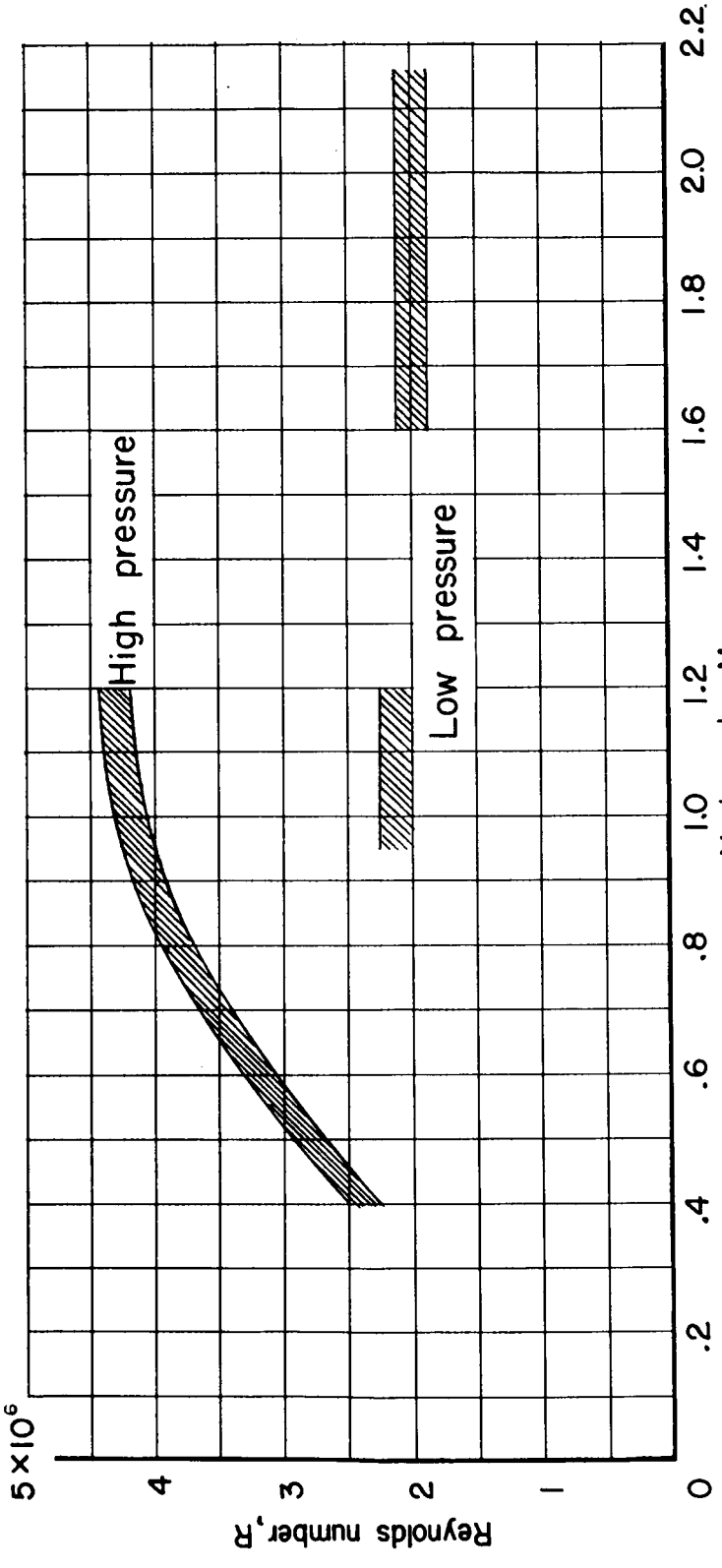

Figure 4.- Representative variations of Reynolds number with Mach number for Langley 8-foot transonic pressure tunnel (M = 0.1 to 1.2) and low-speed test section of the Langley Unitary Plan wind tunnel (M = 1.60 to 2.16).

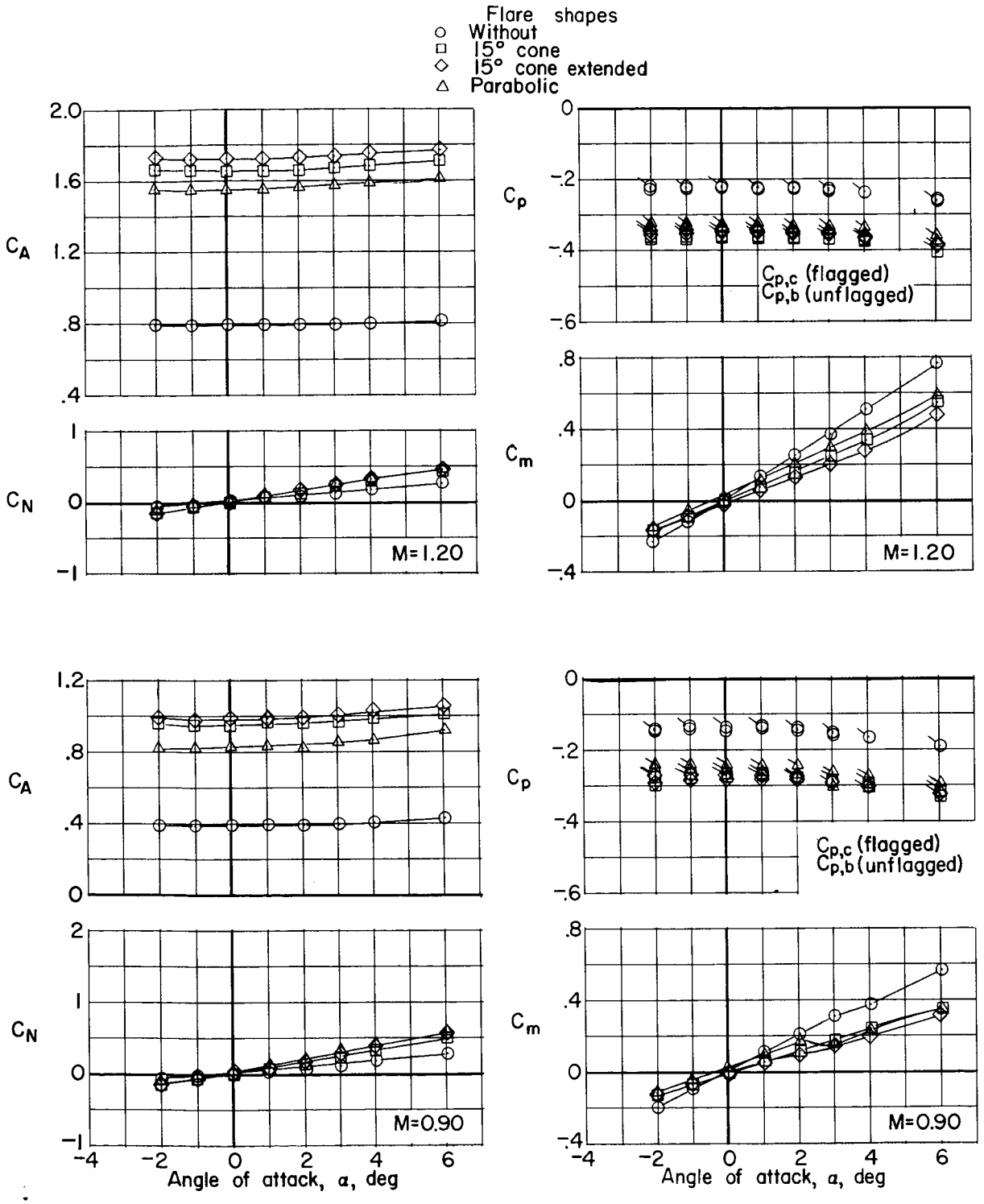

Figure 5.- Longitudinal aerodynamic characteristics of basic booster without and with several axisymmetric base flare shapes. Spherical nose; $\beta = 0^{\circ}$.

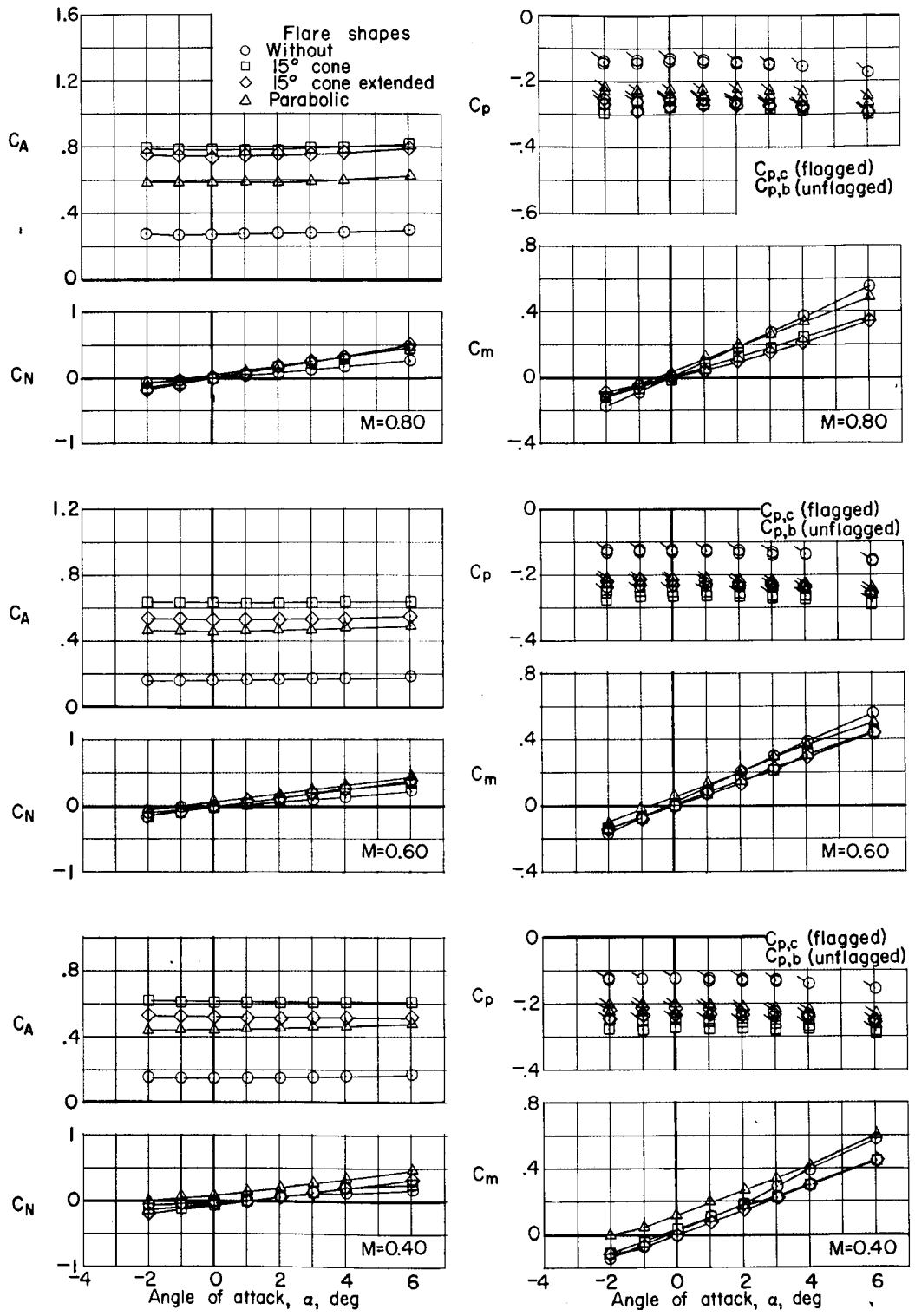

Figure 5.- Concluded.

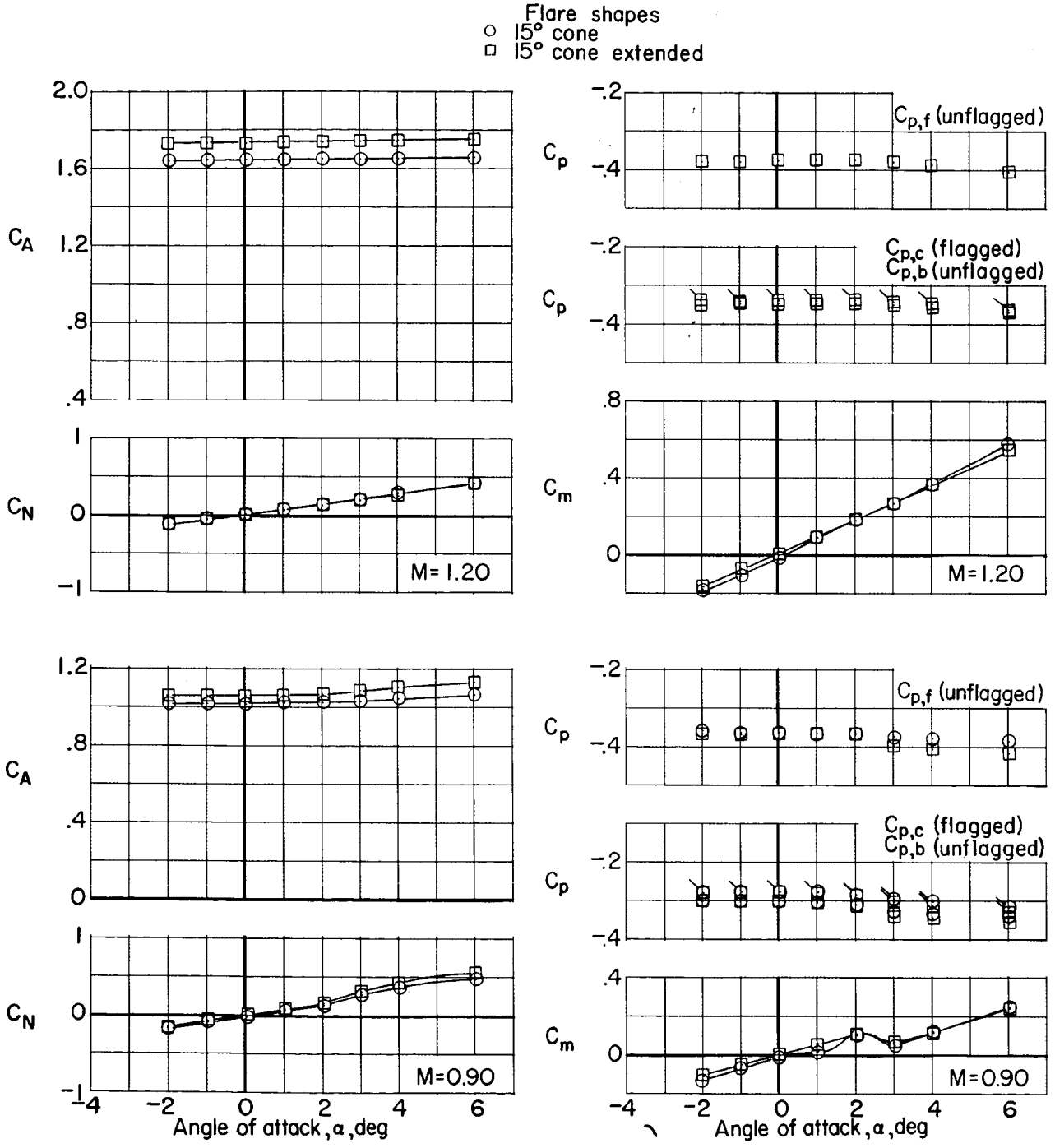

Figure 6.- Longitudinal aerodynamic characteristics of basic booster with vented base flare shapes. $\beta = 0^{\circ}$.

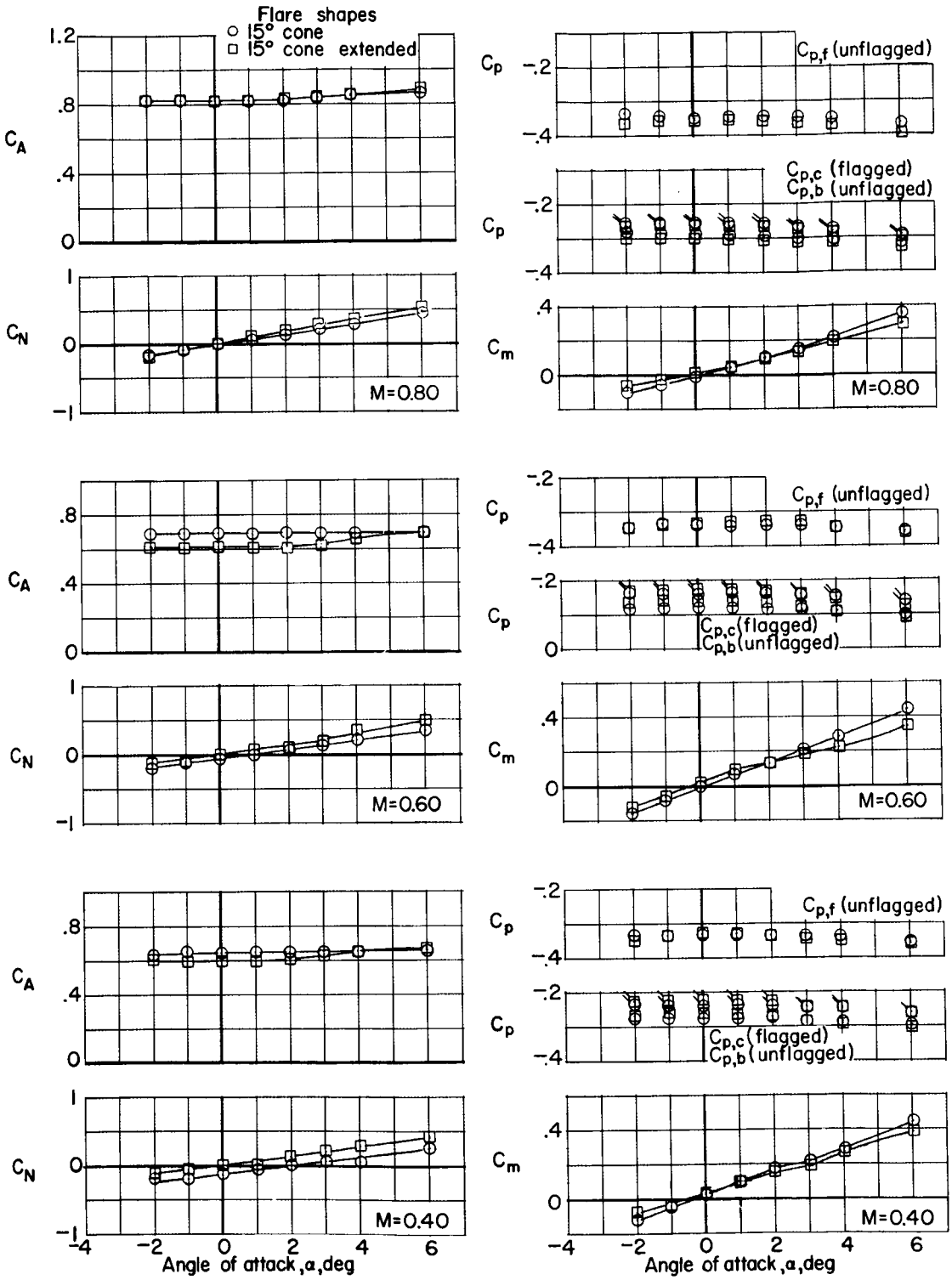

Figure 6.- Concluded.

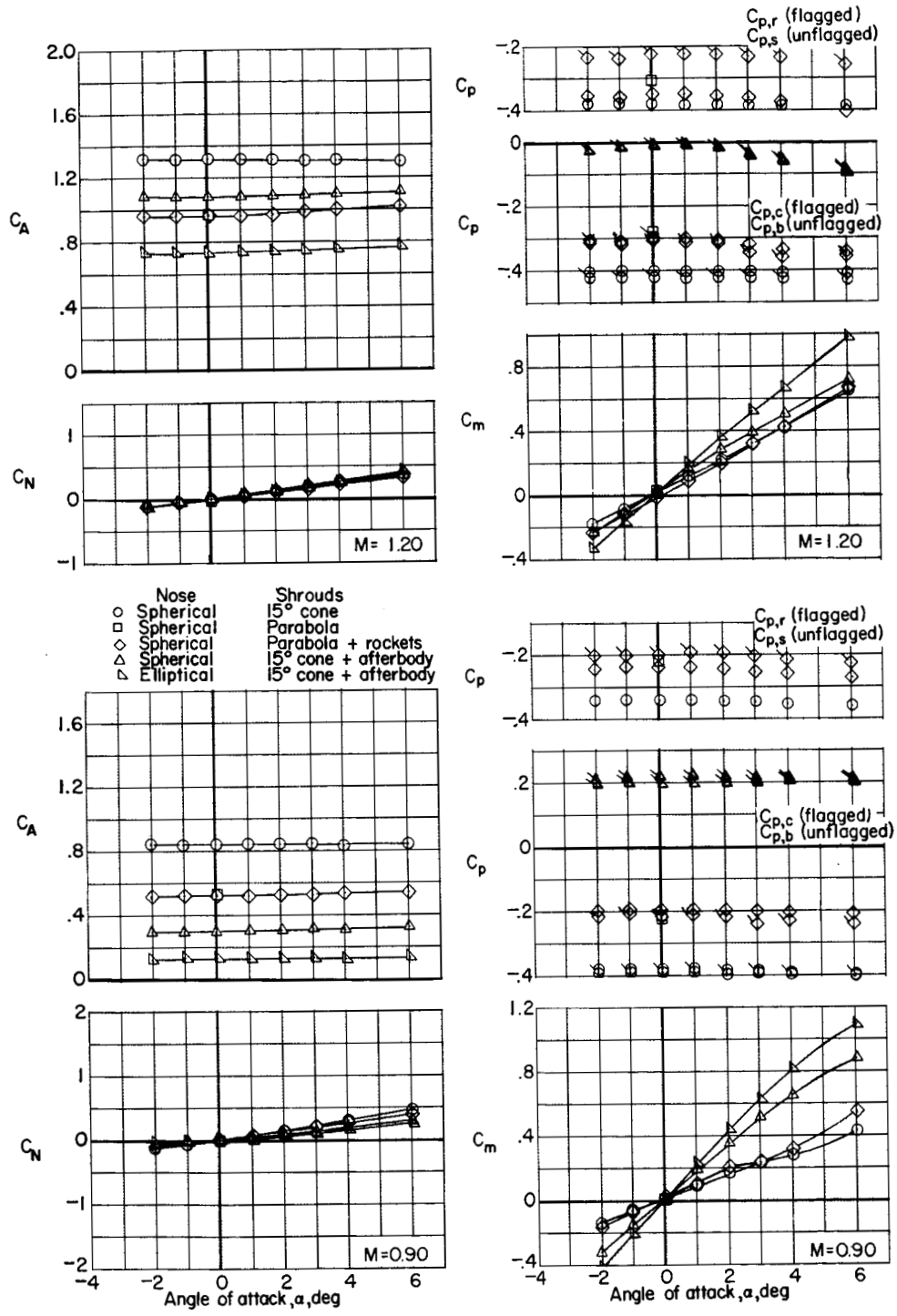

Figure 7.- Longitudinal aerodynamic characteristics of basic booster showing effects of conical and parabolic extended shrouds, rocket engines, afterbody, spherical nose, and a 4:1 elliptic nose. $\beta = 0^{o}$.

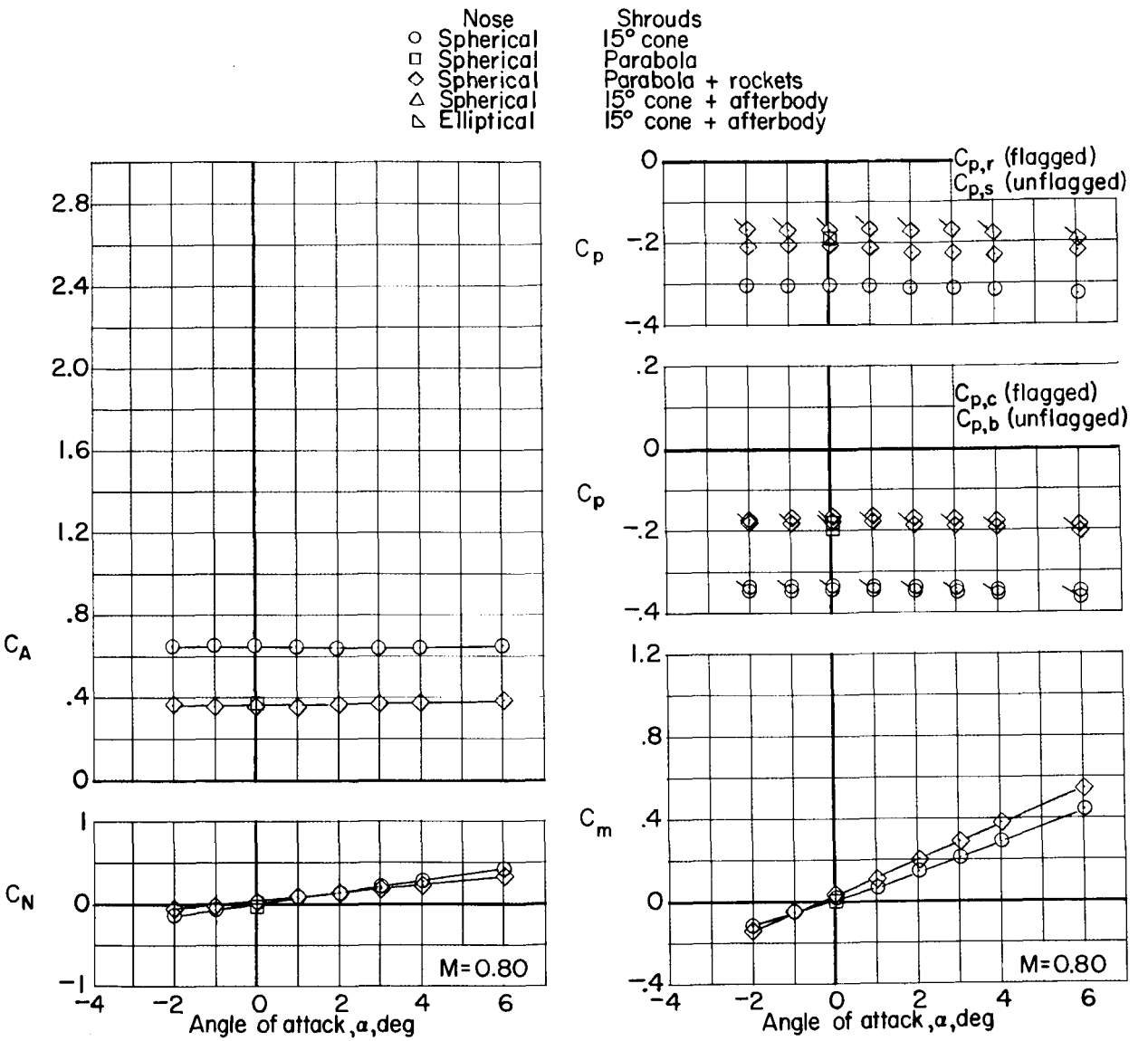

Figure 7.- Continued.

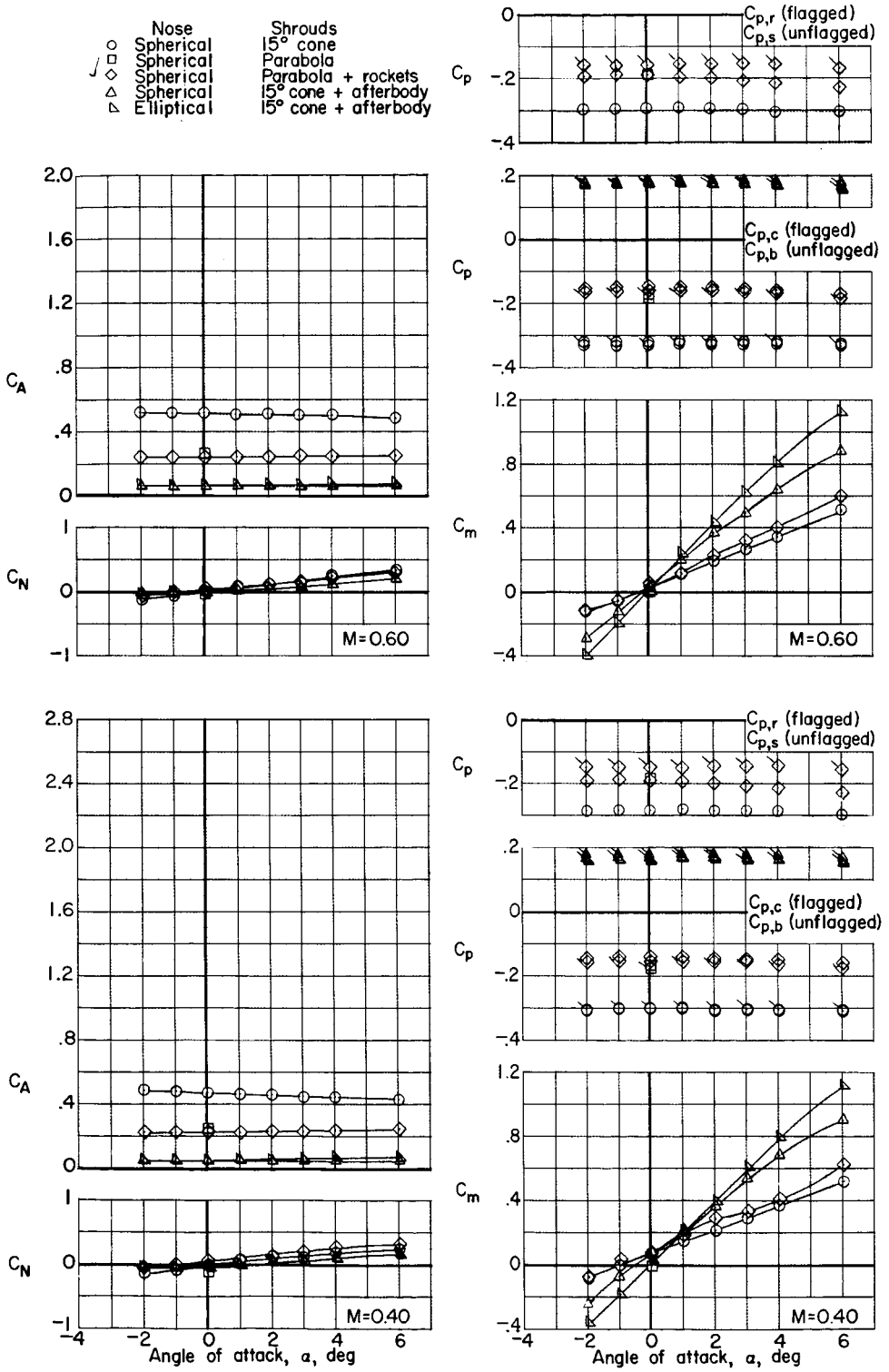

Figure 7.- Concluded.

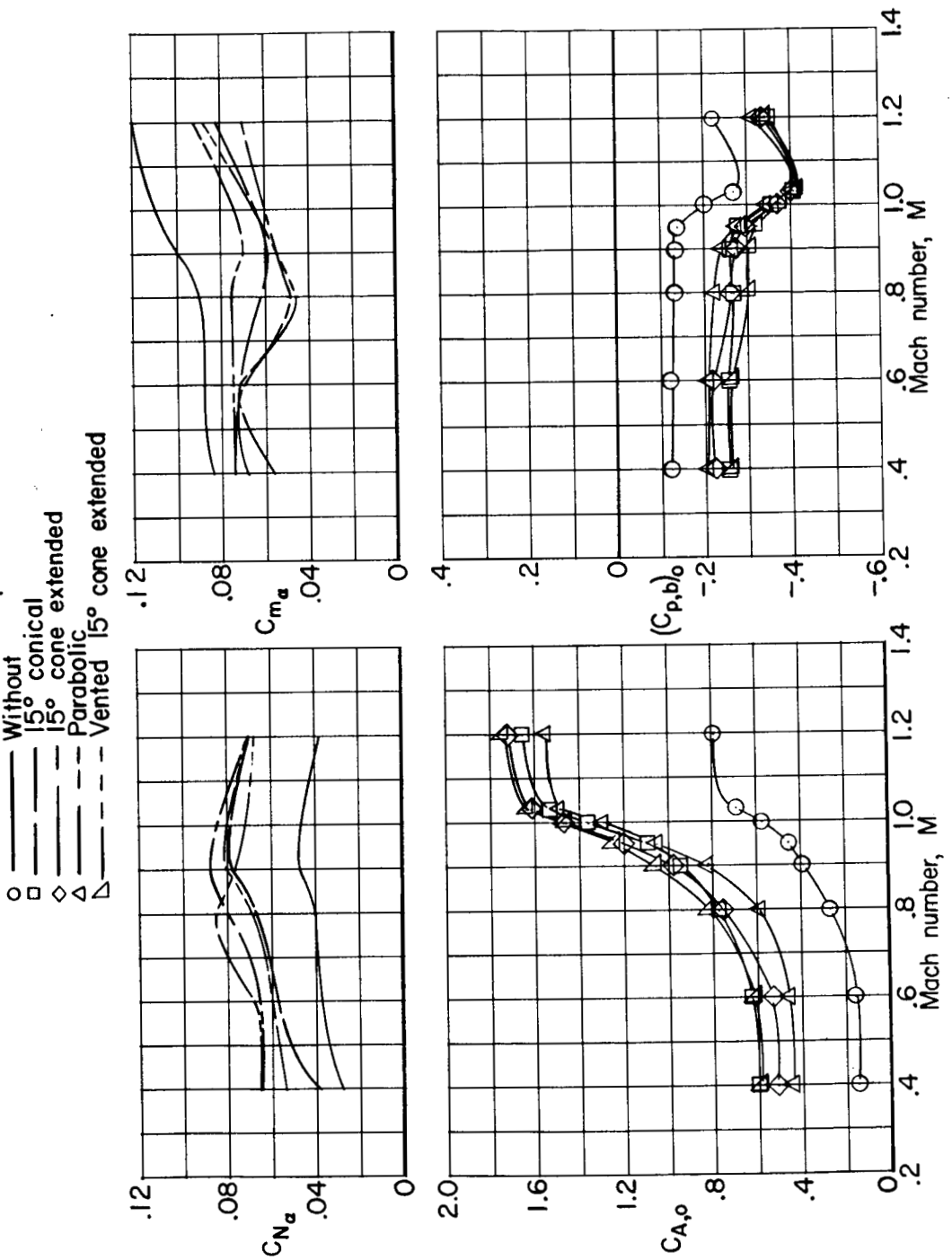

(a) Flare arrangements.

Figure 8.- Variation with Mach number of longitudinal aerodynamic and drag parameters for basic booster with flares, shrouds, rocket engines, and afterbody.

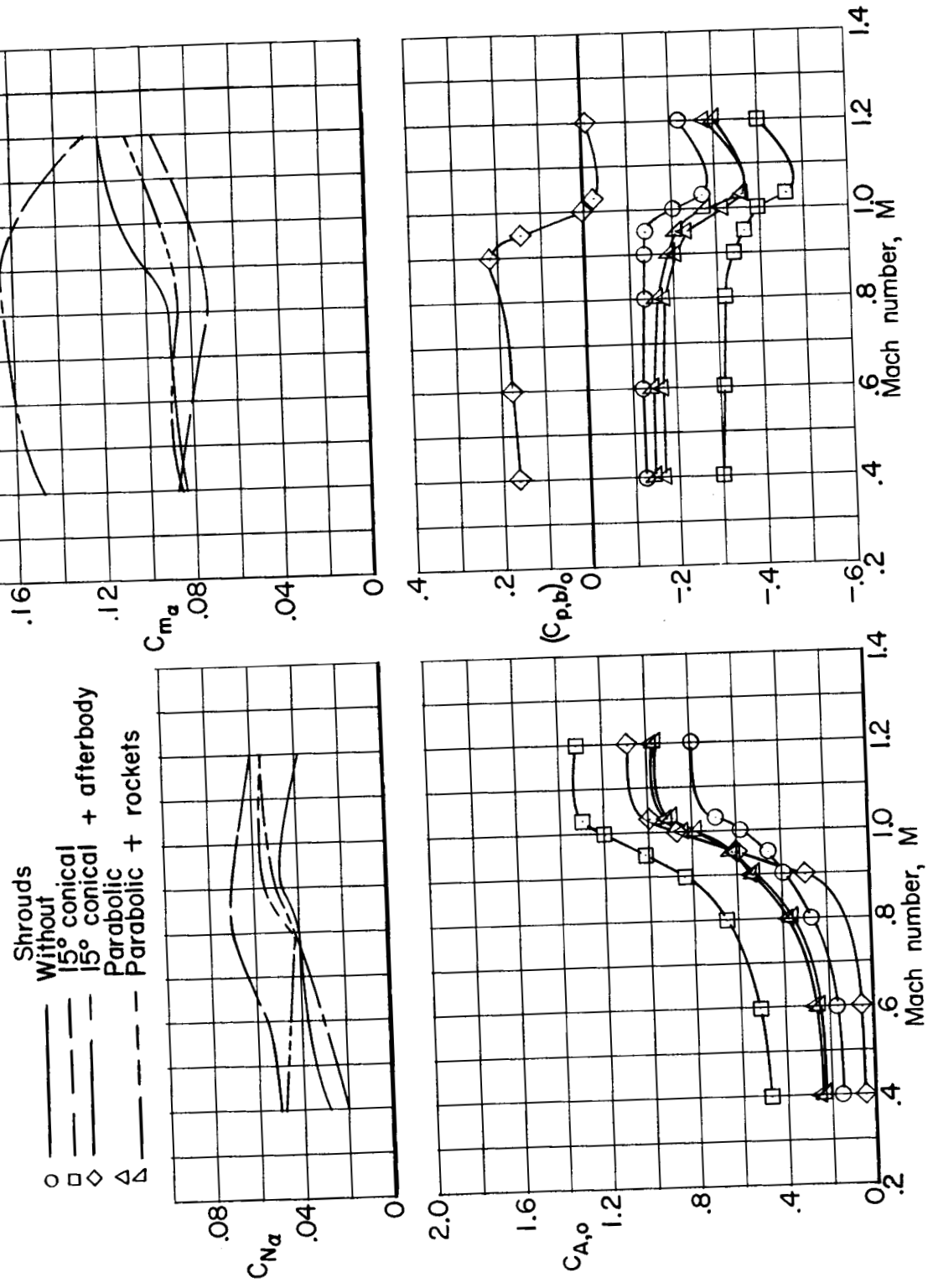

(b) Shroud arrangements.

Figure 8.- Concluded.

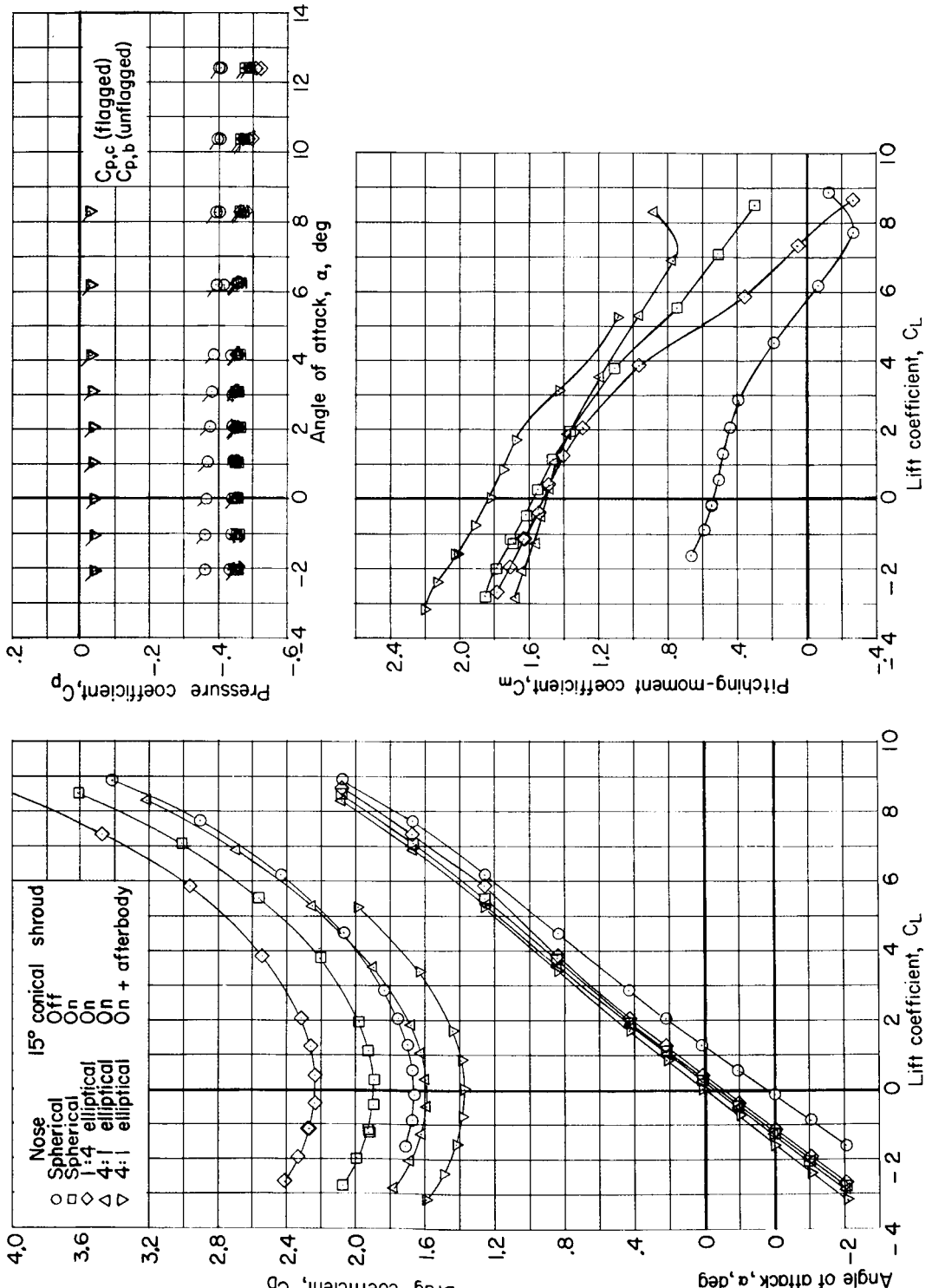

(a) M = 1.20.

Figure 9.- Longitudinal aerodynamic characteristics of reusable booster with 55° clipped delta wing for several nose, shroud, and afterbody arrangements. $\beta = 0°$.

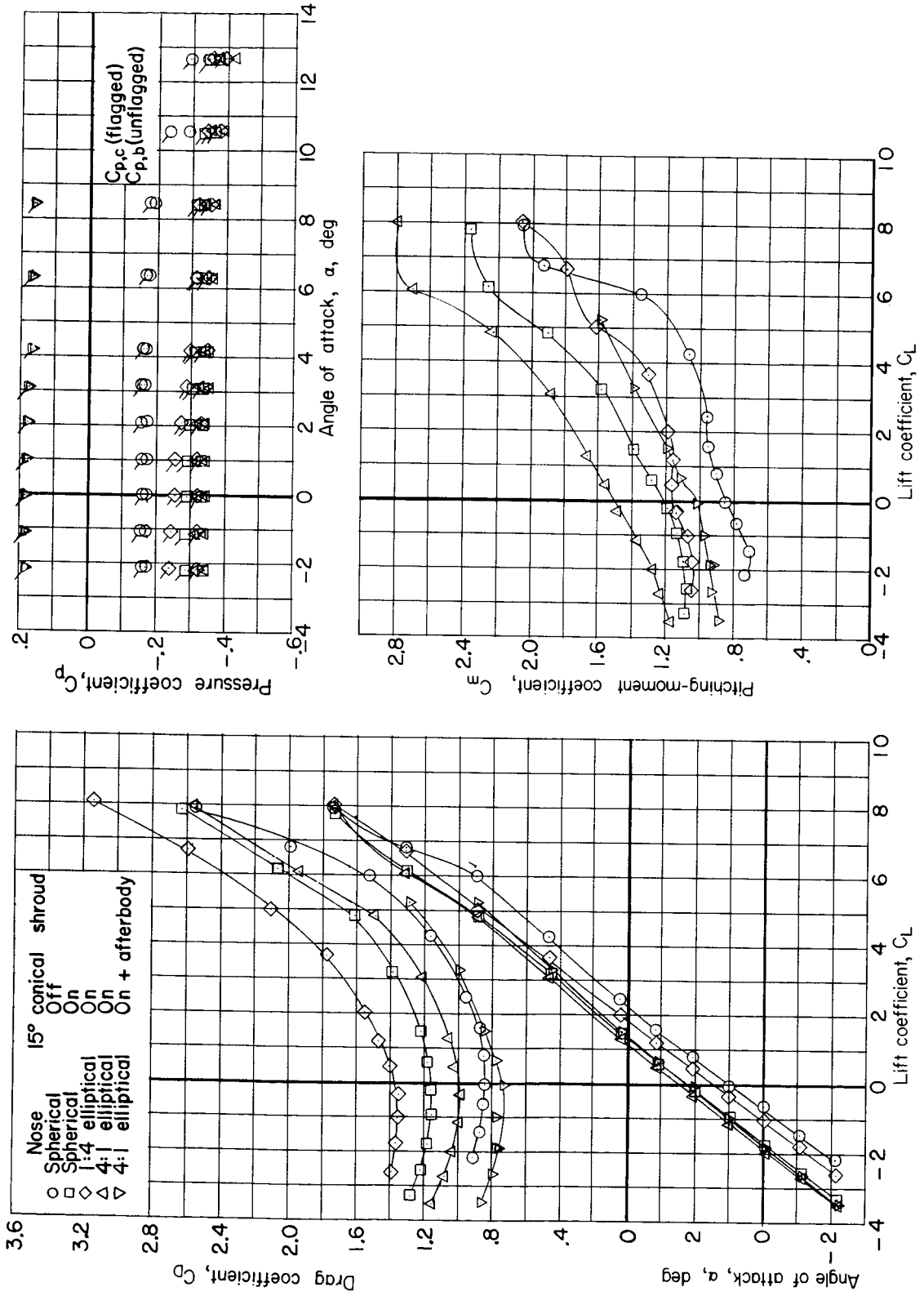

(b) M = 0.90.

Figure 9.- Continued.

(c) M = 0.60.

Figure 9.- Continued.

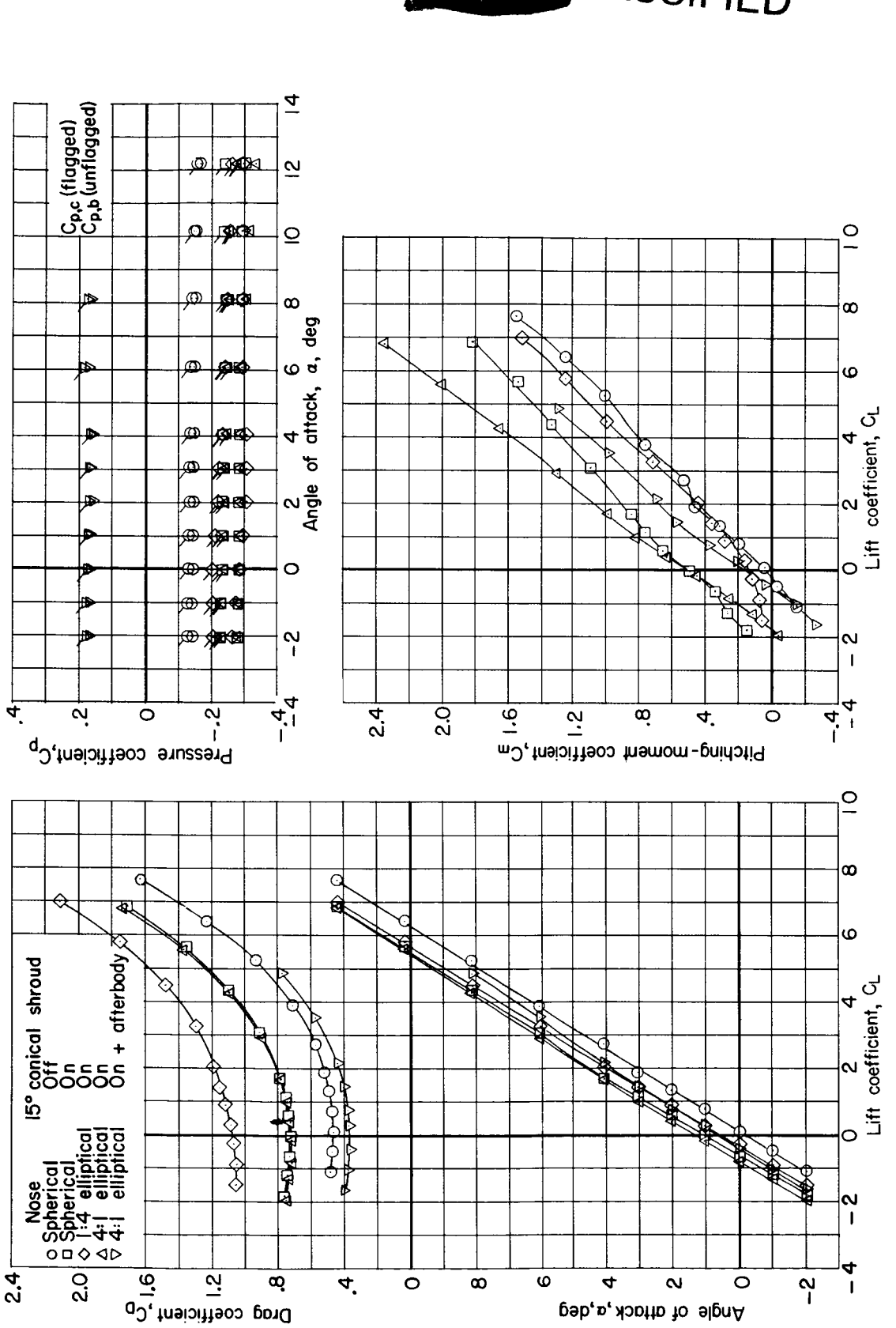

(d) M = 0.40.

Figure 9.- Concluded.

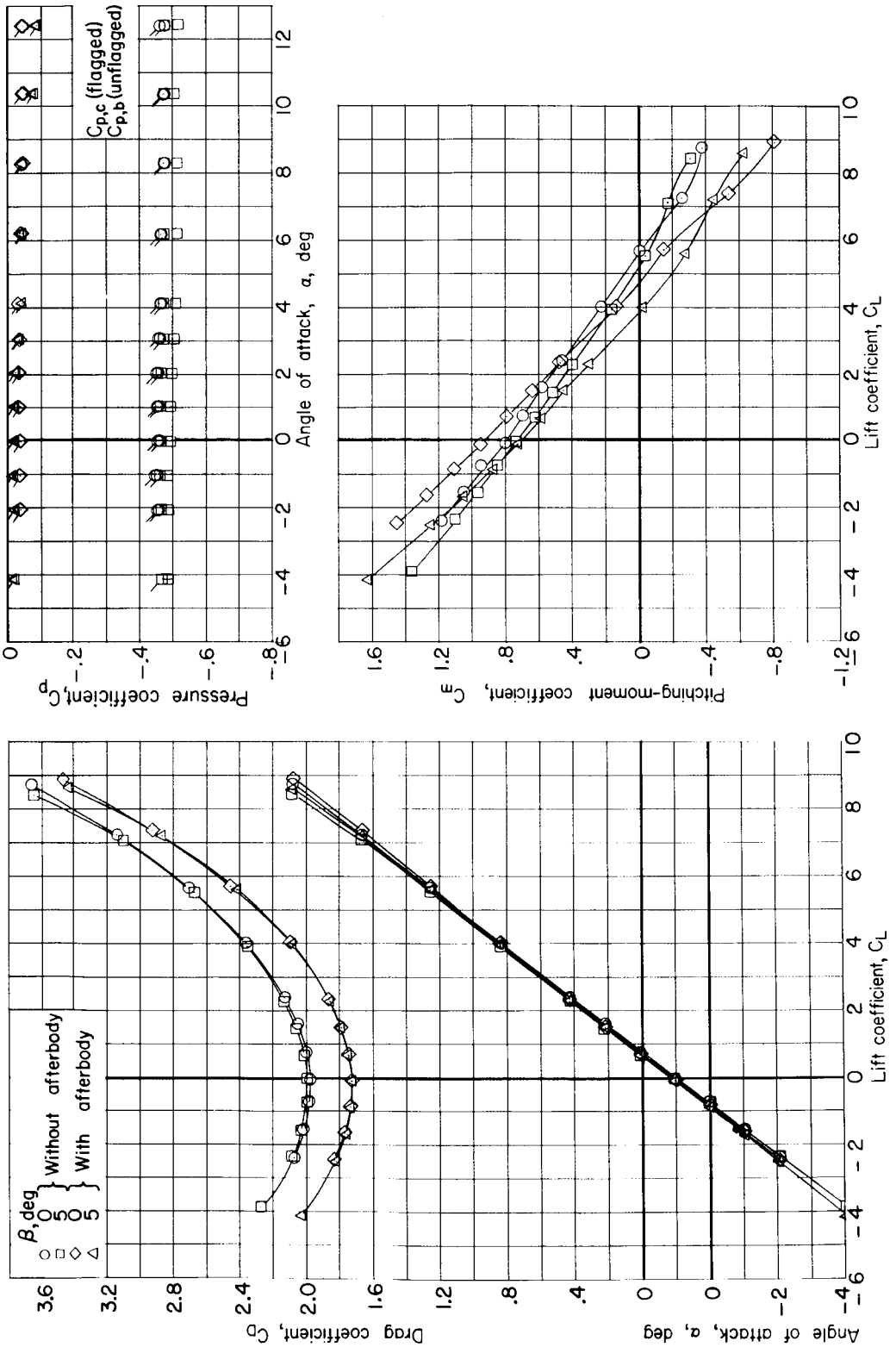

(a) M = 1.20.

Figure 10.- Longitudinal aerodynamic characteristics of reusable booster with 55° clipped delta wing, spherical nose, shrouds, and flyback engine nacelles both without and with afterbody fairing. β = 0° and 5°.

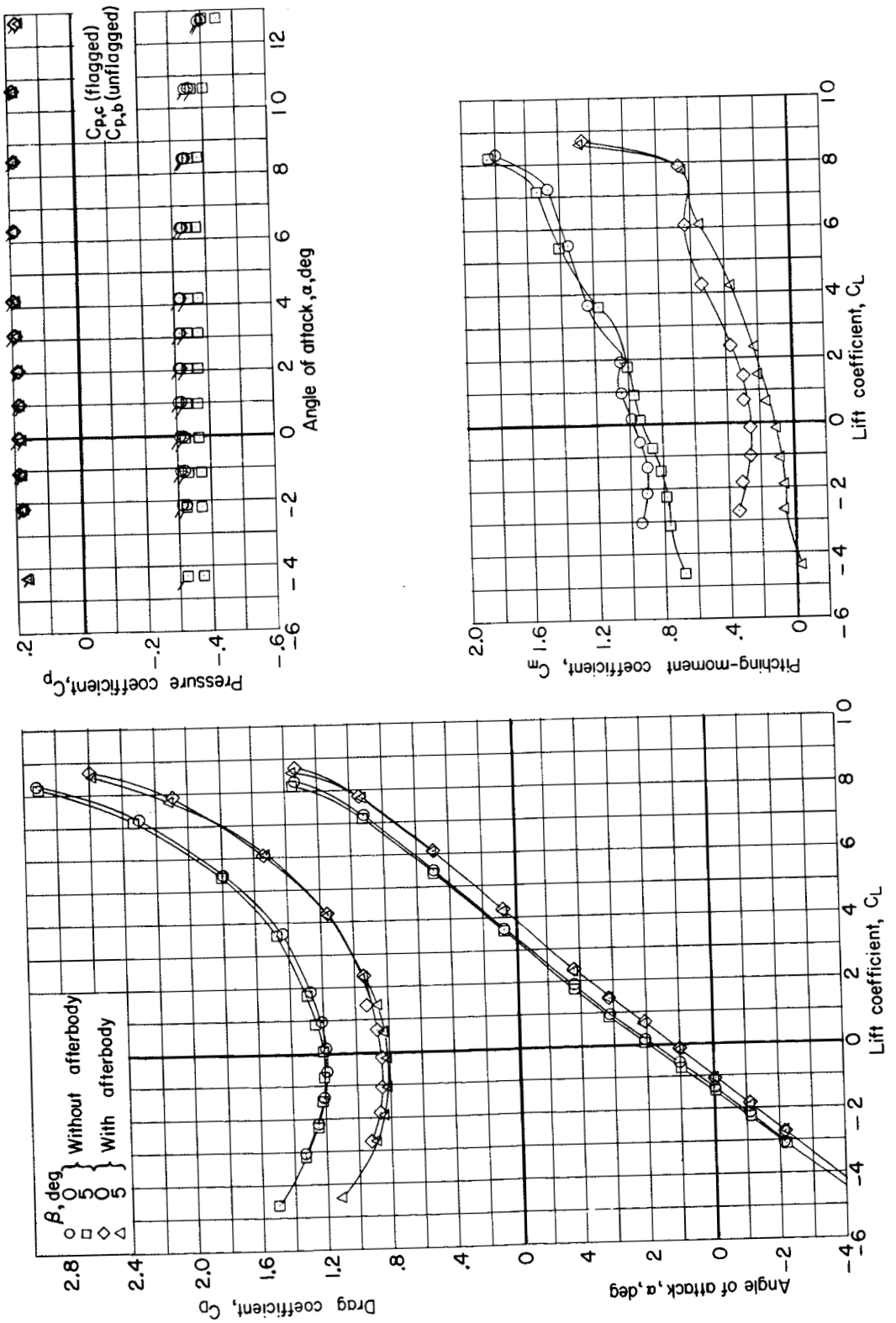

(b) M = 0.90.

Figure 10.- Continued.

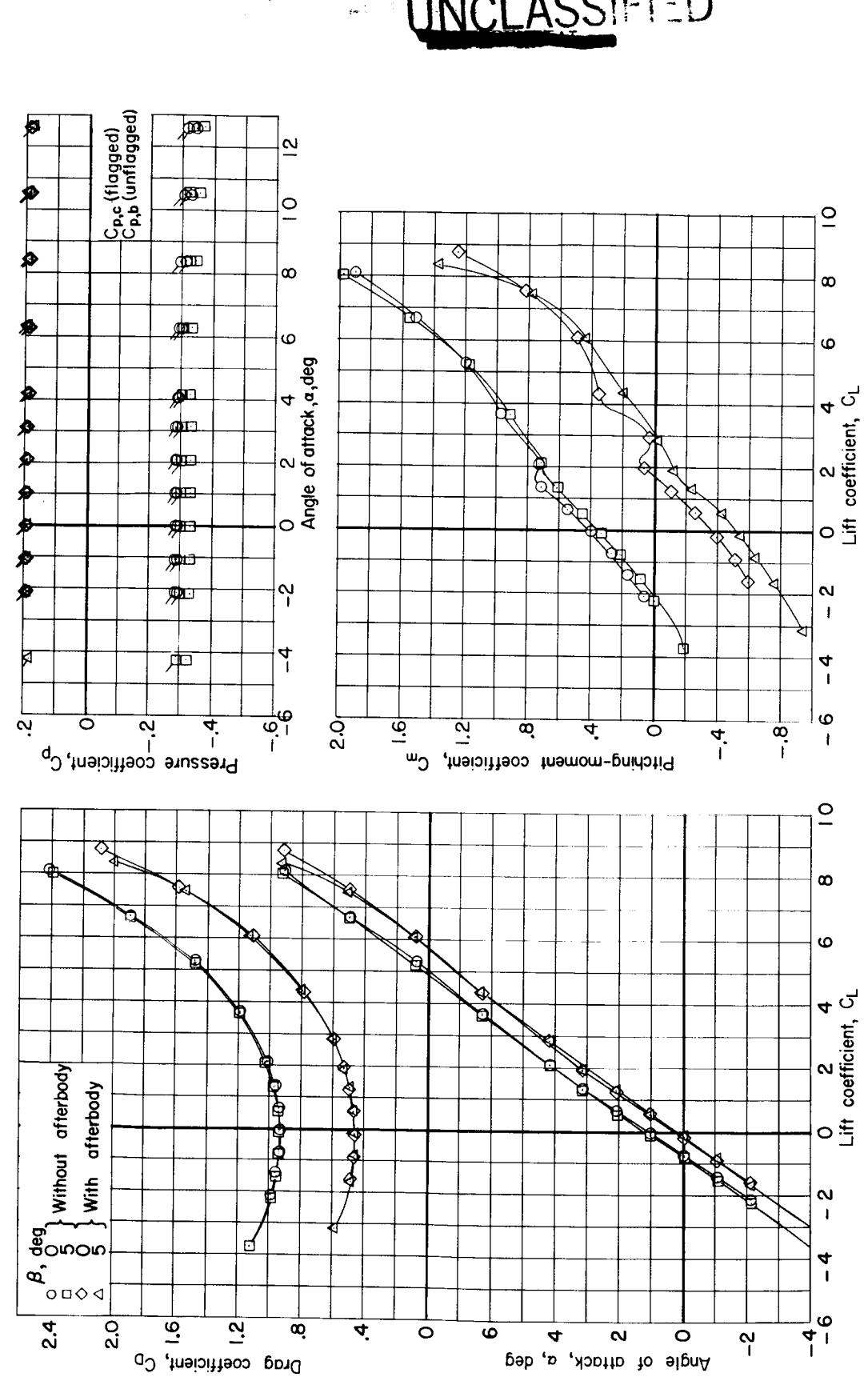

(c) M = 0.80.

Figure 10.- Continued.

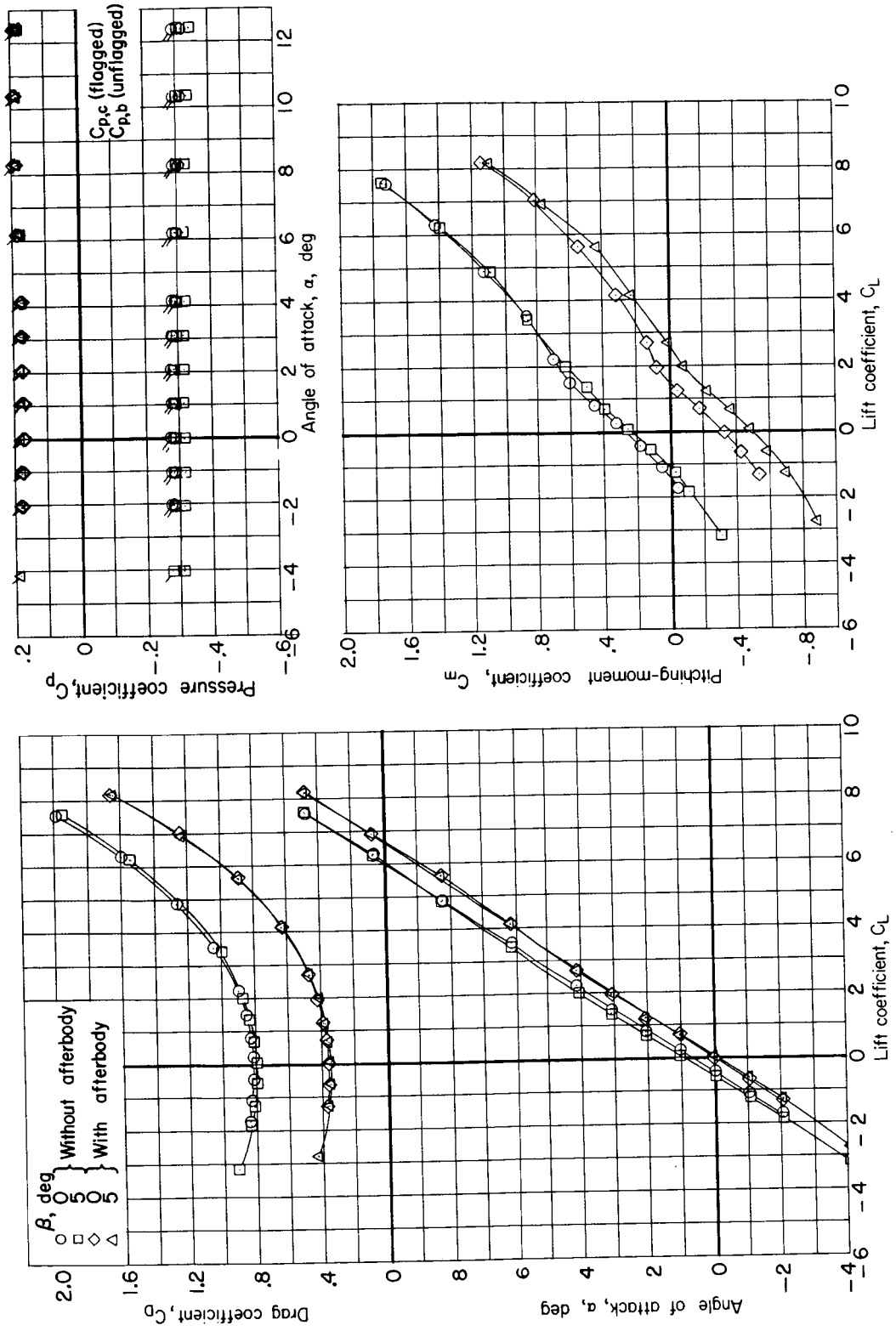

(d) M = 0.60.

Figure 10.- Continued.

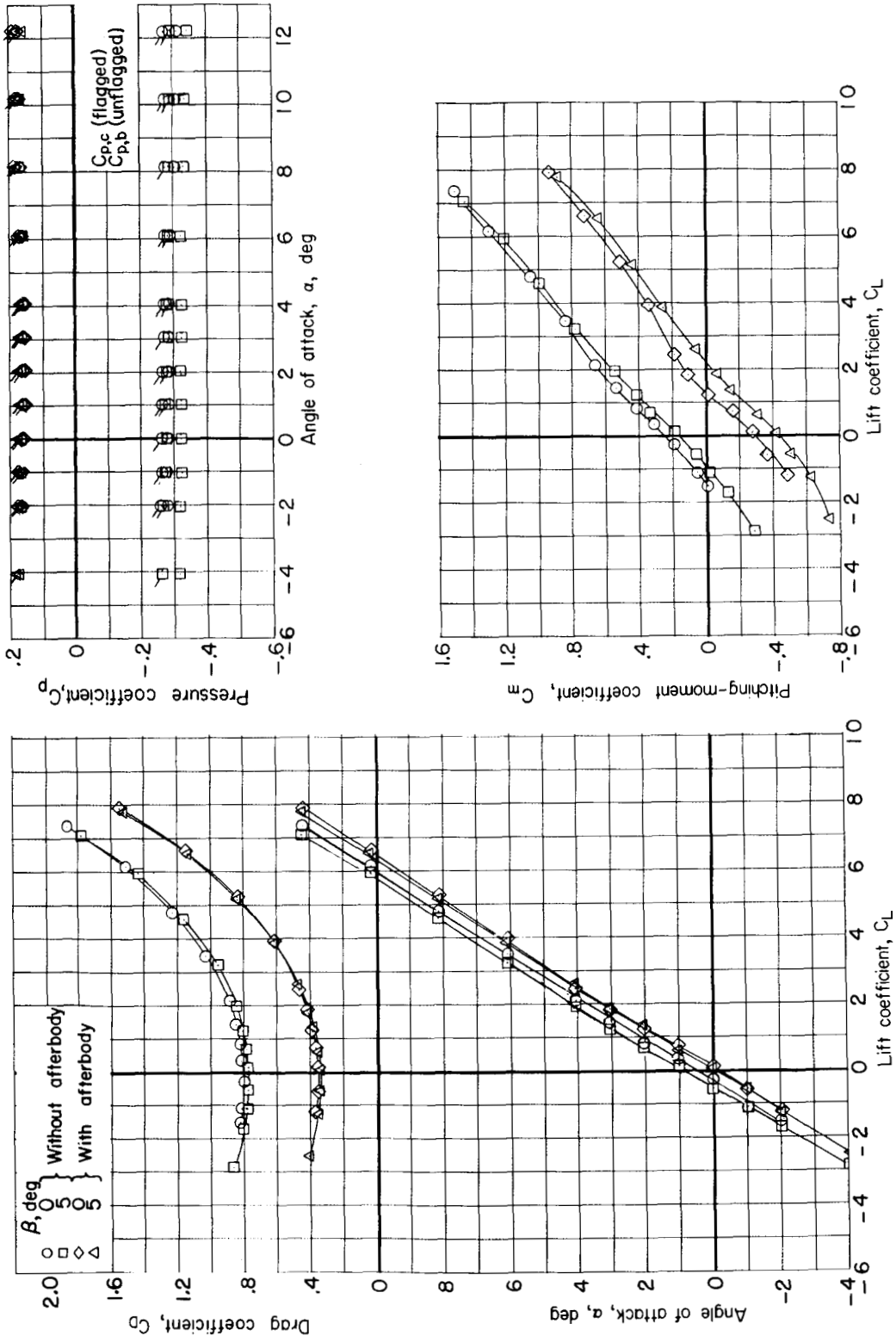

(e) M = 0.40.

Figure 10.- Concluded.

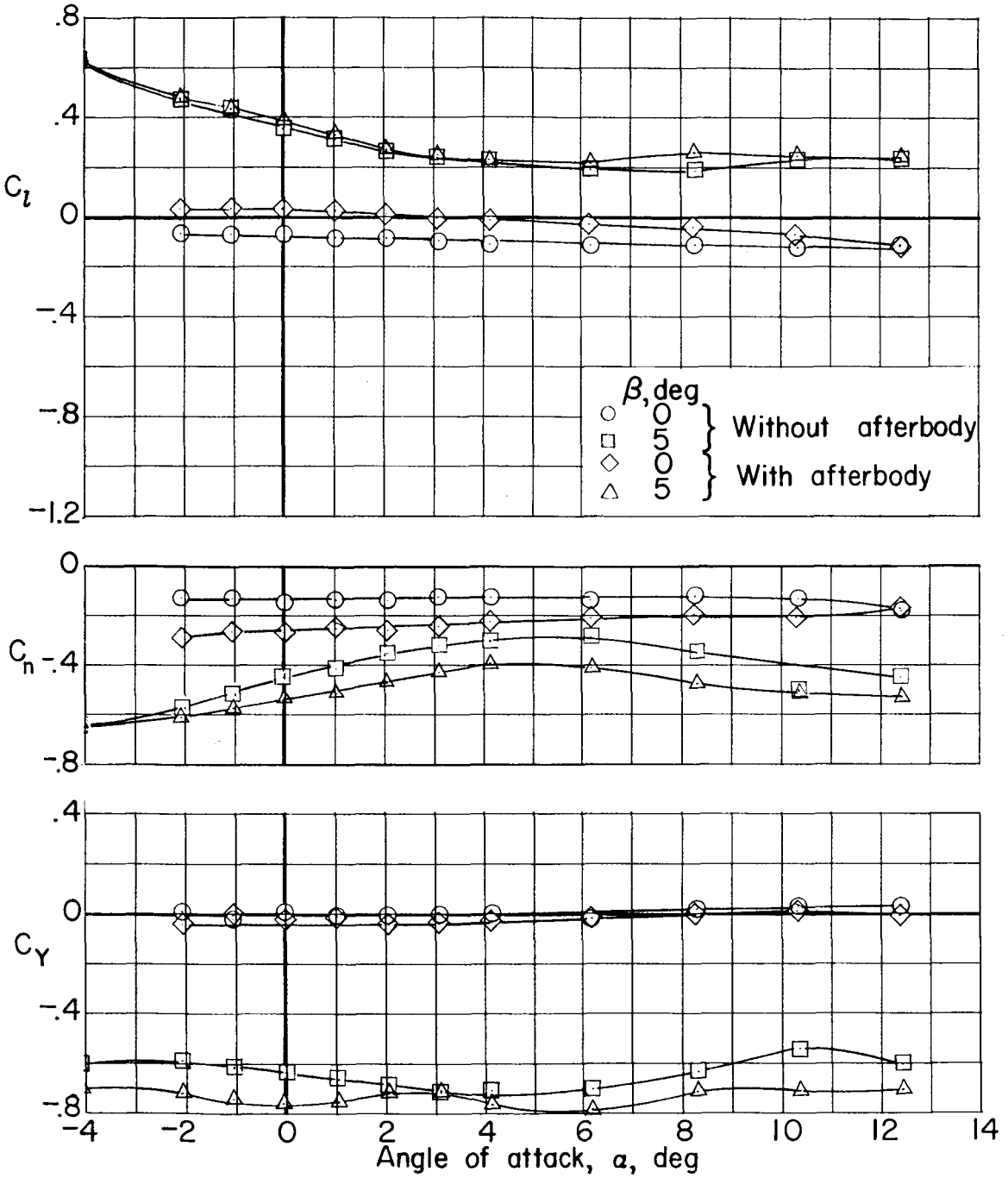

(a) M = 1.20.

Figure 11.- Lateral aerodynamic characteristics of reusable booster with 55° clipped delta wing, spherical nose, shrouds, and flyback engine nacelles both with and without afterbody fairing. β = 0° and 5°.

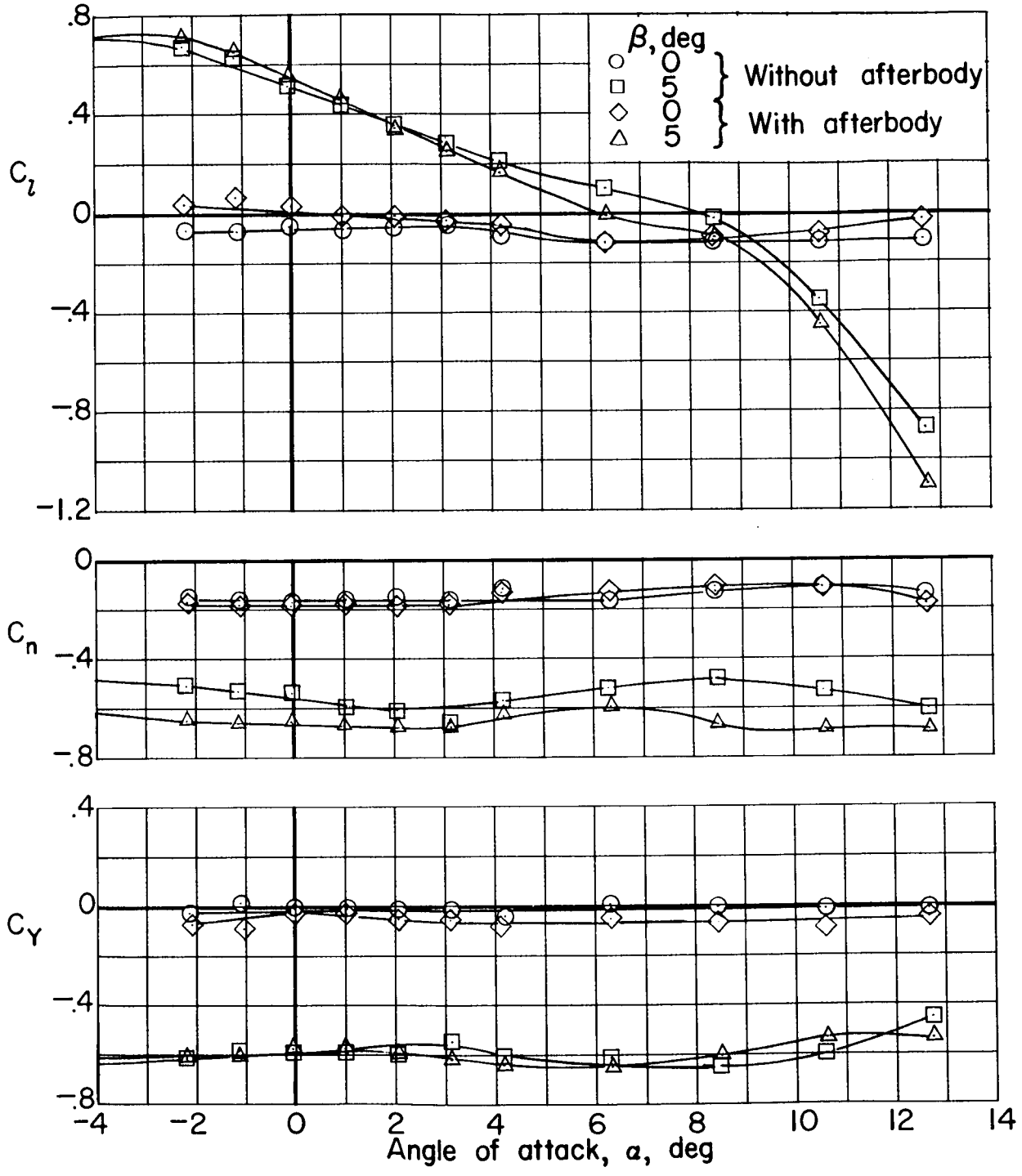

(b) M = 0.90.

Figure 11.- Continued.

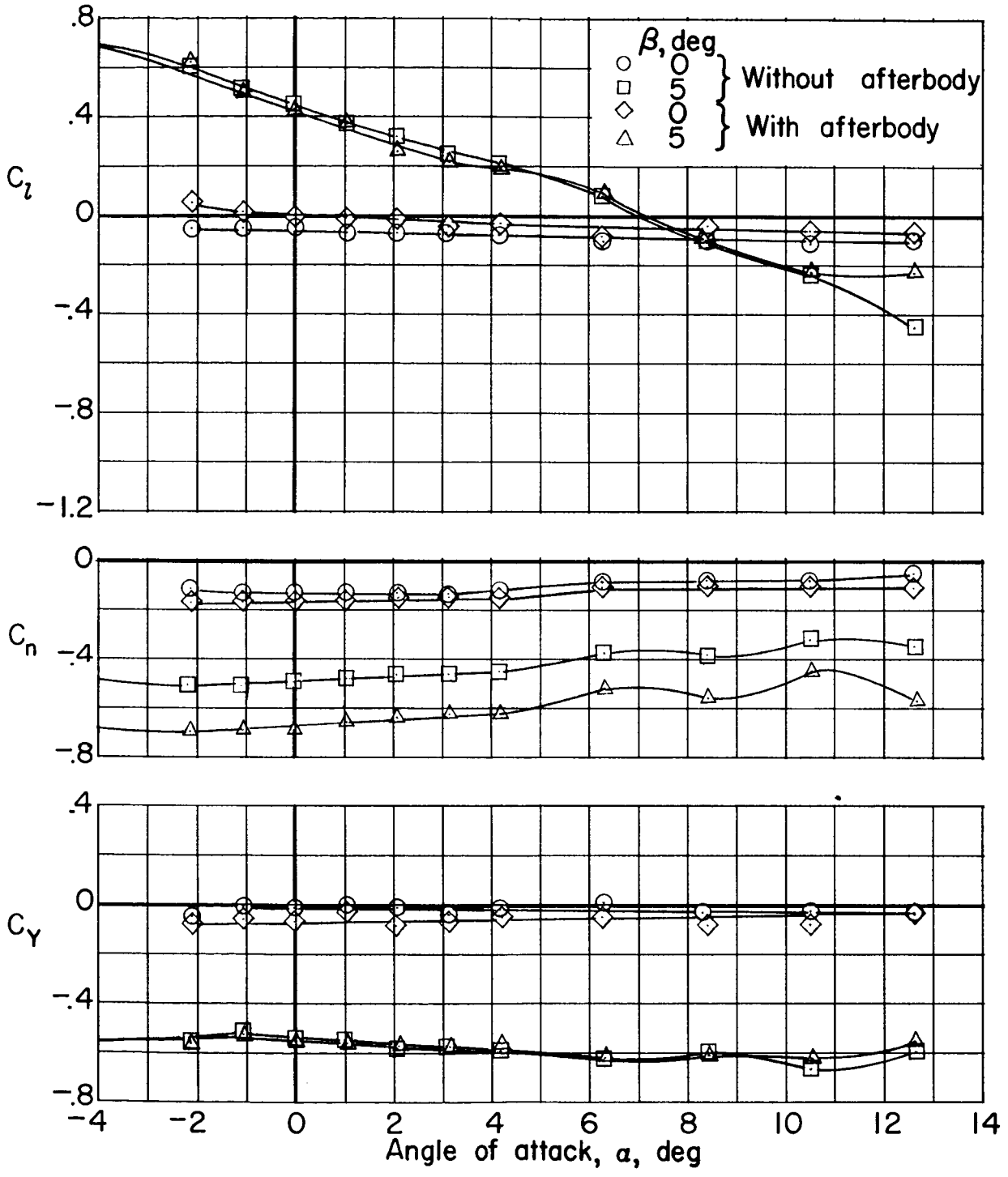

(c) M = 0.80.

Figure 11.- Continued.

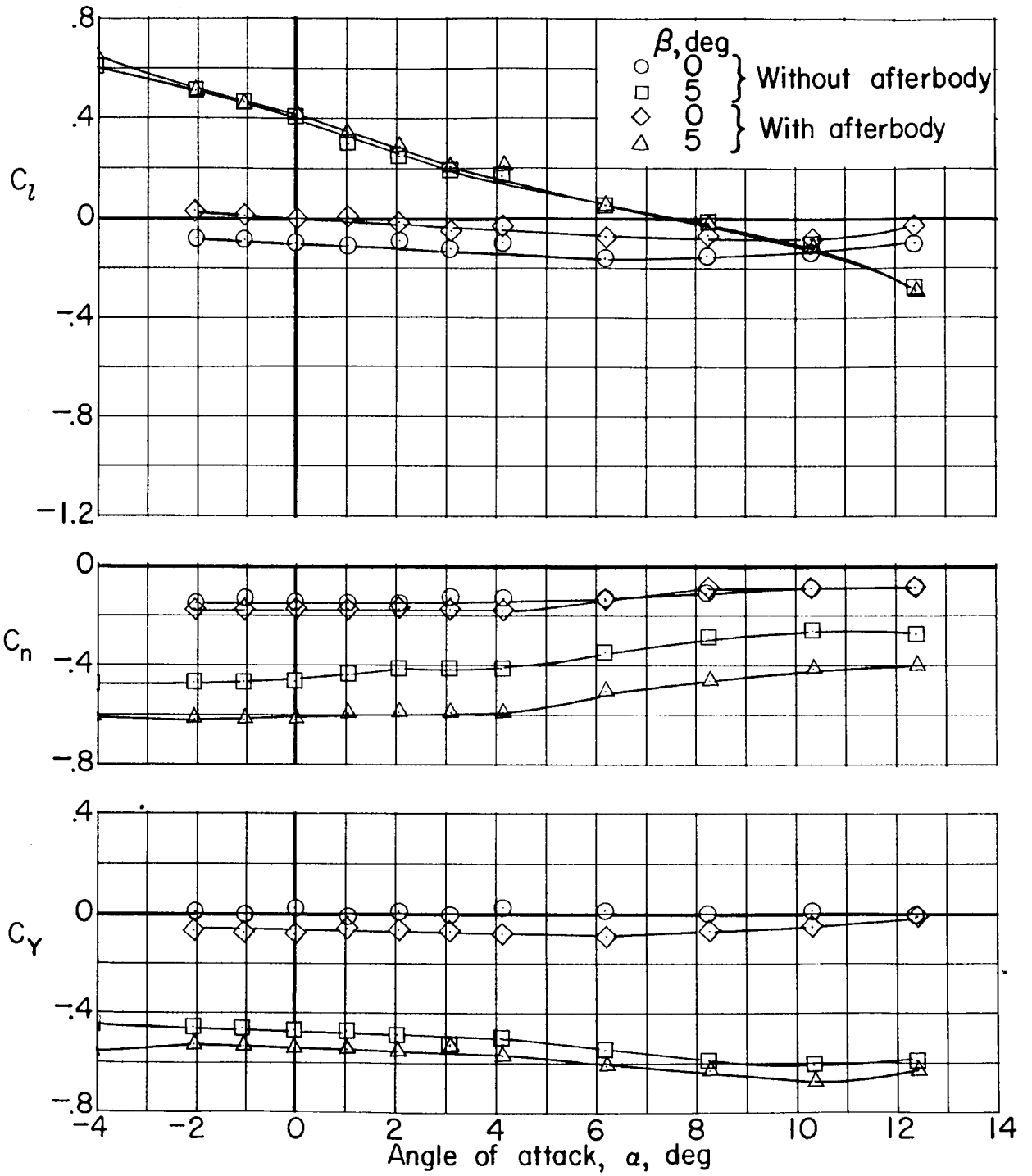

(d) M = 0.60.

Figure 11.- Continued.

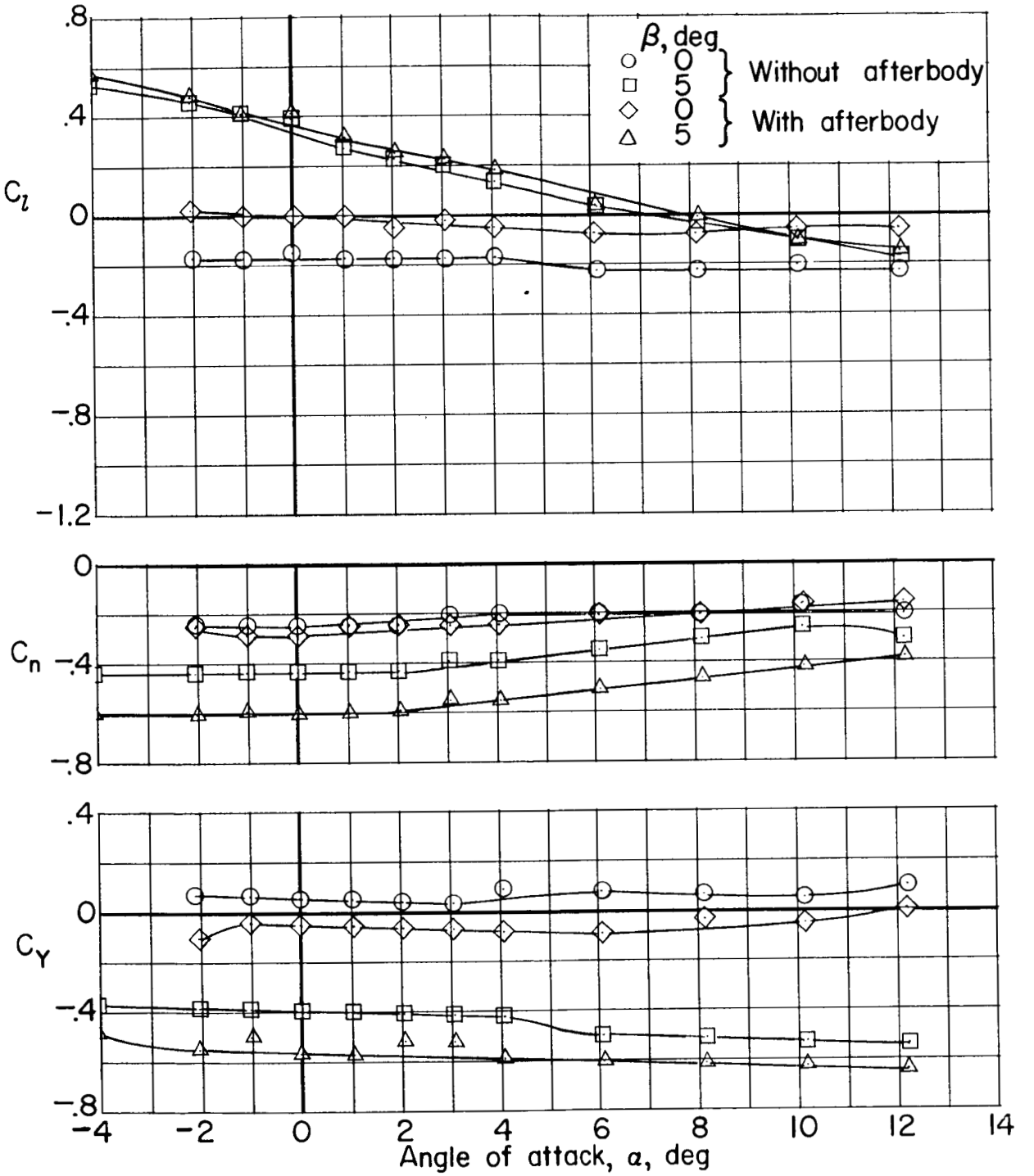

(e) M = 0.40.

Figure 11.- Concluded.

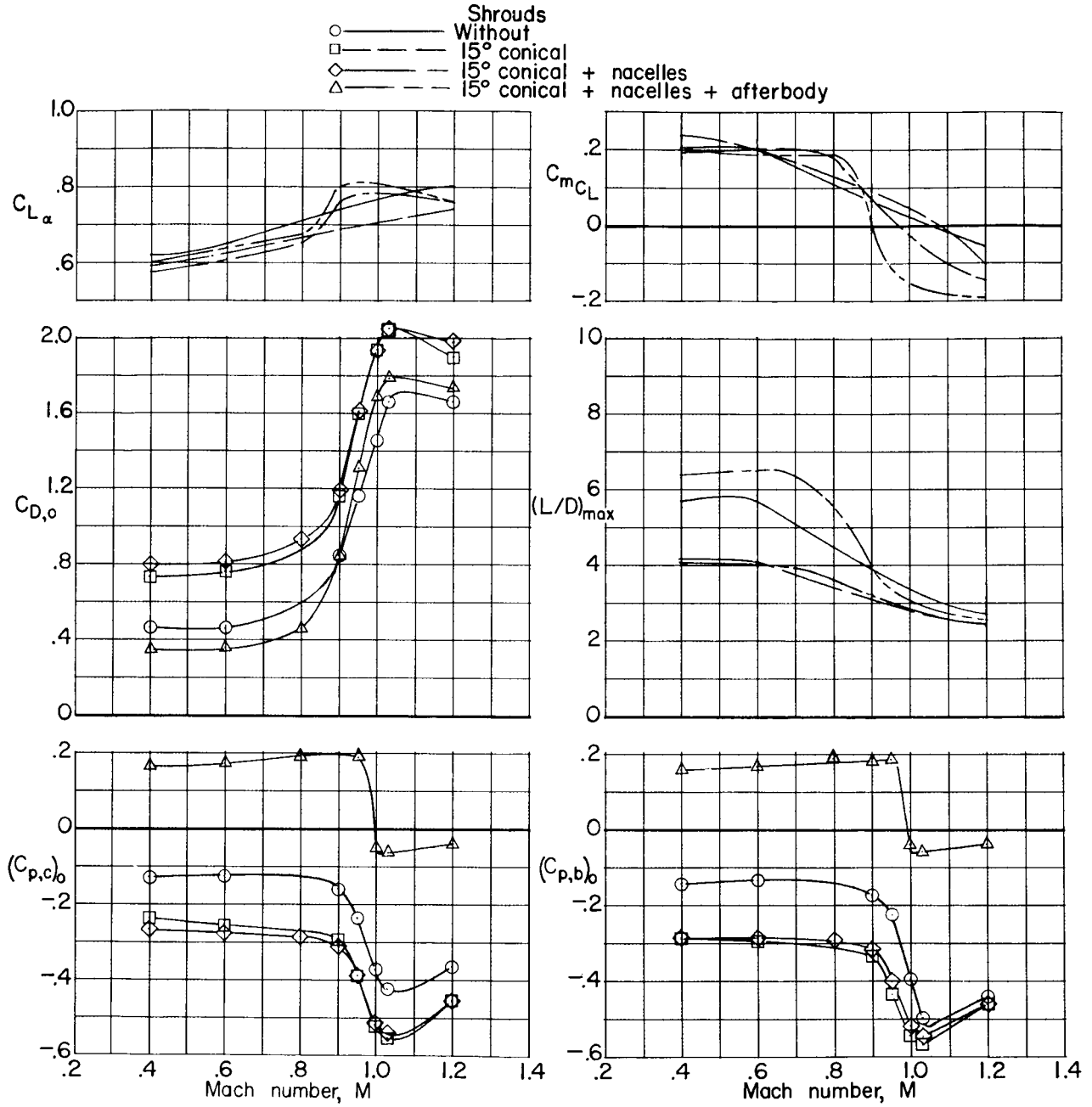

Figure 12.- Variation with Mach number of longitudinal stability and drag parameters for reusable booster with 55° clipped delta wing and spherical nose including effects of shrouds, nacelles, and afterbody.

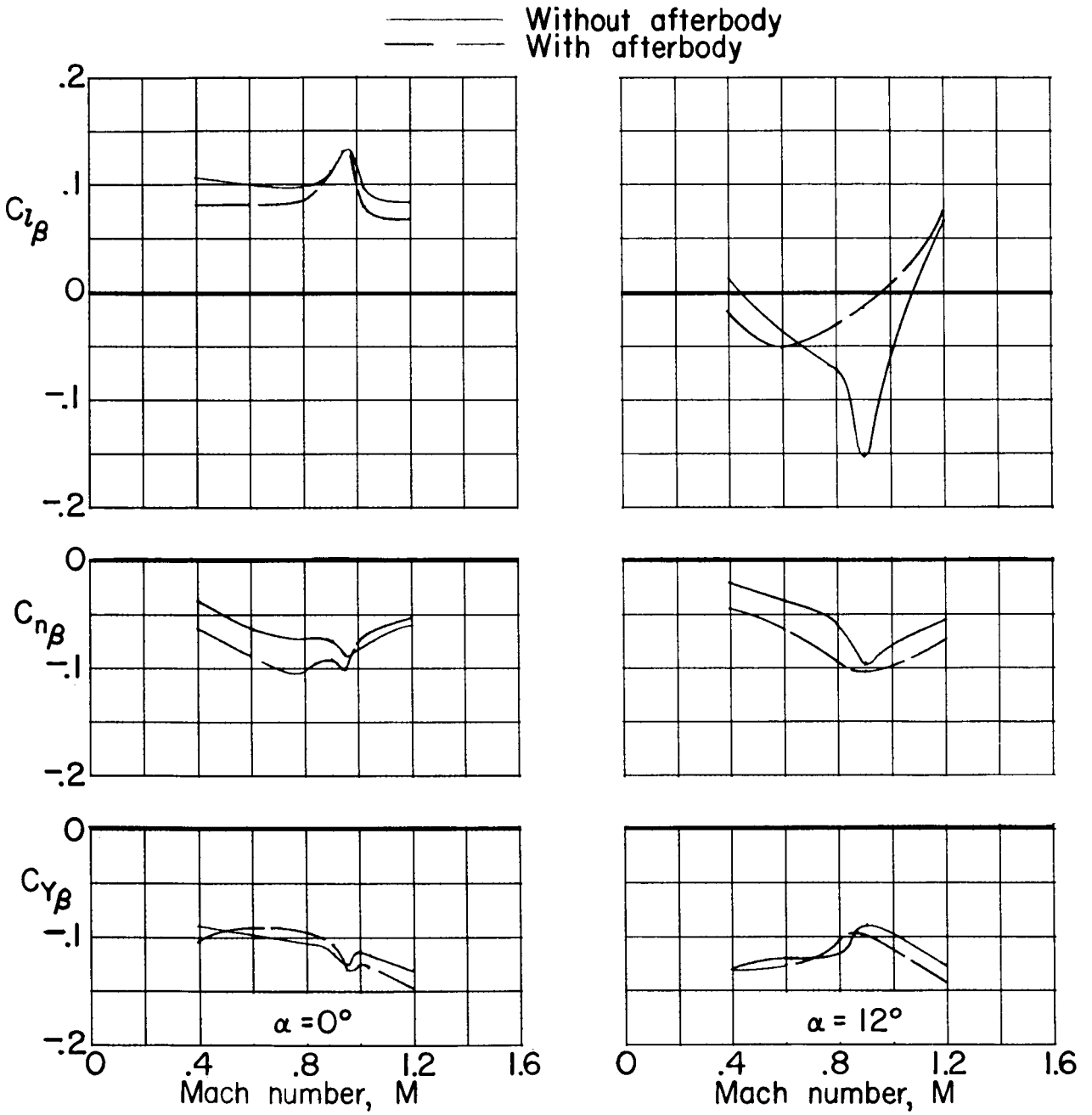

Figure 13.- Variation with Mach number of lateral-directional aerodynamic parameters for reusable booster with 55° clipped delta wing, spherical nose, 15° conical shrouds, and flyback engine nacelles.

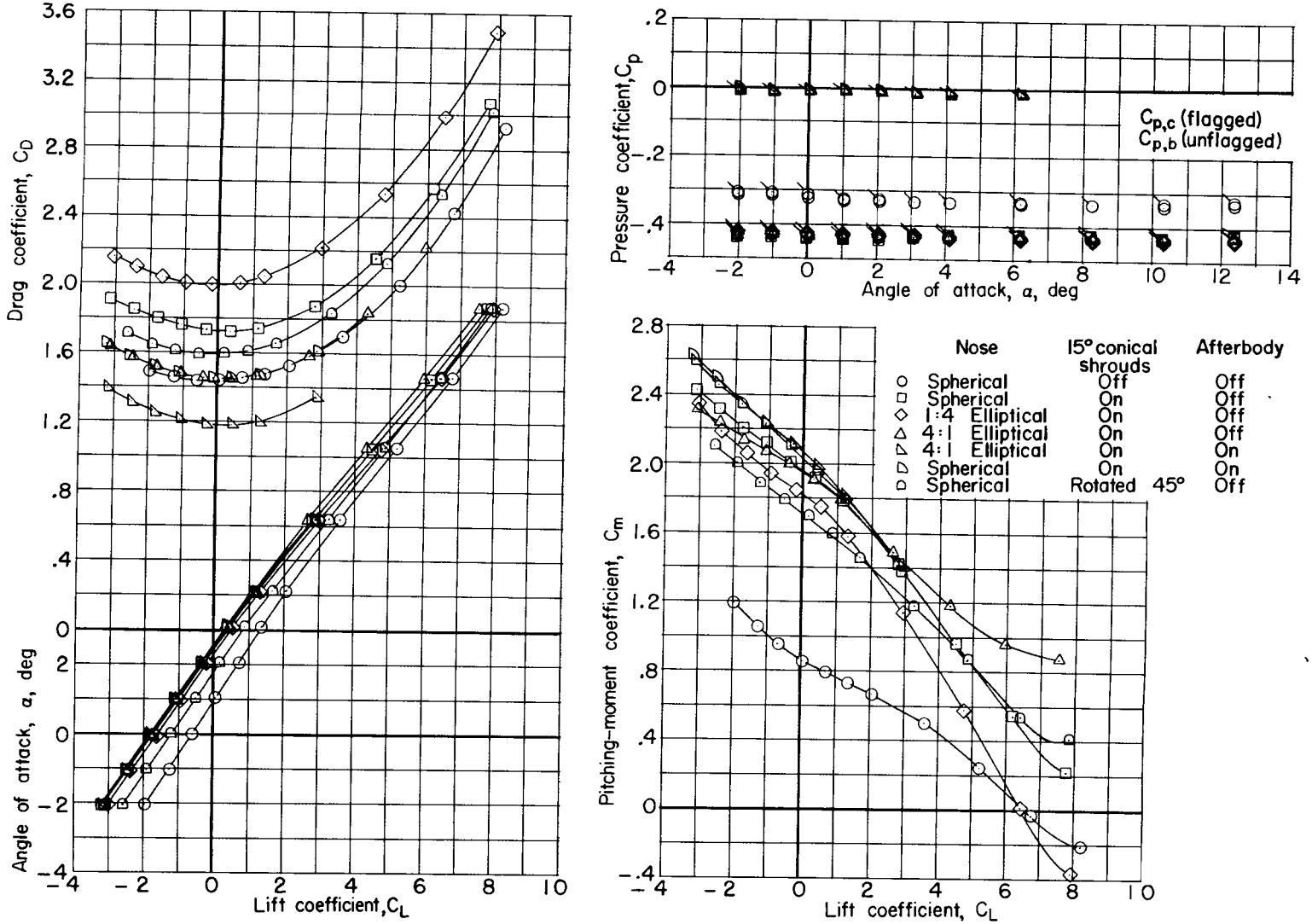

(a) M = 1.20.

Figure 14.- Longitudinal aerodynamic characteristics of reusable booster with 65° swept trapezoidal wing, various arrangements of noses, shrouds, and without and with afterbody. $\beta = 0°$.

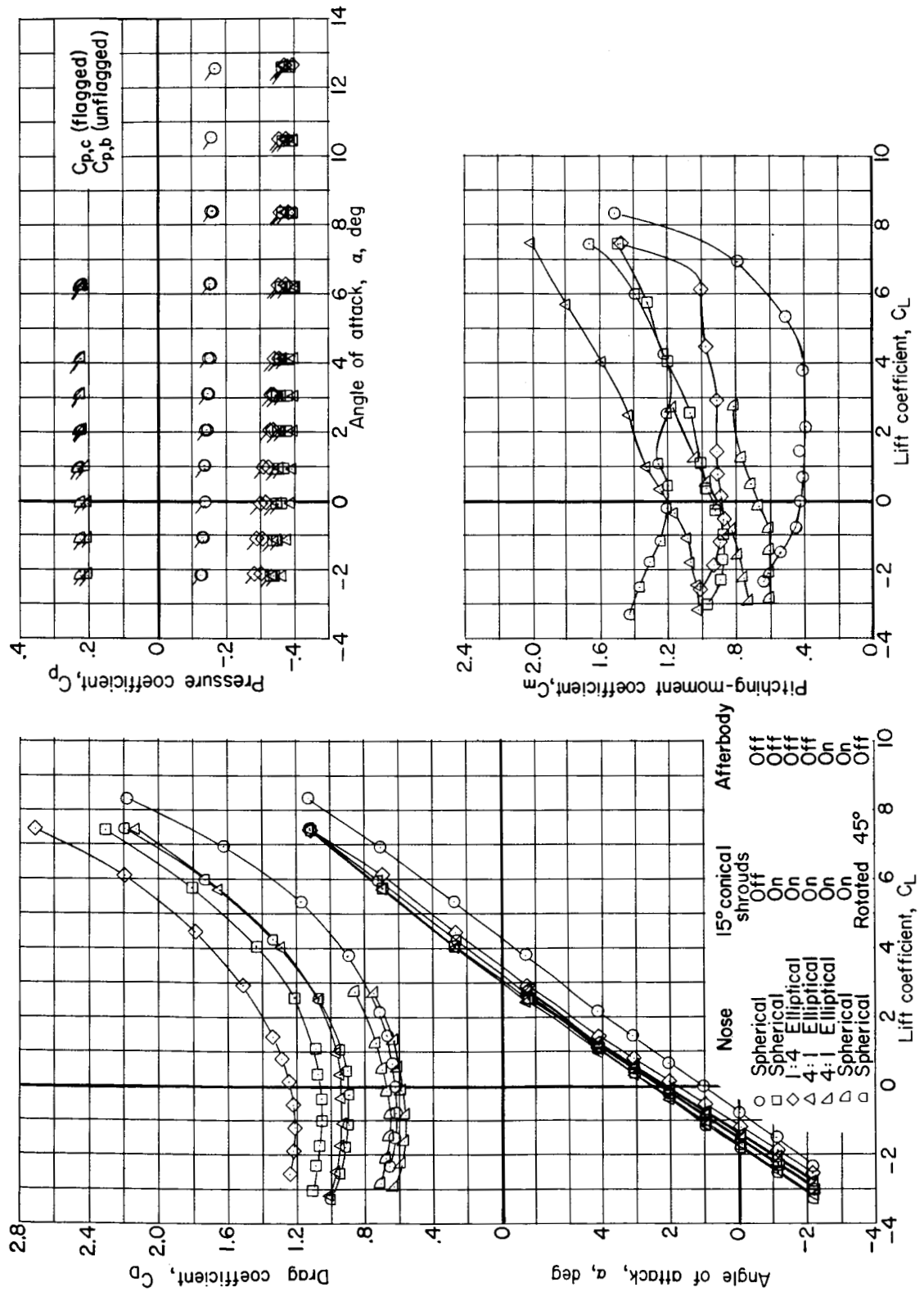

(b) M = 0.90.

Figure 14.- Continued.

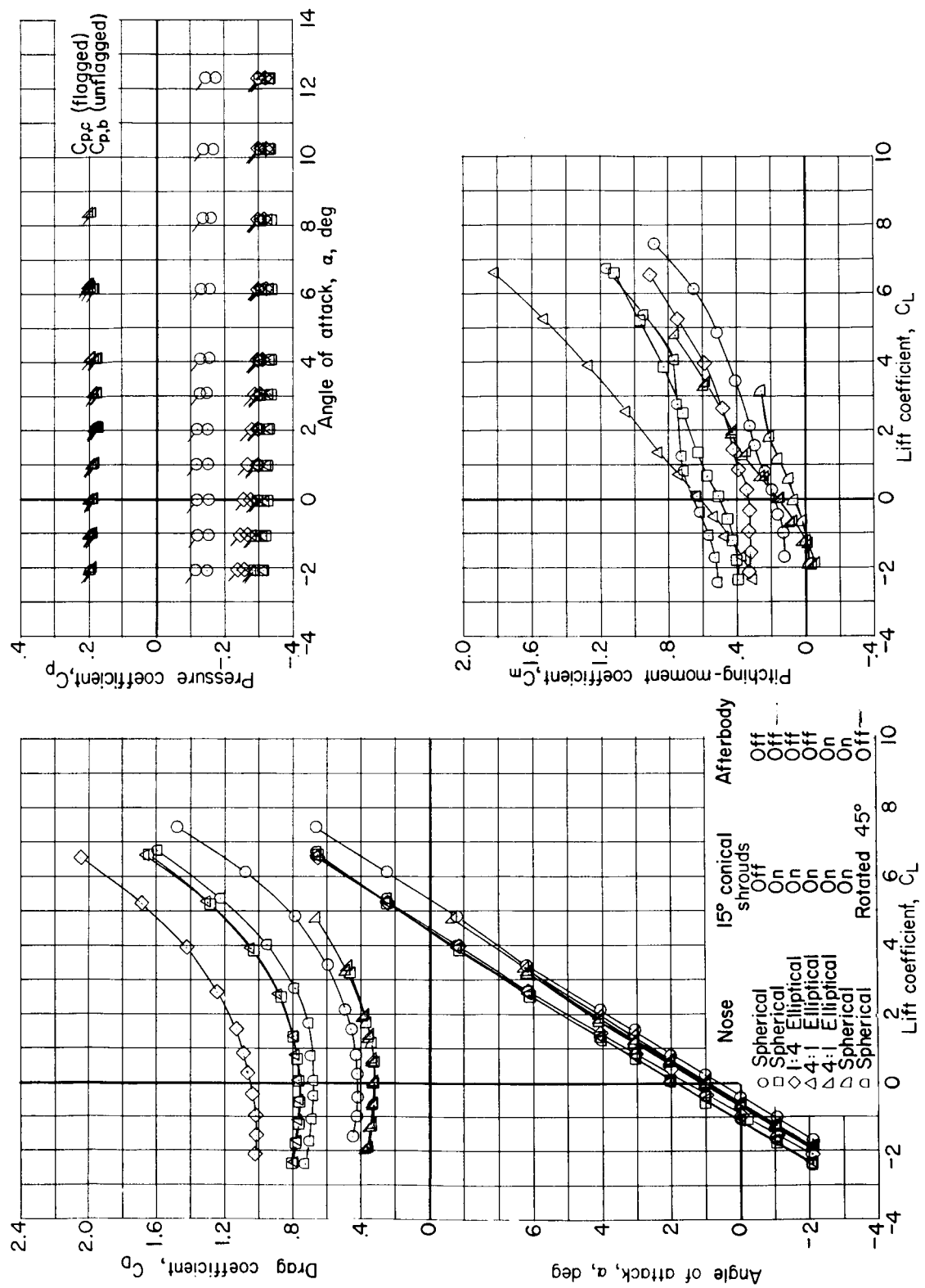

(c) M = 0.60.

Figure 14.- Continued.

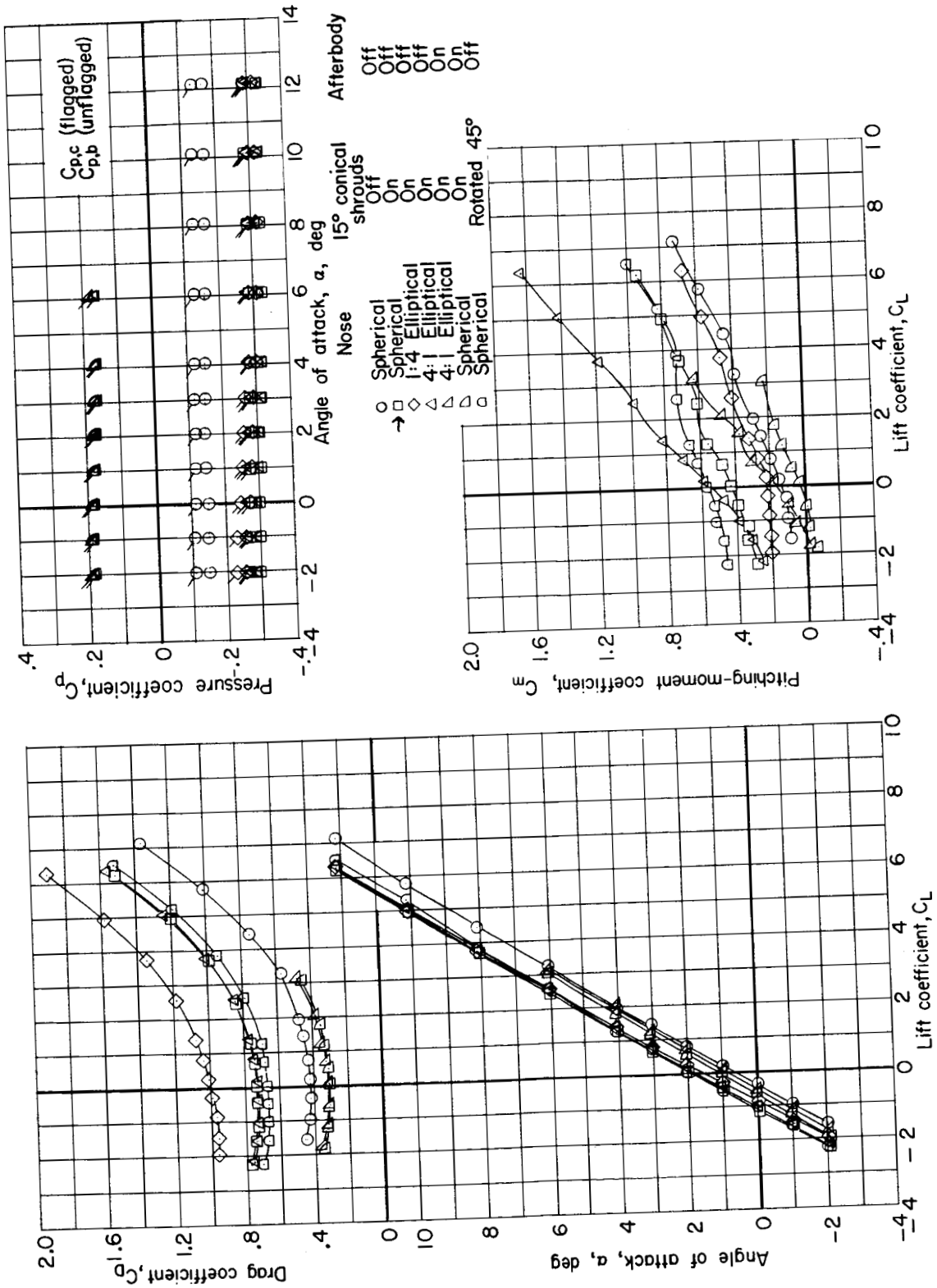

(d) M = 0.40.

Figure 14.- Concluded.

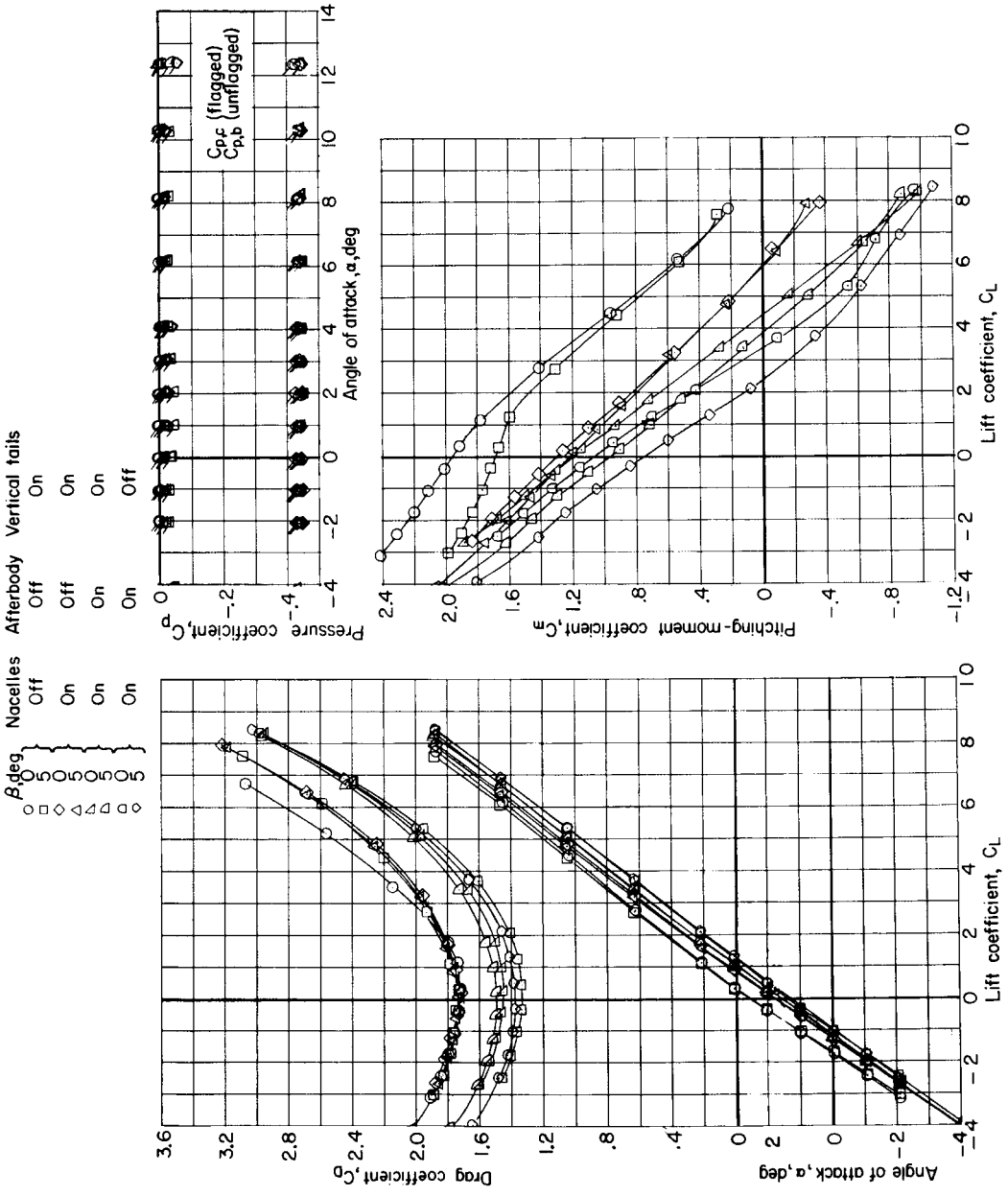

(a) M = 1.20.

Figure 15.- Longitudinal aerodynamic characteristics of reusable booster with 65° swept trapezoidal wing, spherical nose, 15° shrouds, without and with flyback engine nacelles and afterbody. β = 0° and 5°.

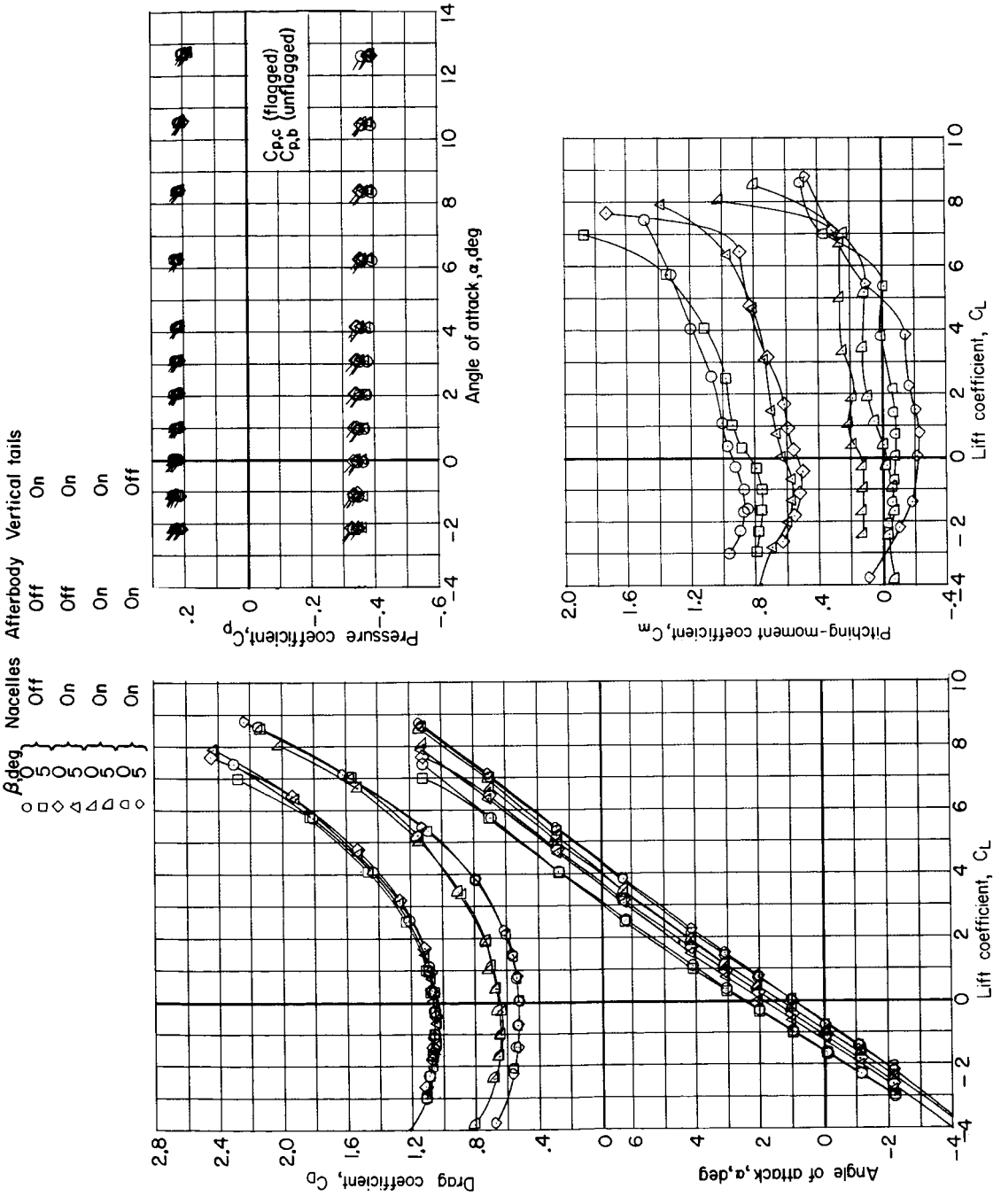

(b) M = 0.90.

Figure 15.- Continued.

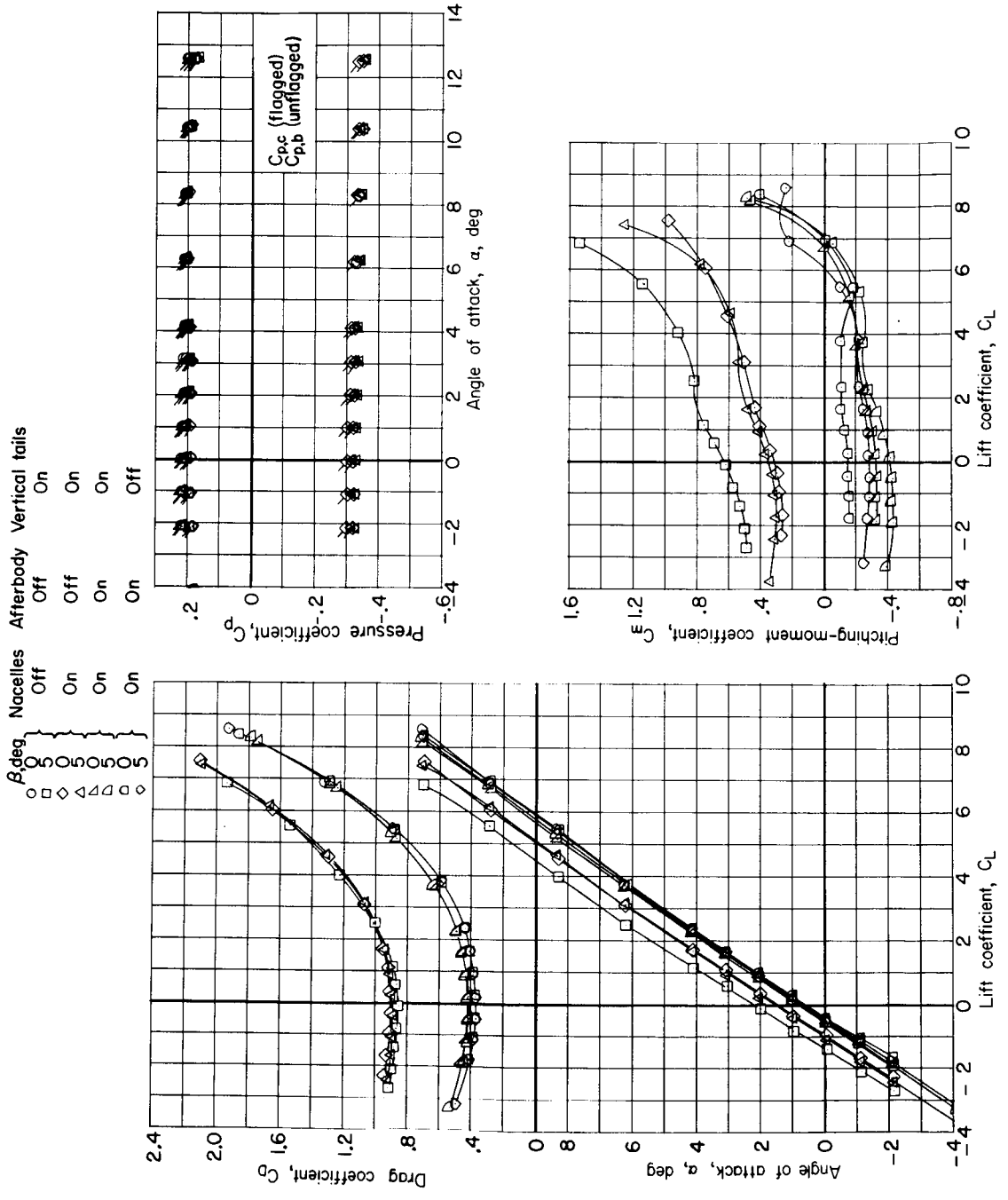

(c) M = 0.80.

Figure 15.- Continued.

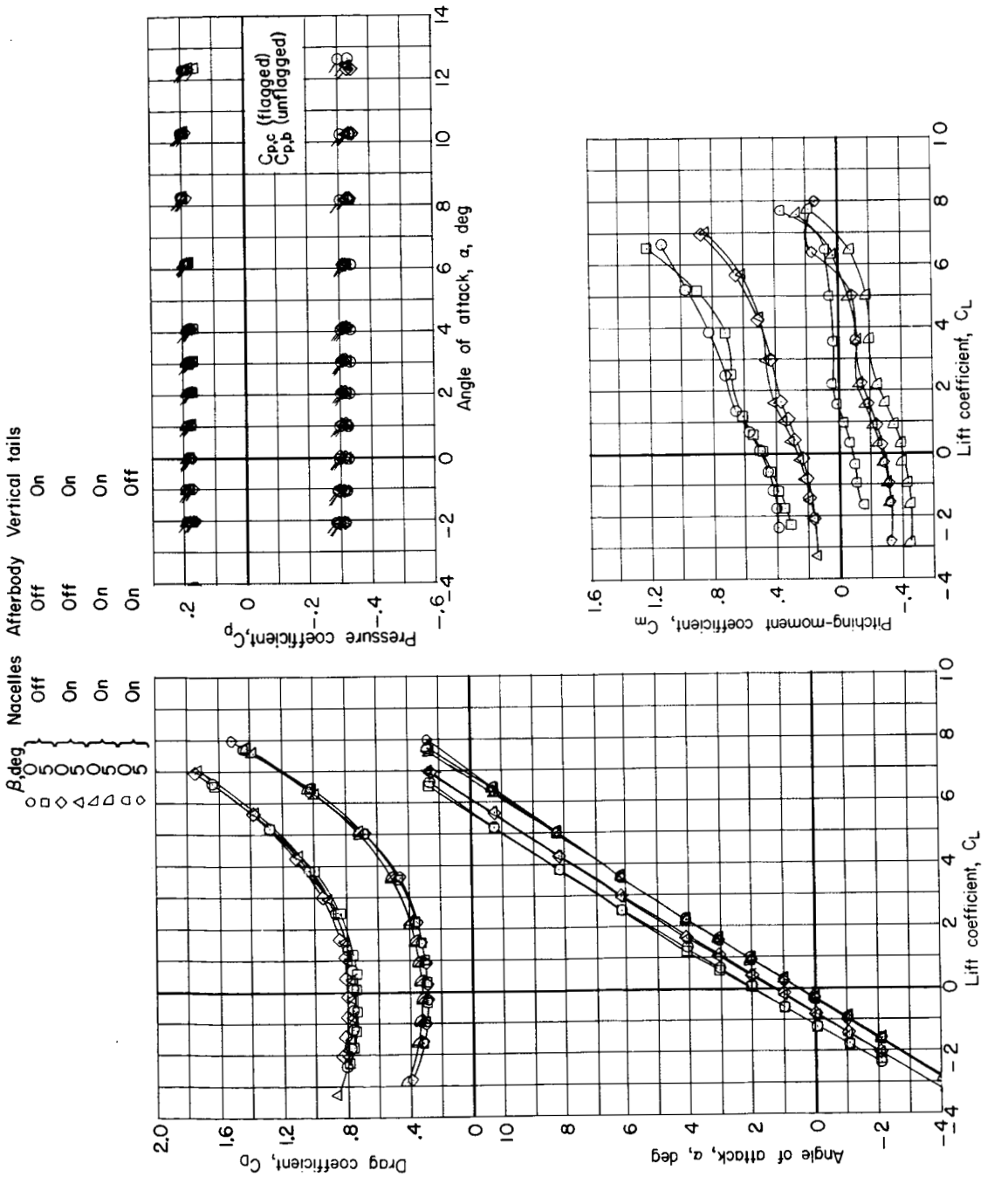

(d) M = 0.60.

Figure 15.- Continued.

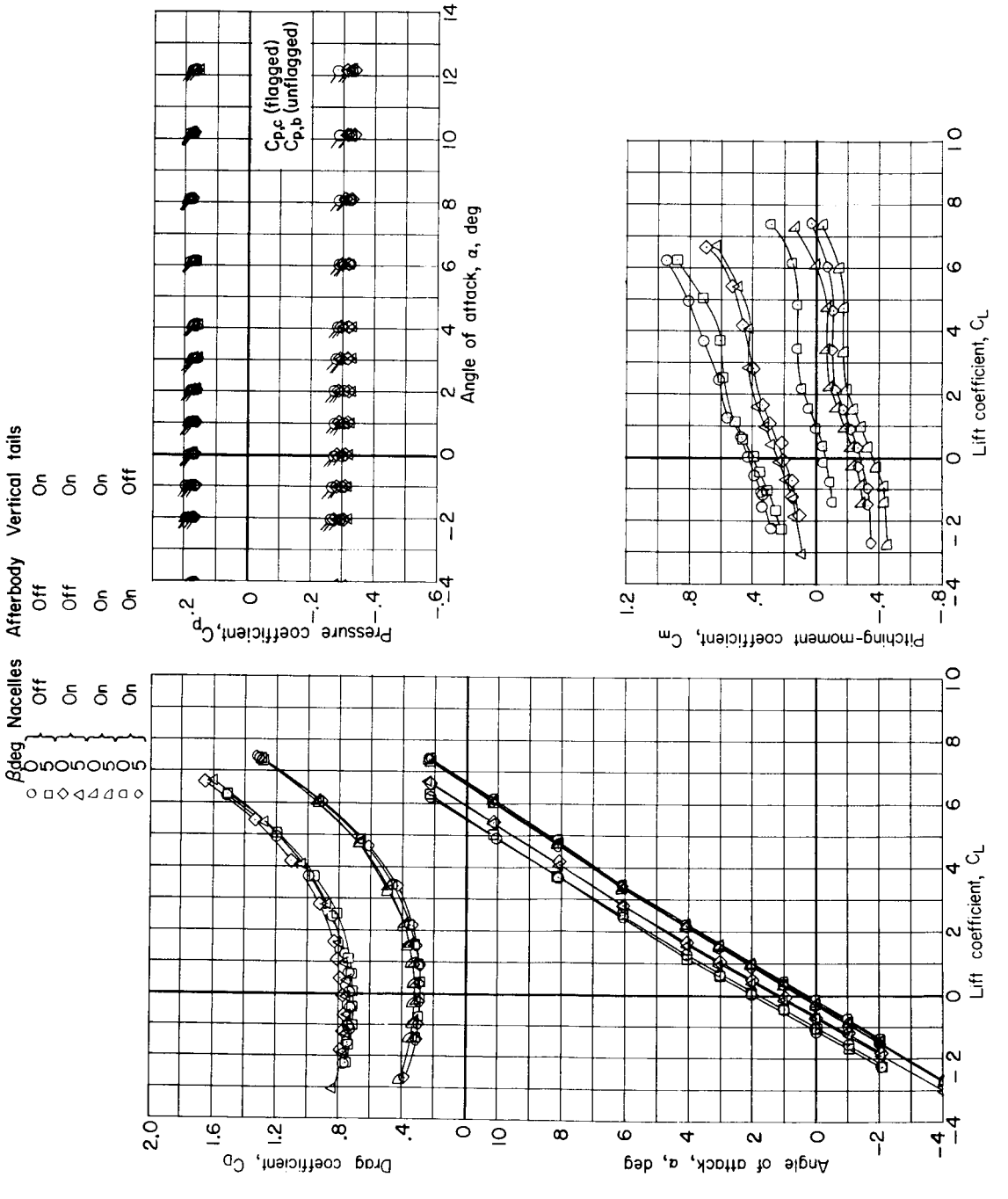

(e) M = 0.40.

Figure 15.- Concluded.

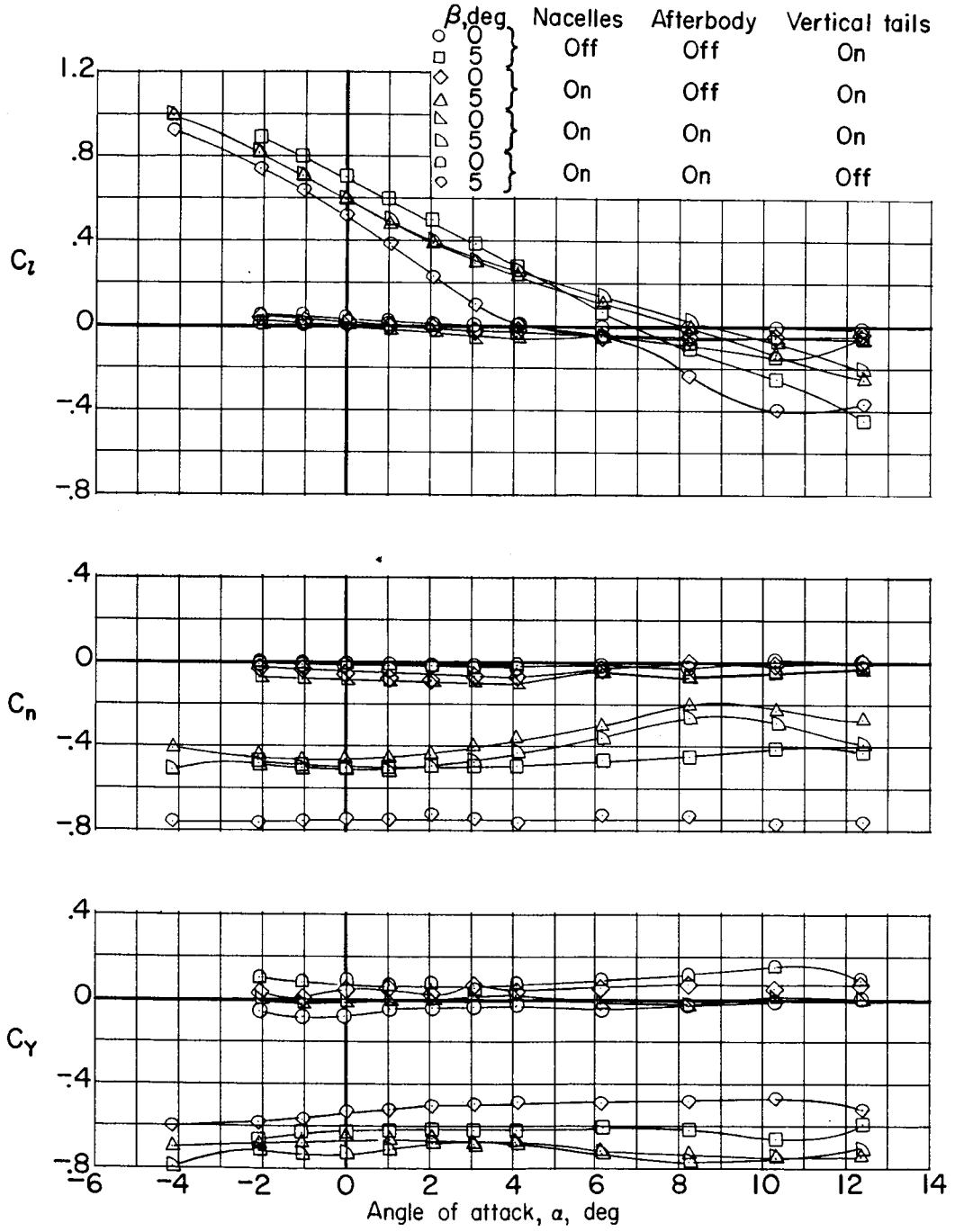

(a) M = 1.20.

Figure 16.- Lateral aerodynamic characteristics of reusable booster with 65° swept trapezoidal wing, spherical nose, 15° shrouds, without and with flyback engine nacelles, afterbody, and vertical tails.

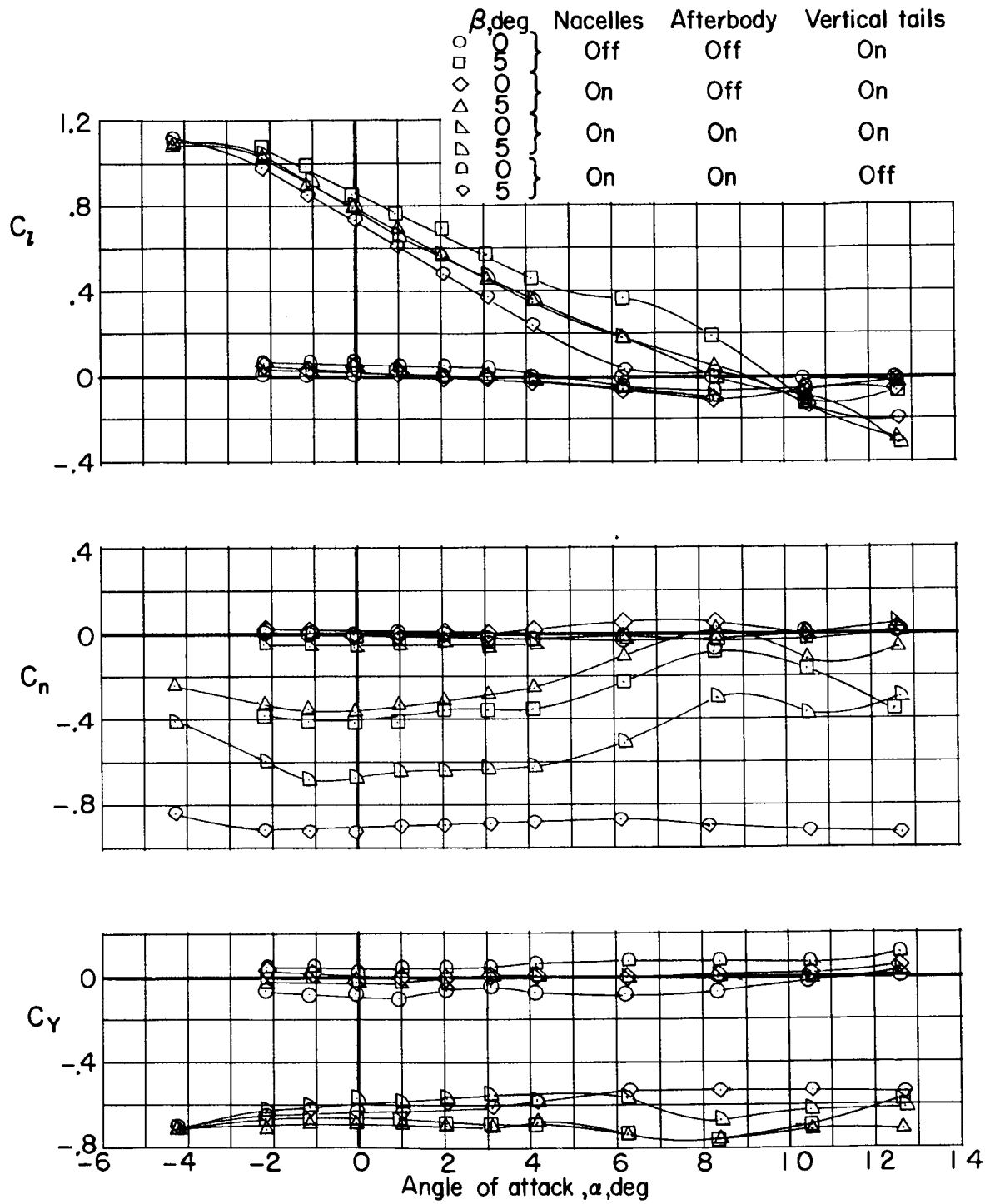

(b) M = 0.90.

Figure 16.- Continued.

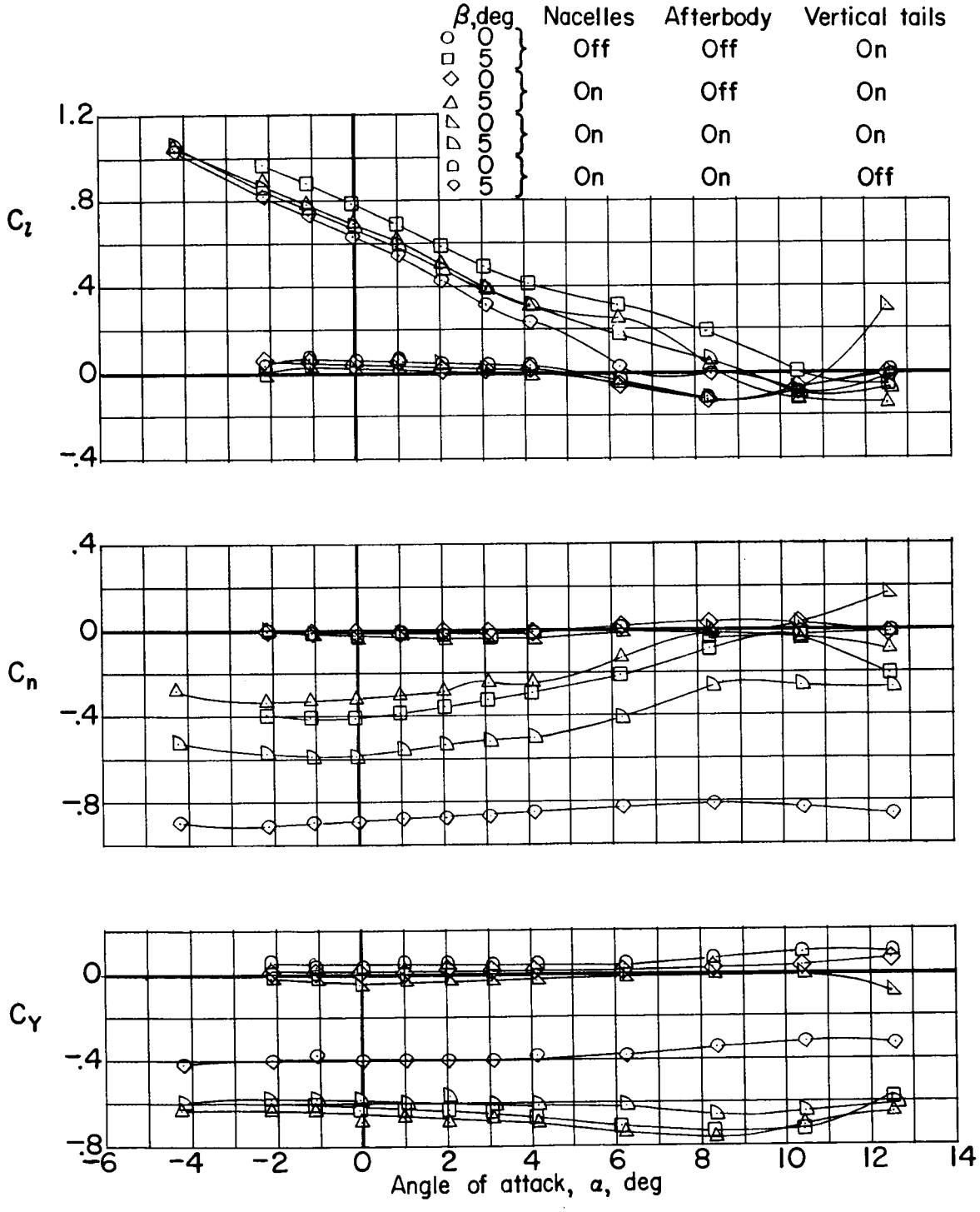

(c) M = 0.80.

Figure 16.- Continued.

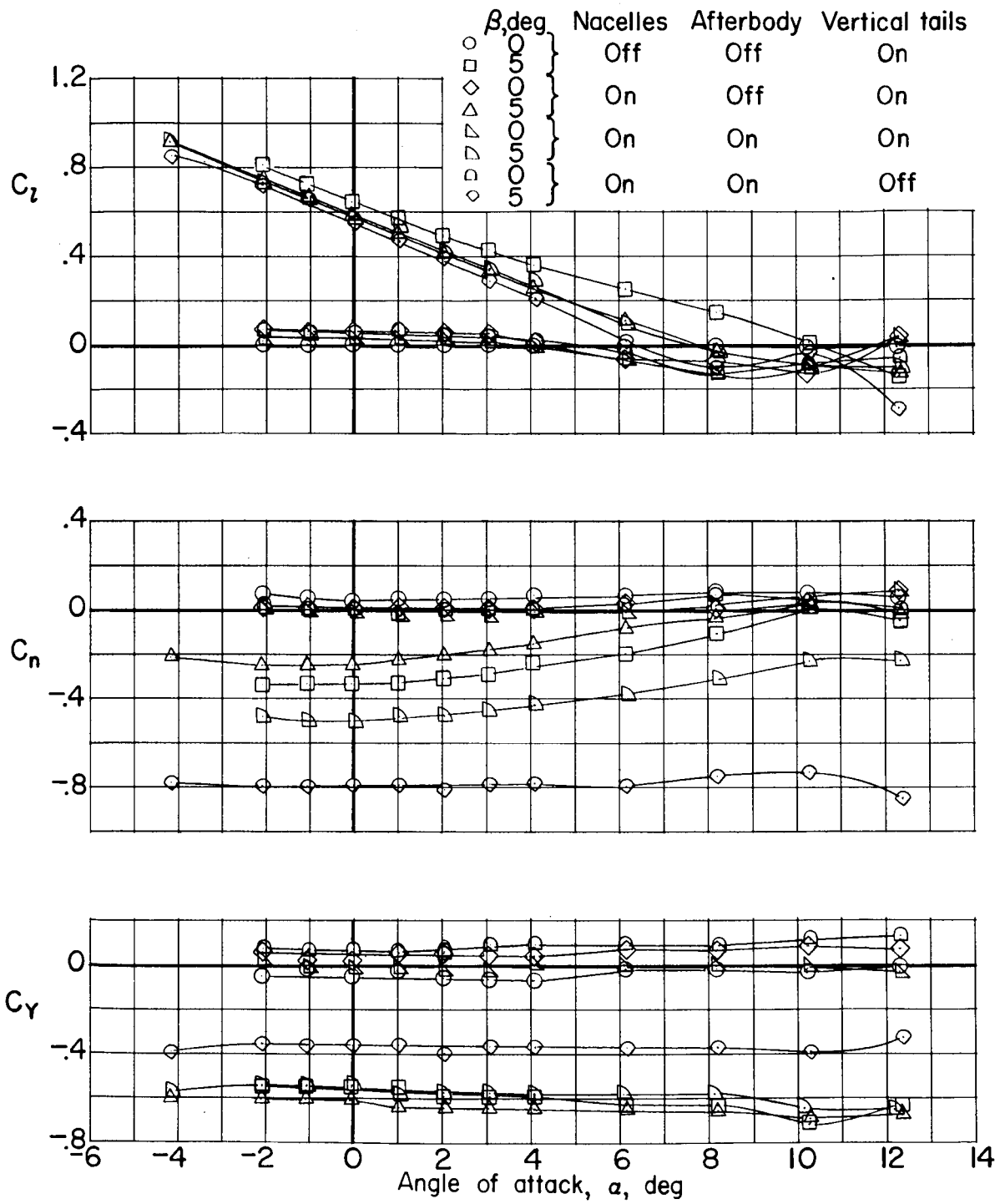

(d) M = 0.60.

Figure 16.- Continued.

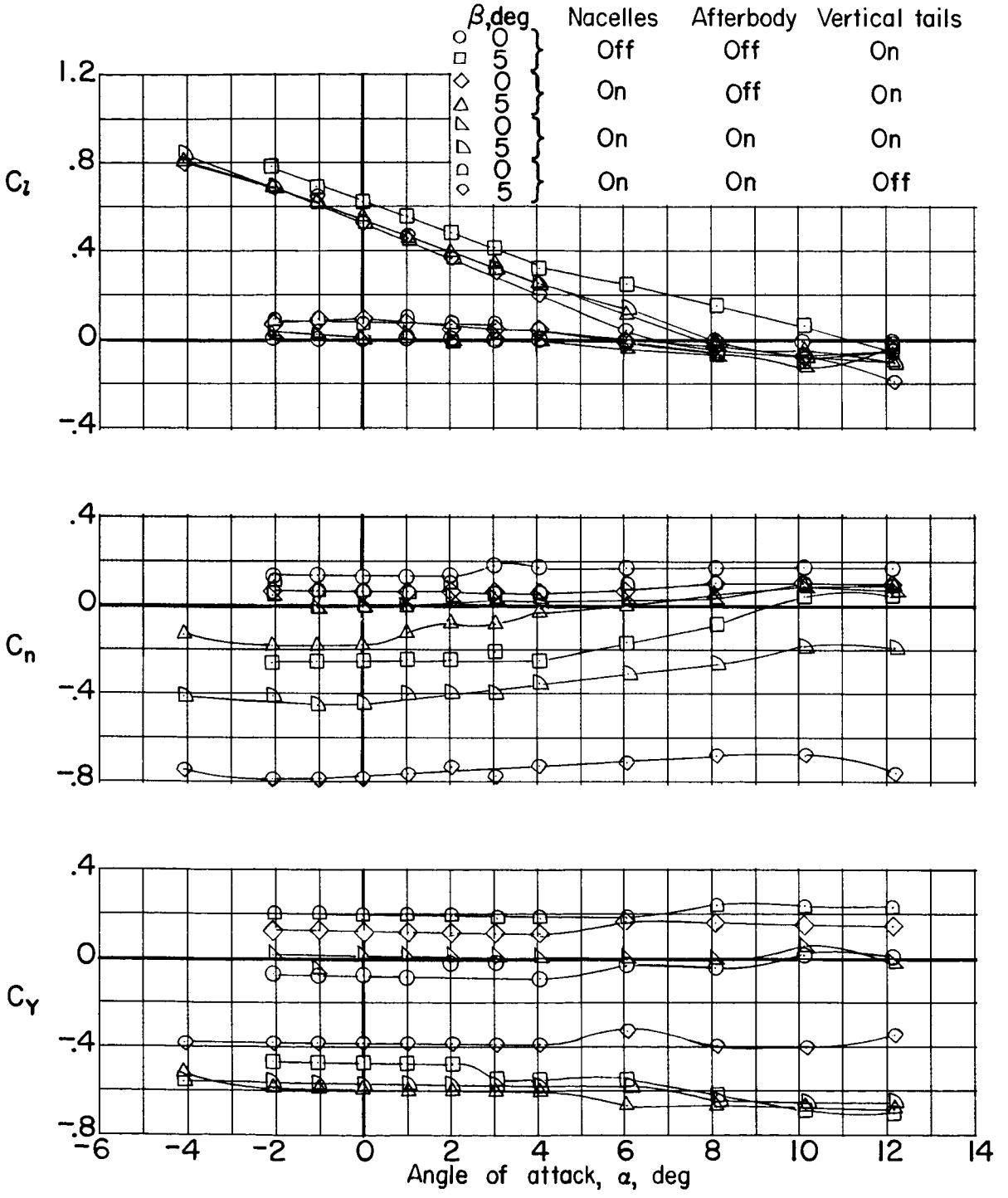

(e) M = 0.40.

Figure 16.- Concluded.

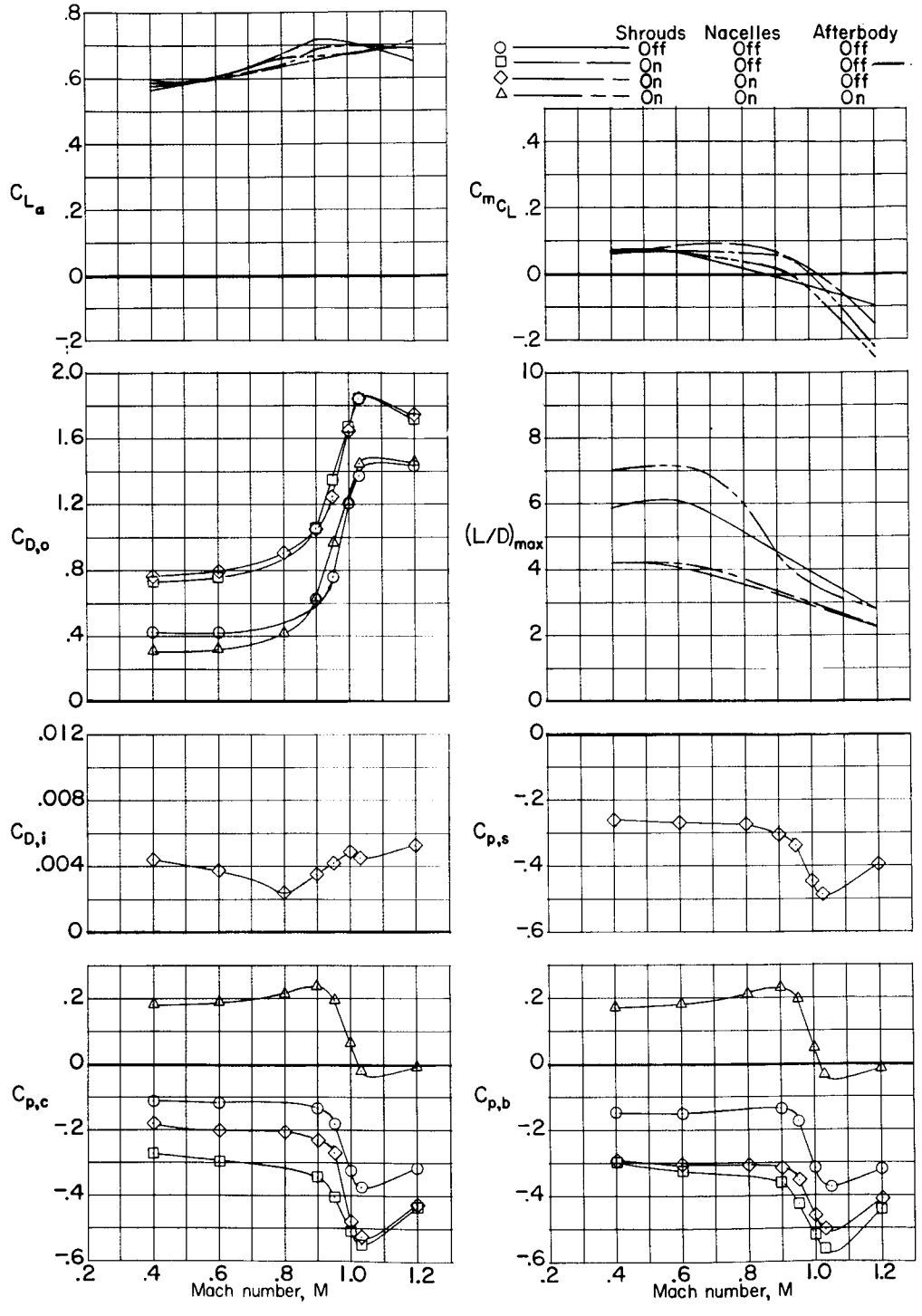

Figure 17.- Variation with Mach number of longitudinal stability and drag parameters for reusable booster with 65° swept trapezoidal wing and spherical nose including effects of shrouds, fly-back engine nacelles, and afterbody.

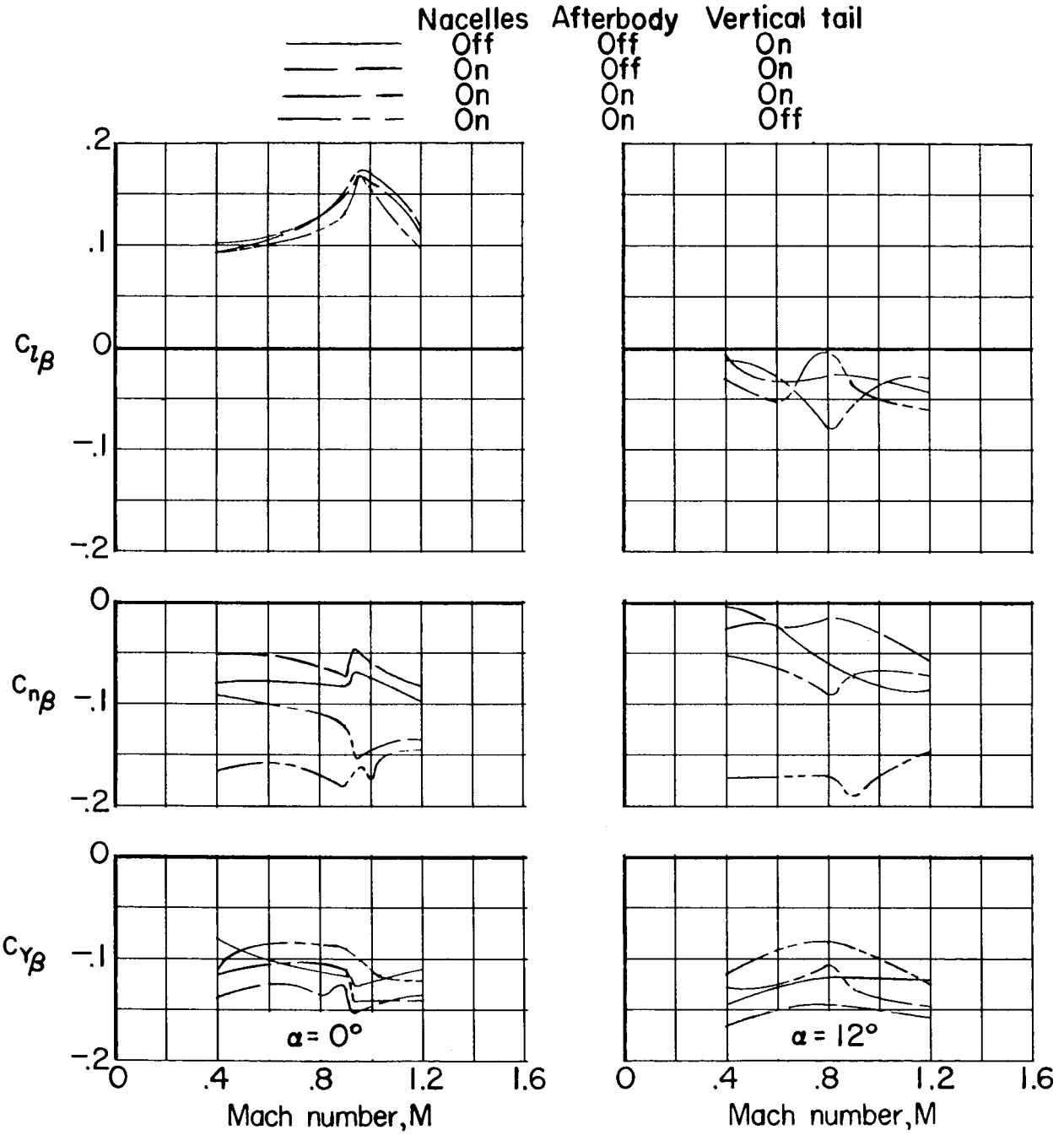

Figure 18.- Variation with Mach number of lateral-directional stability parameters for reusable booster with 65° swept trapezoidal wing, spherical nose, and shrouds showing effects of nacelles, afterbody, and vertical tails.

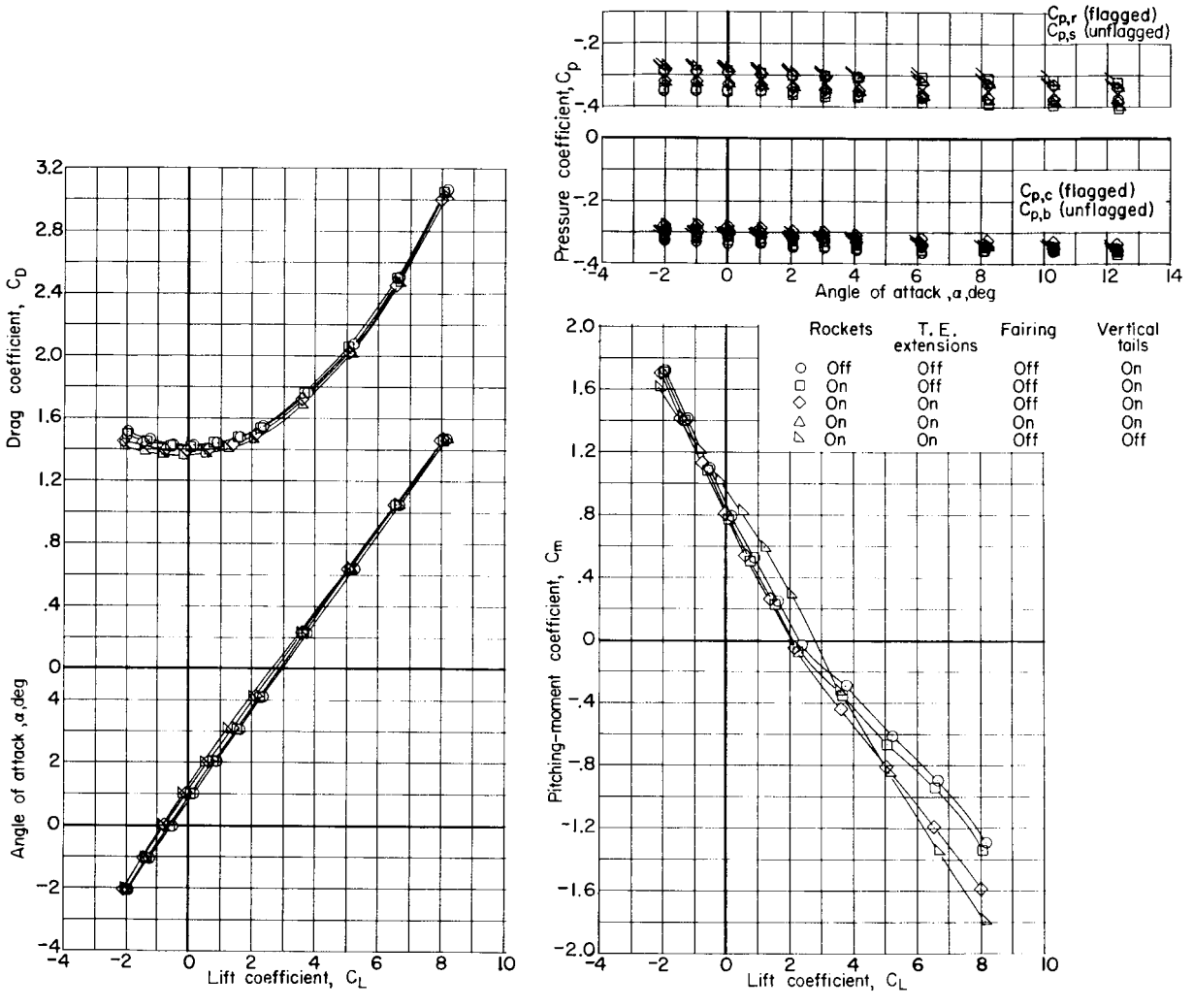

(a) M = 1.20.

Figure 19.- Longitudinal aerodynamic characteristics of modified reusable booster with 65° swept trapezoidal wing moved rearward 0.19D, outboard vertical tails, parabolic shrouds rotated 45° including effects of rocket engines, trailing-edge extension, base fairing, with and without vertical tails. $\beta = 0°$.

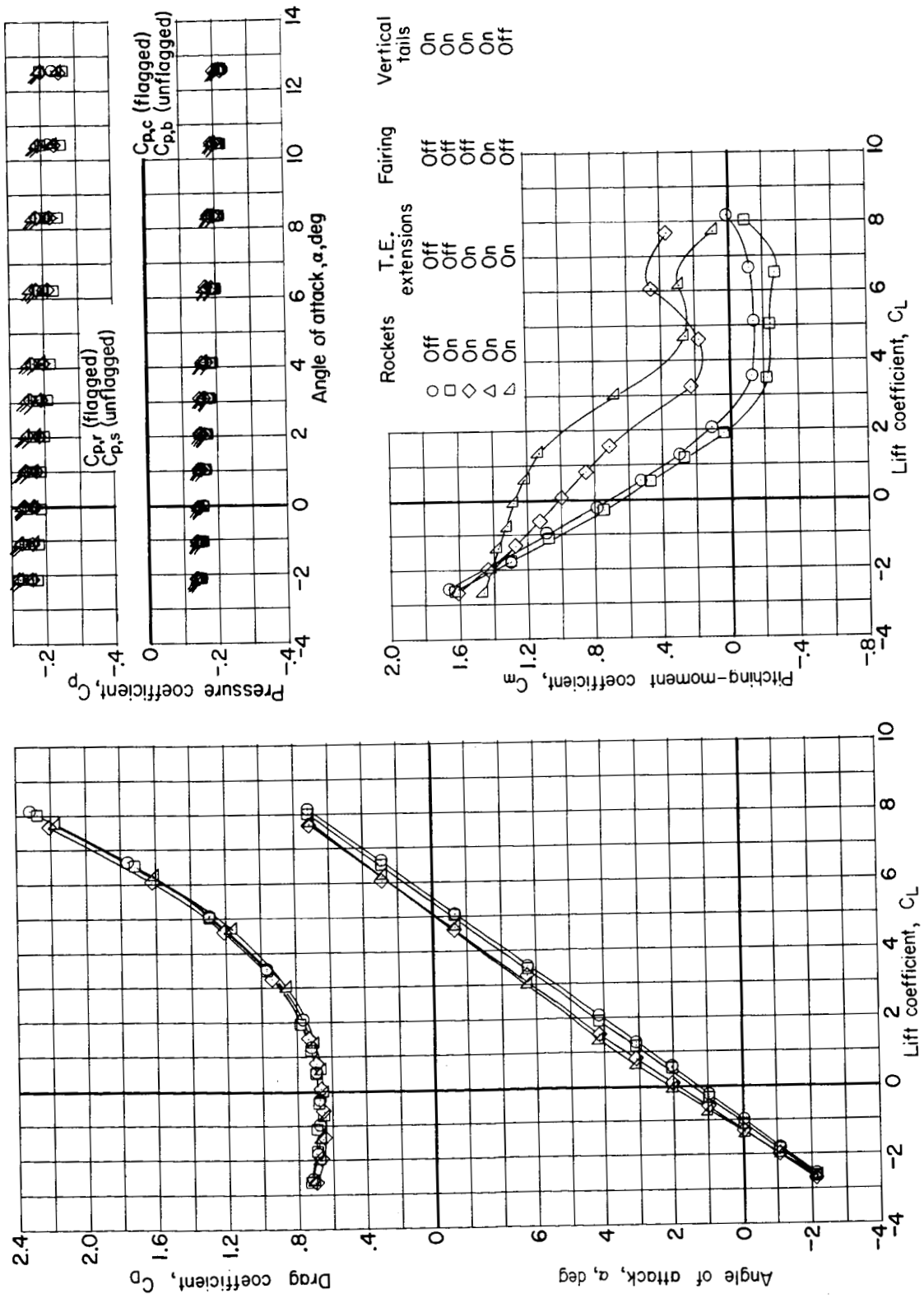

(b) M = 0.90.

Figure 19.- Continued.

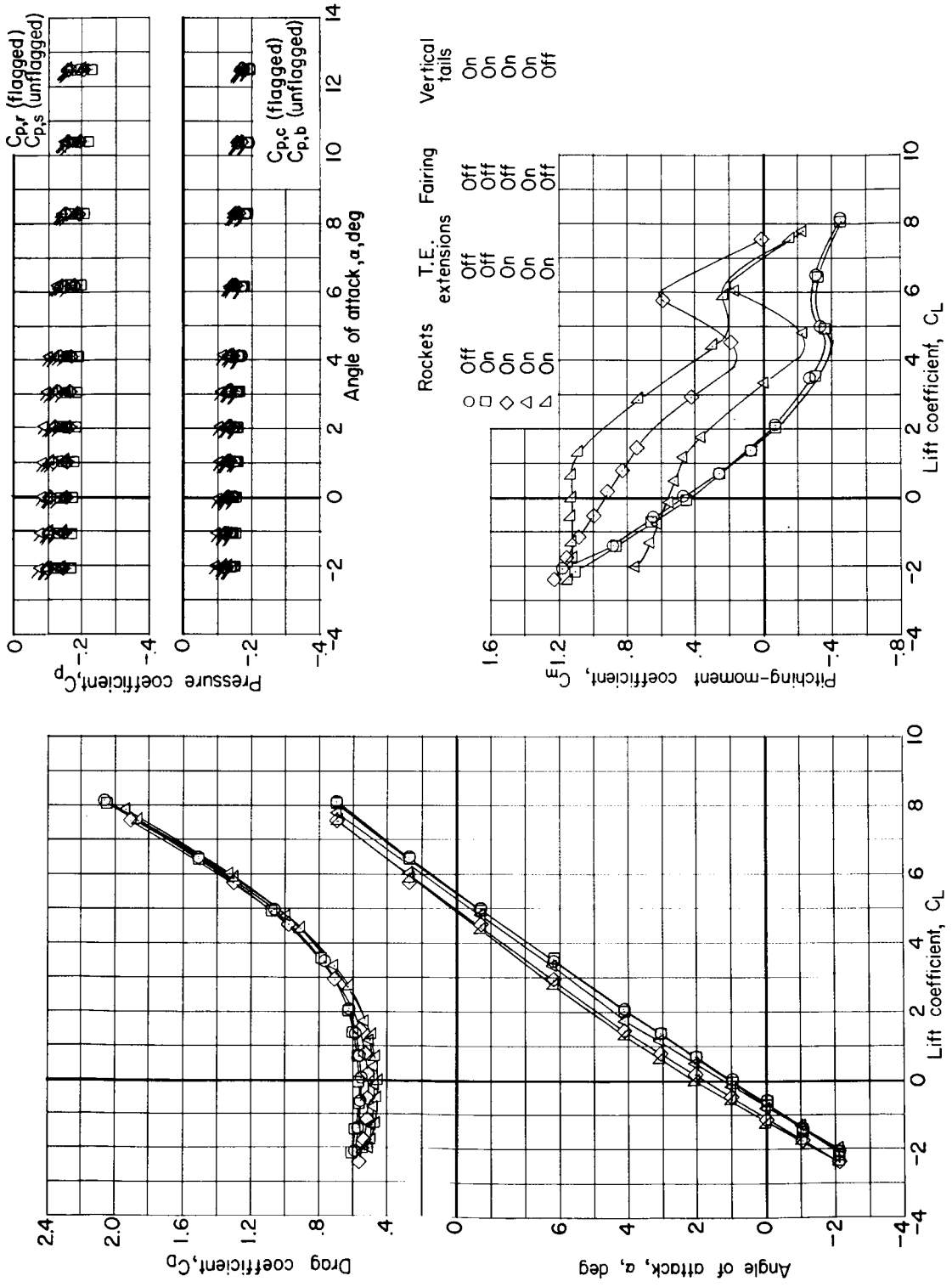

(c) M = 0.80.

Figure 19.- Continued.

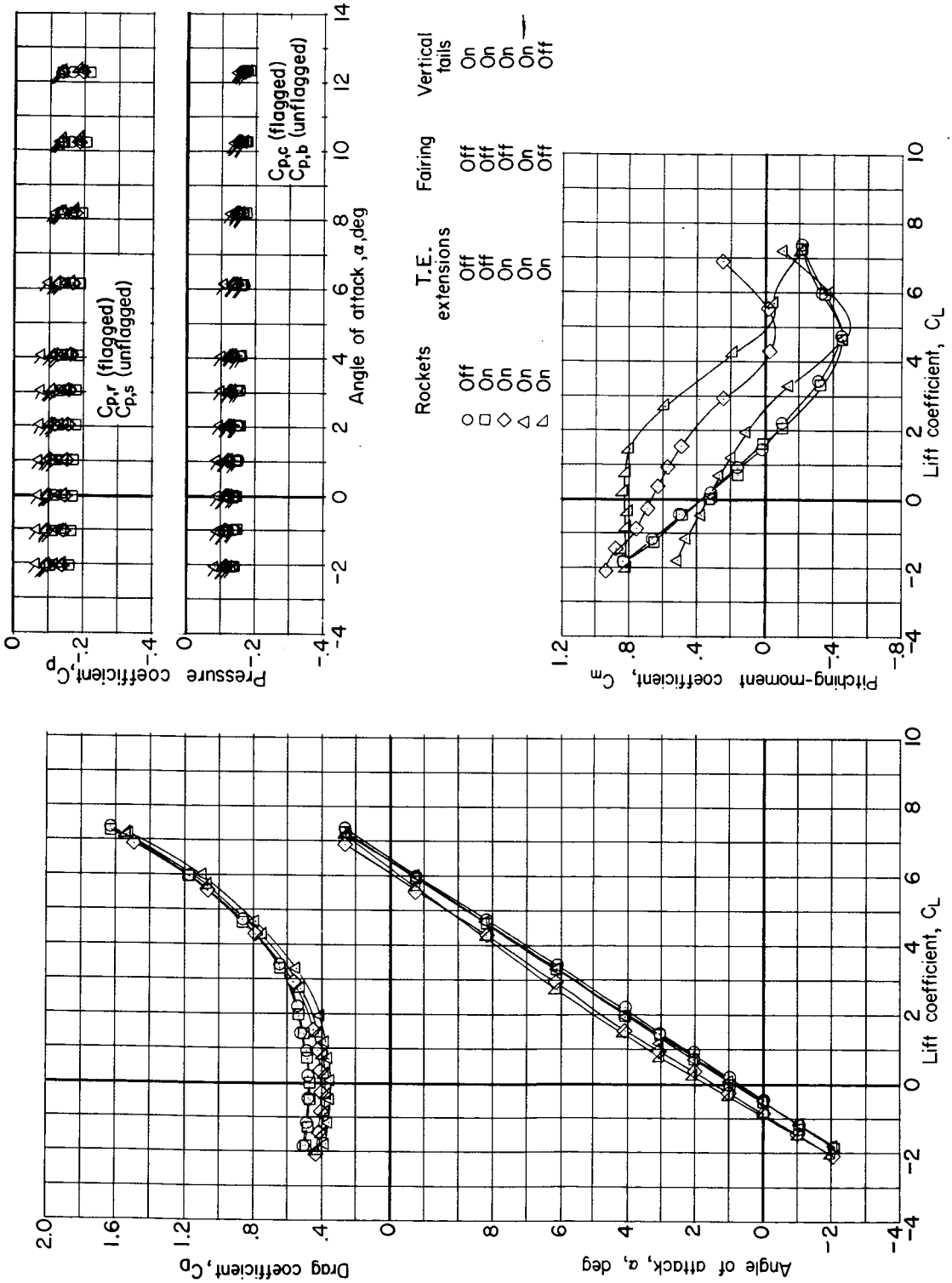

(d) M = 0.60.

Figure 19.- Continued.

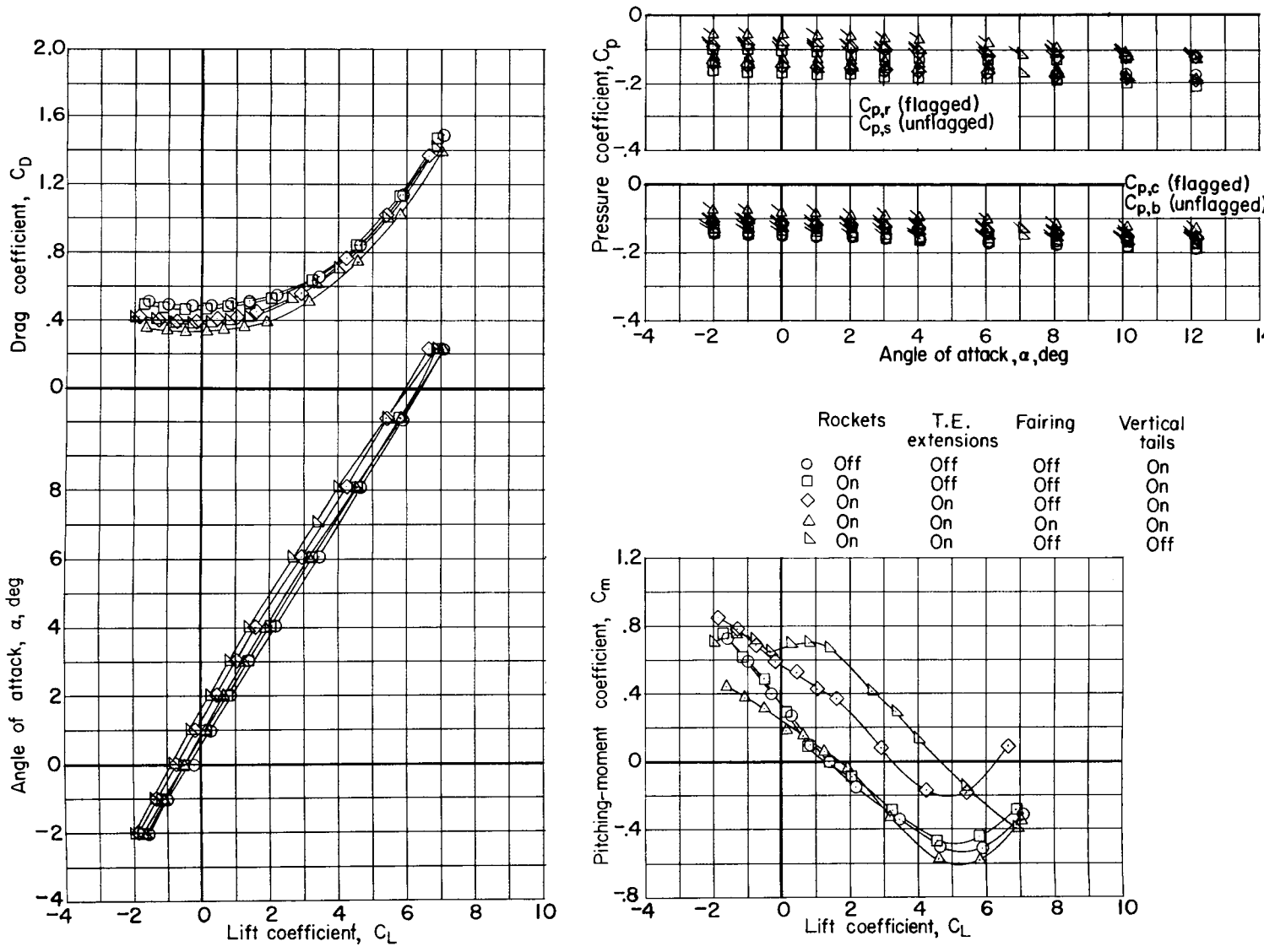

(e) M = 0.40.

Figure 19.- Concluded.

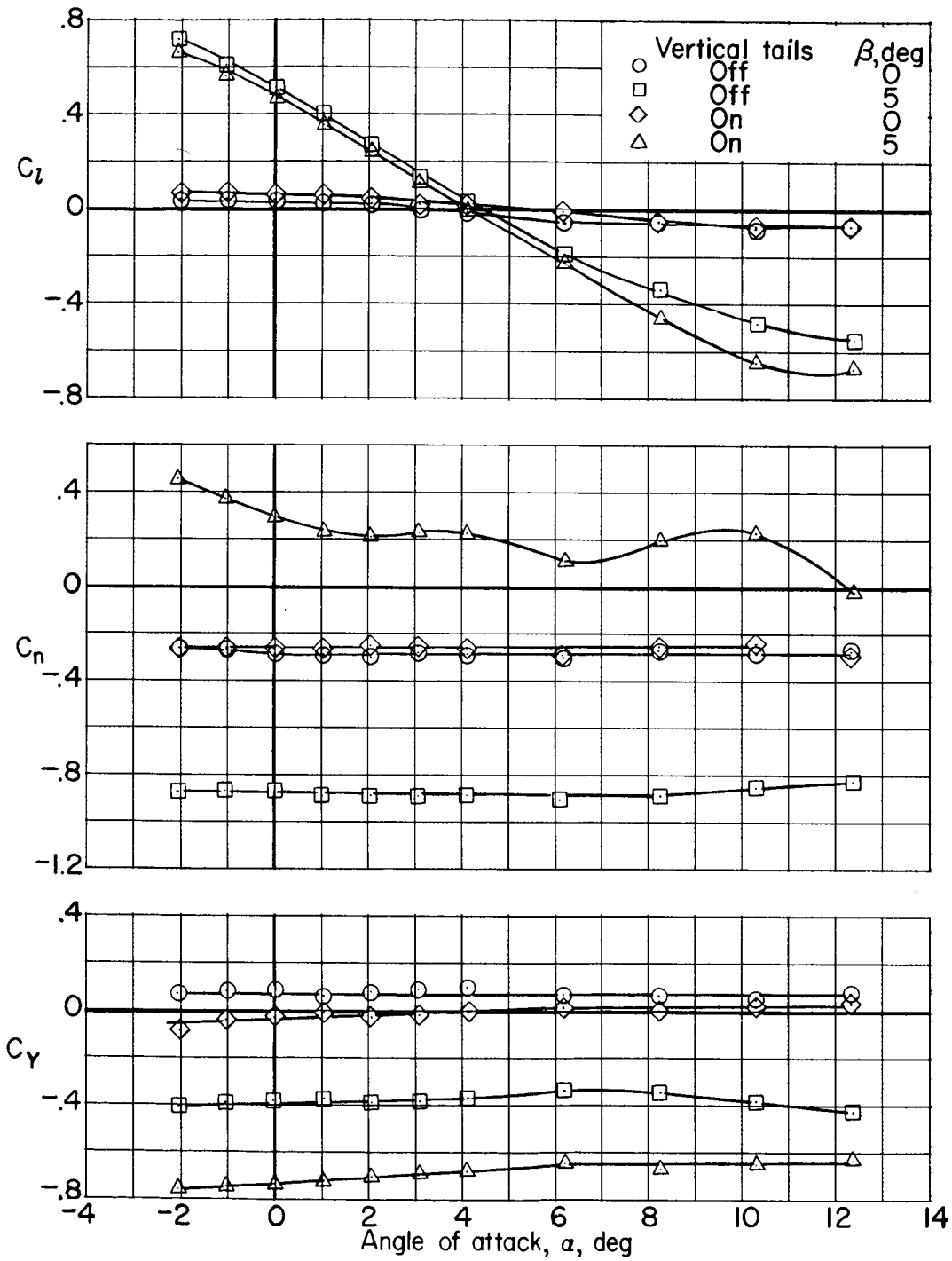

(a) M = 1.20.

Figure 20.- Lateral-directional aerodynamic characteristics of modified reusable booster without and with vertical tails. $\beta = 0^{\circ}$ and 5°.

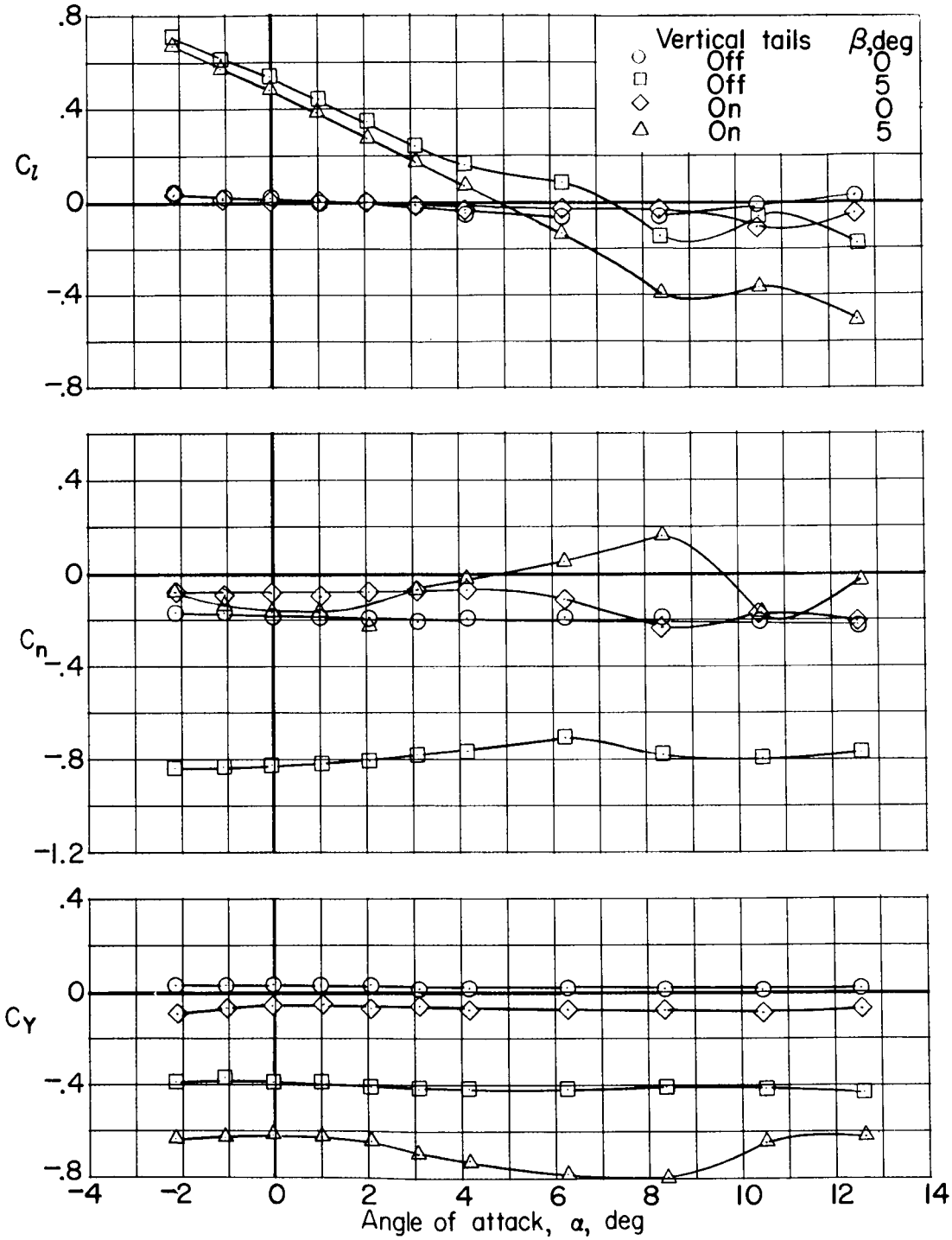

(b) M = 0.90.

Figure 20.- Continued.

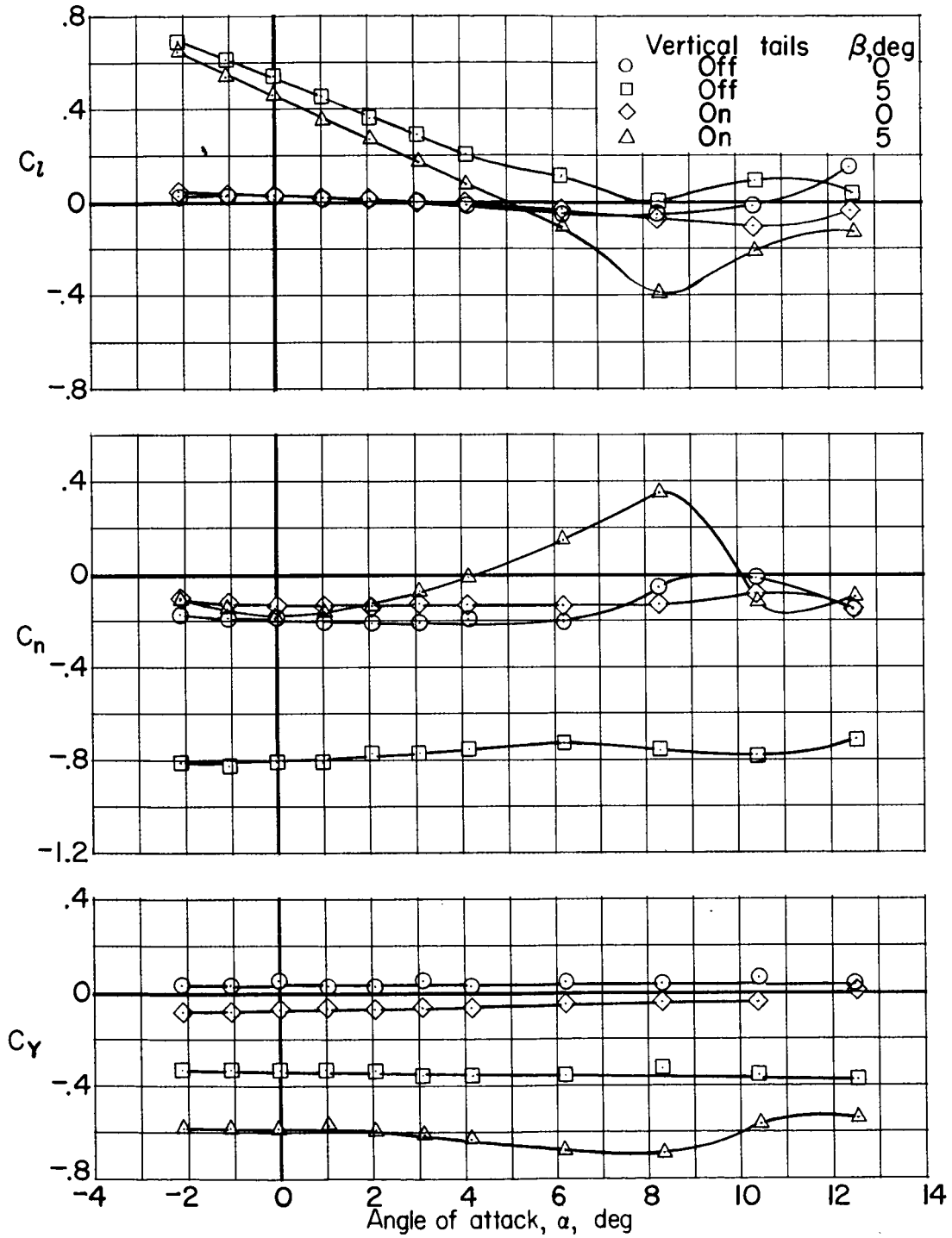

(c) M = 0.80.

Figure 20.- Continued.

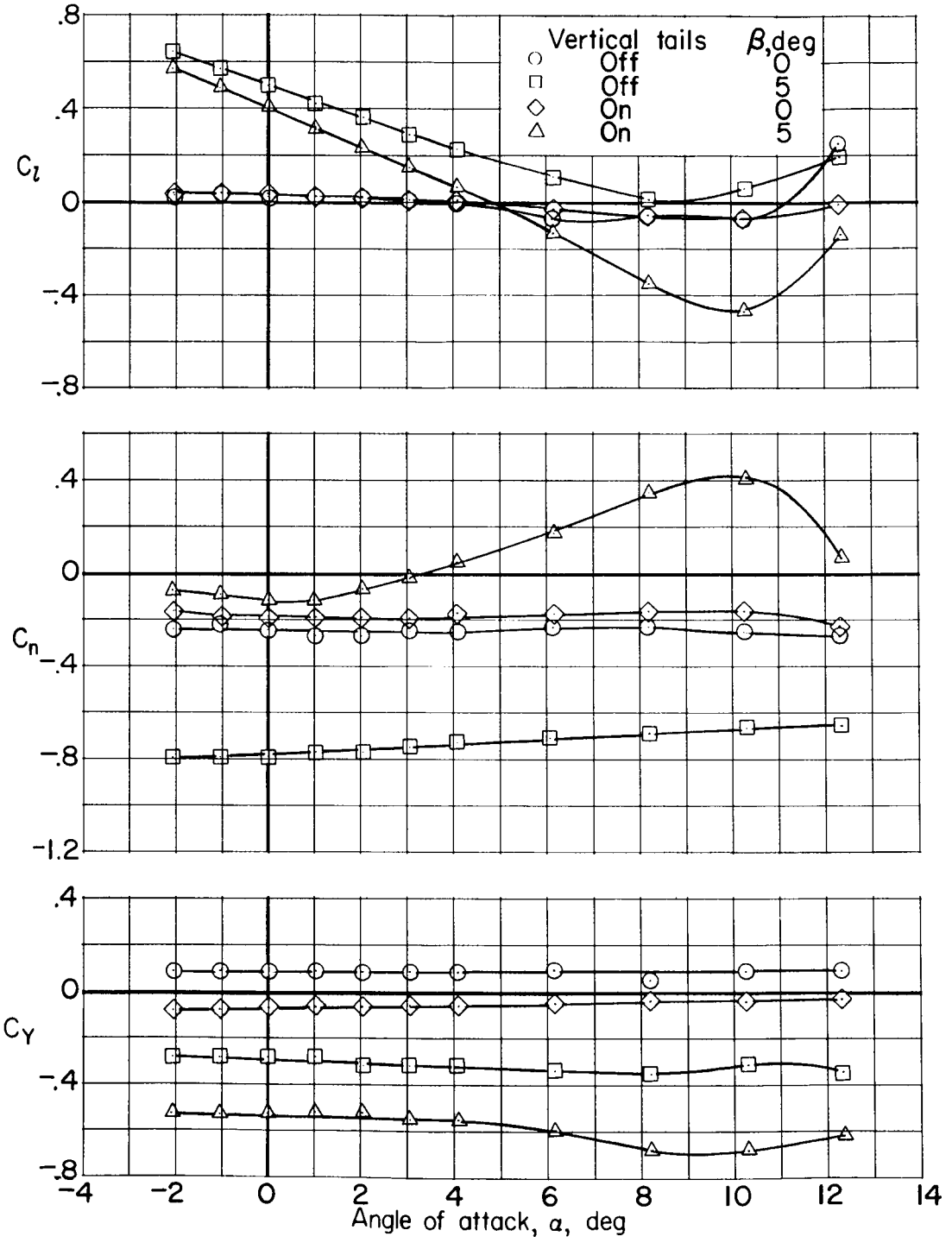

(d) M = 0.60.

Figure 20.- Continued.

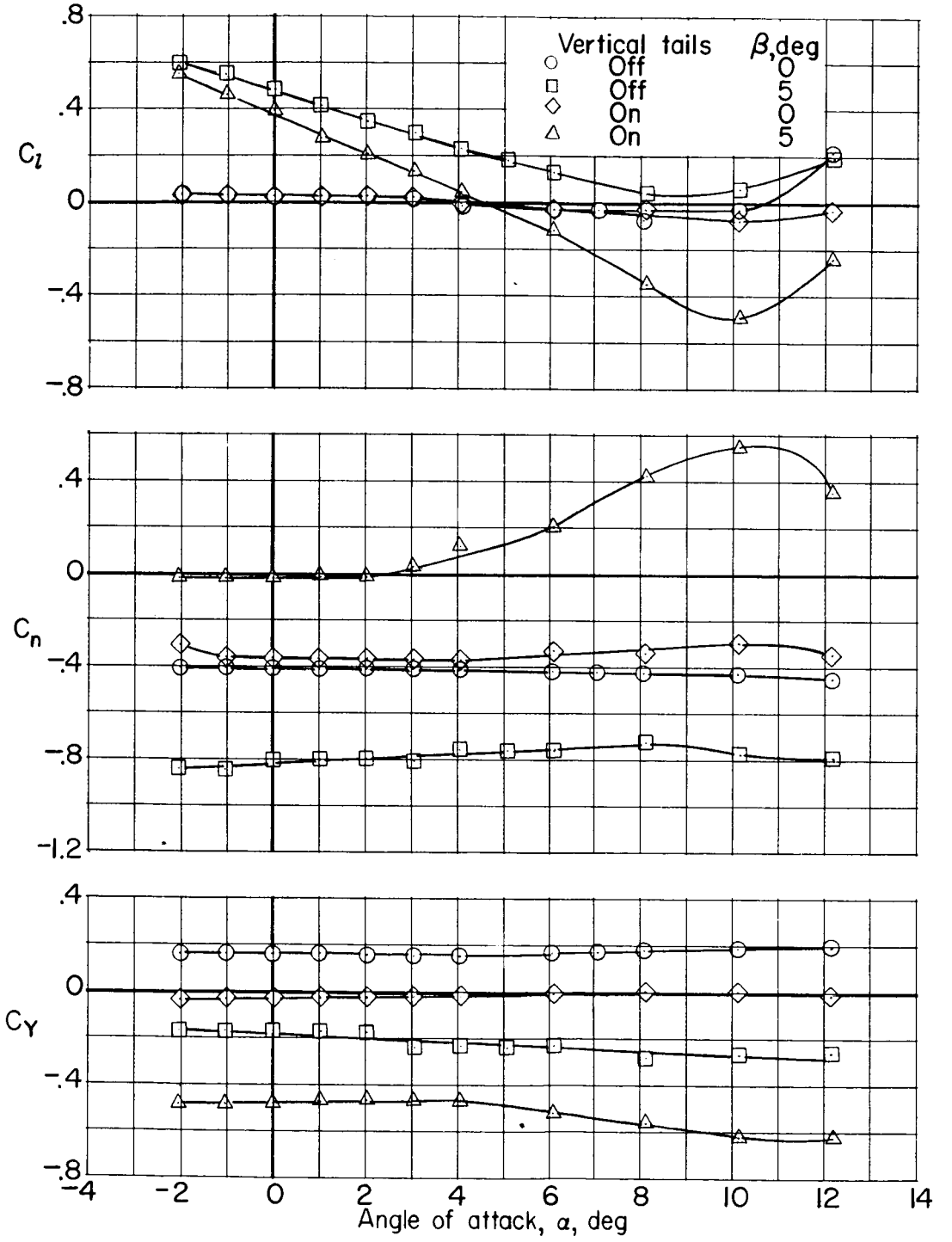

(e) M = 0.40.

Figure 20.- Concluded.

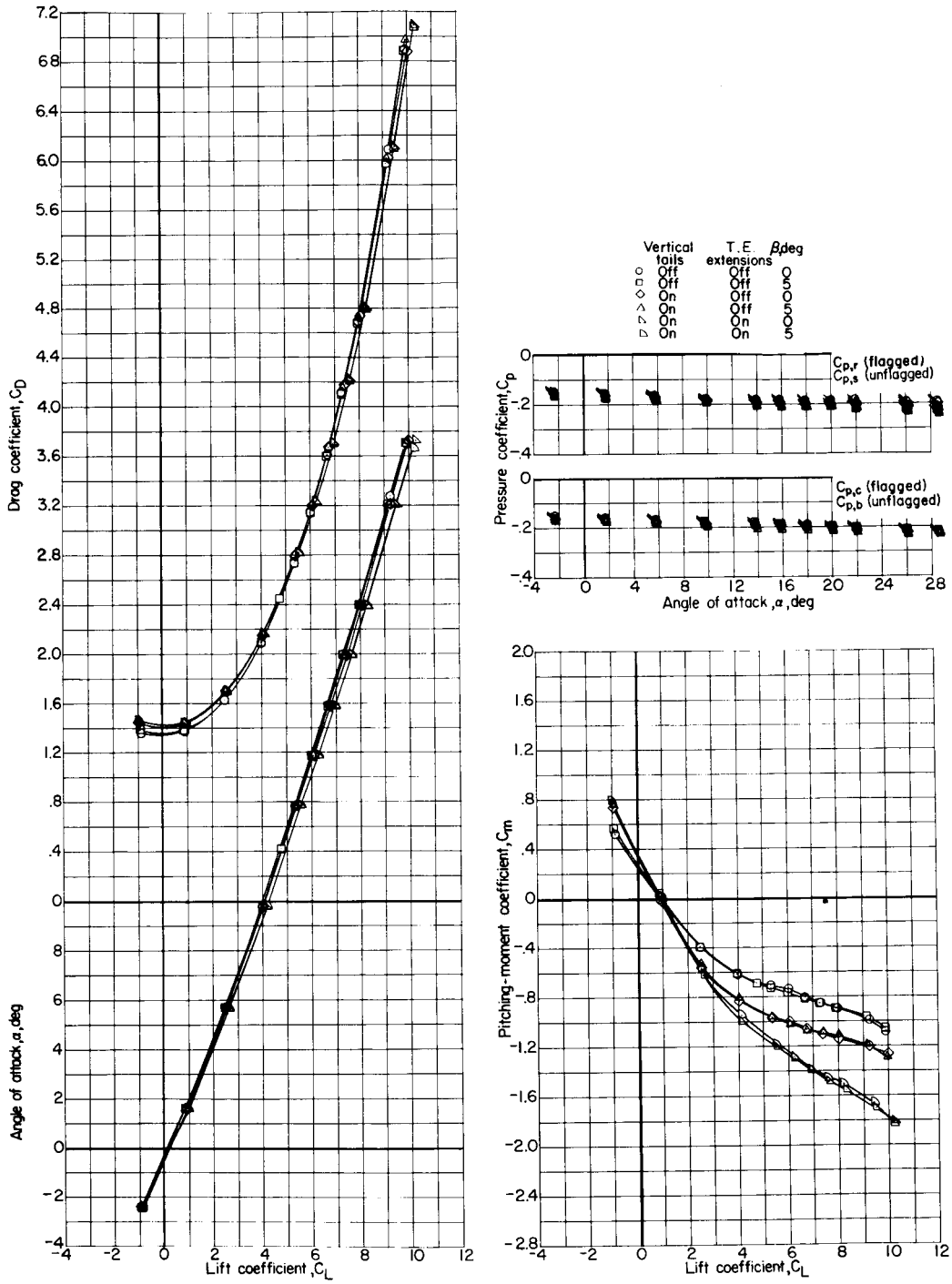

(a) M = 2.16.

Figure 21.- Supersonic longitudinal aerodynamic characteristics of modified reusable booster without and with vertical tails and trailing-edge extensions. $\beta = 0^o$ and 5^o.

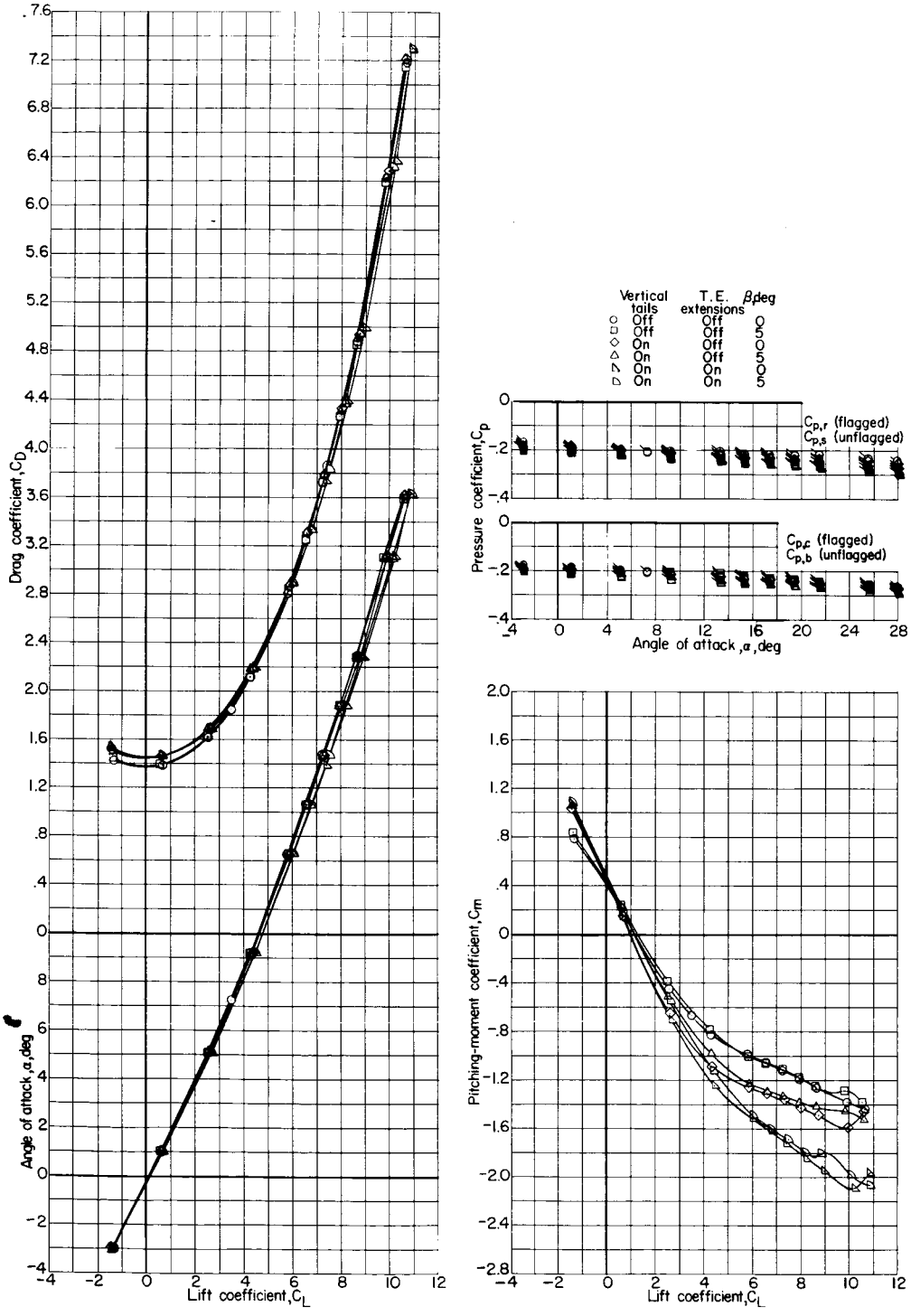

(b) M = 1.90.

Figure 21.- Continued.

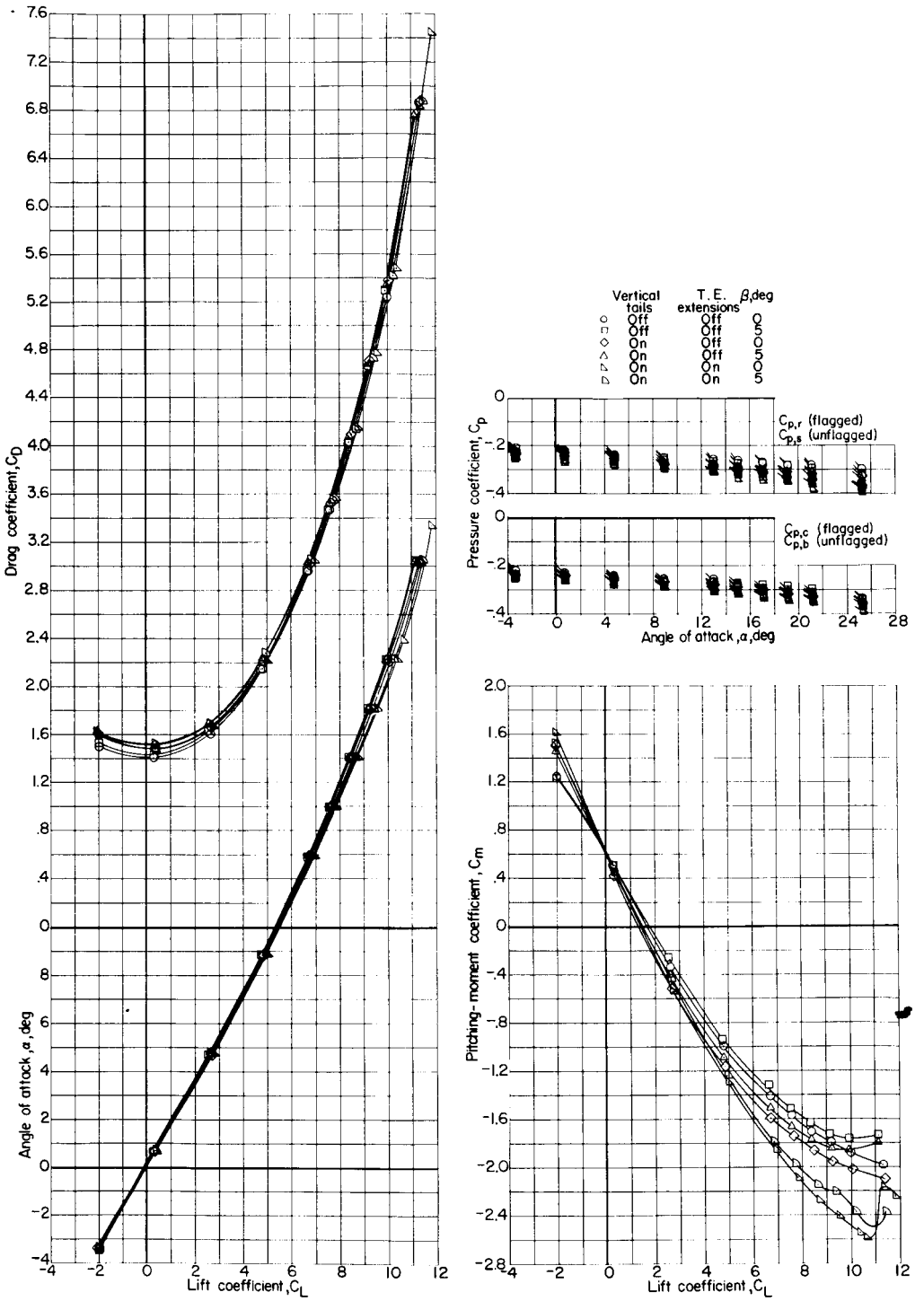

(c) M = 1.60.

Figure 21.- Concluded.

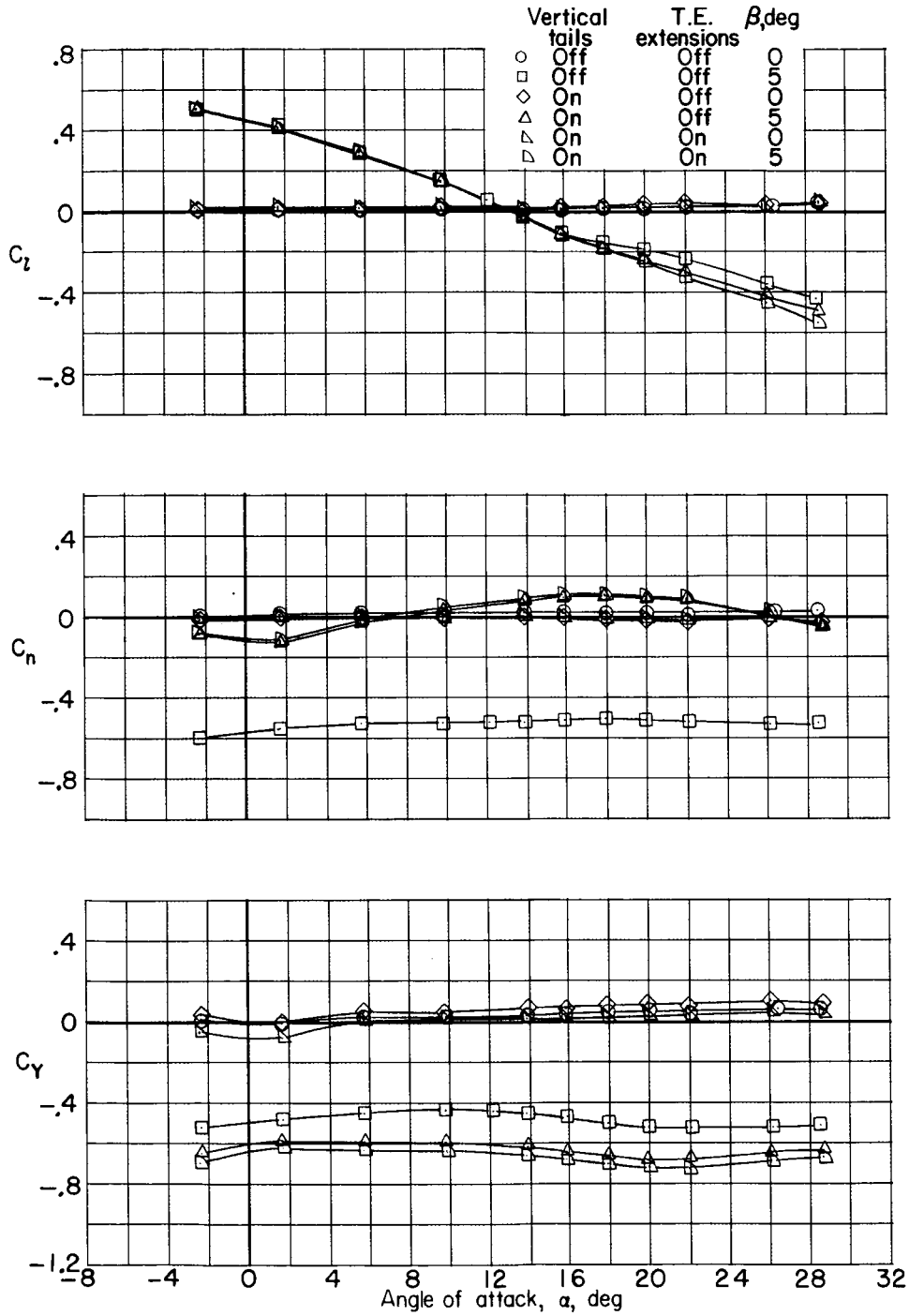

(a) M = 2.16.

Figure 22.- Supersonic lateral-directional aerodynamic characteristics of modified reusable booster without and with vertical tails and trailing-edge extensions. $\beta = 0^\circ$ and 5°.

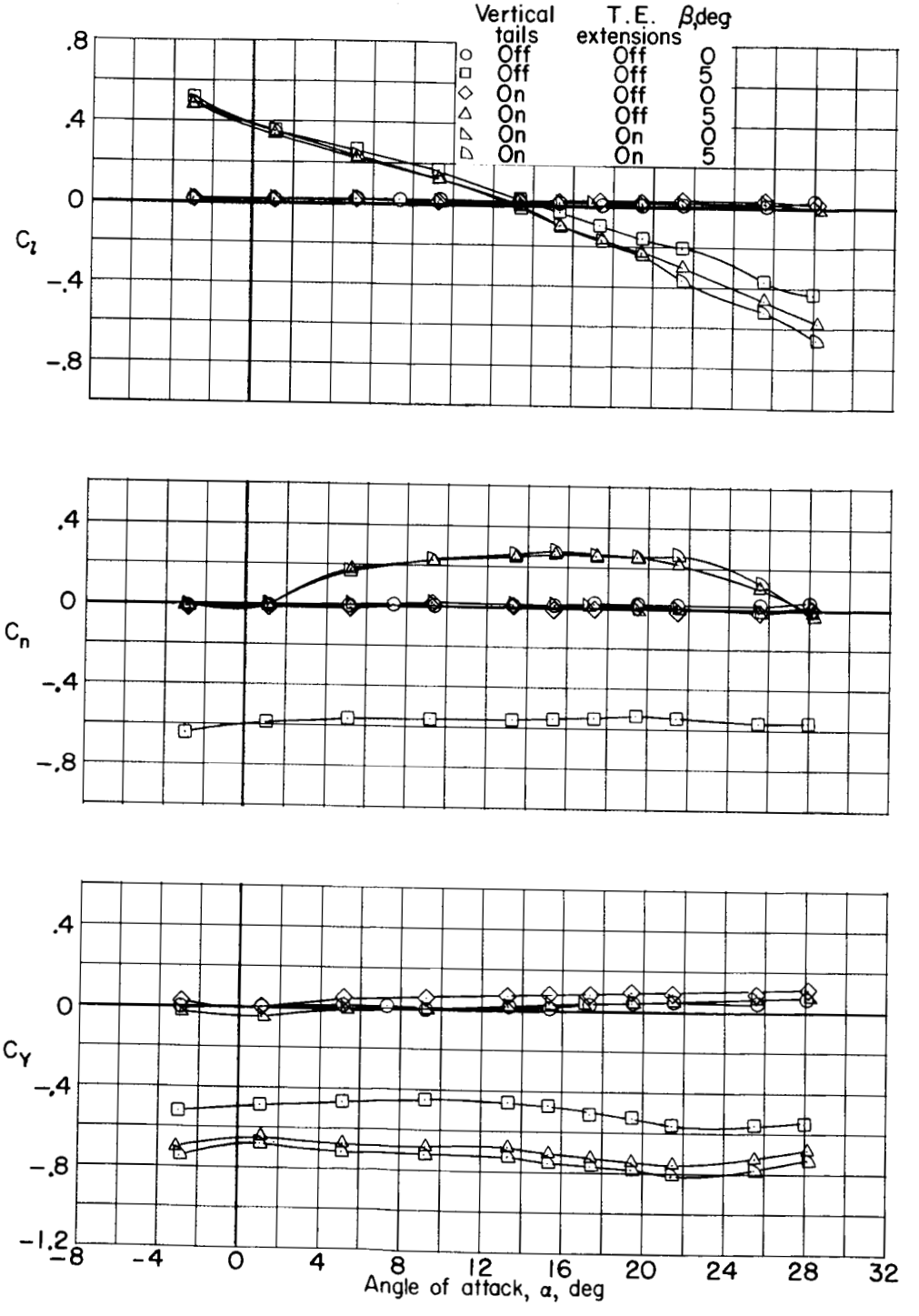

(b) M = 1.90.

Figure 22.- Continued.

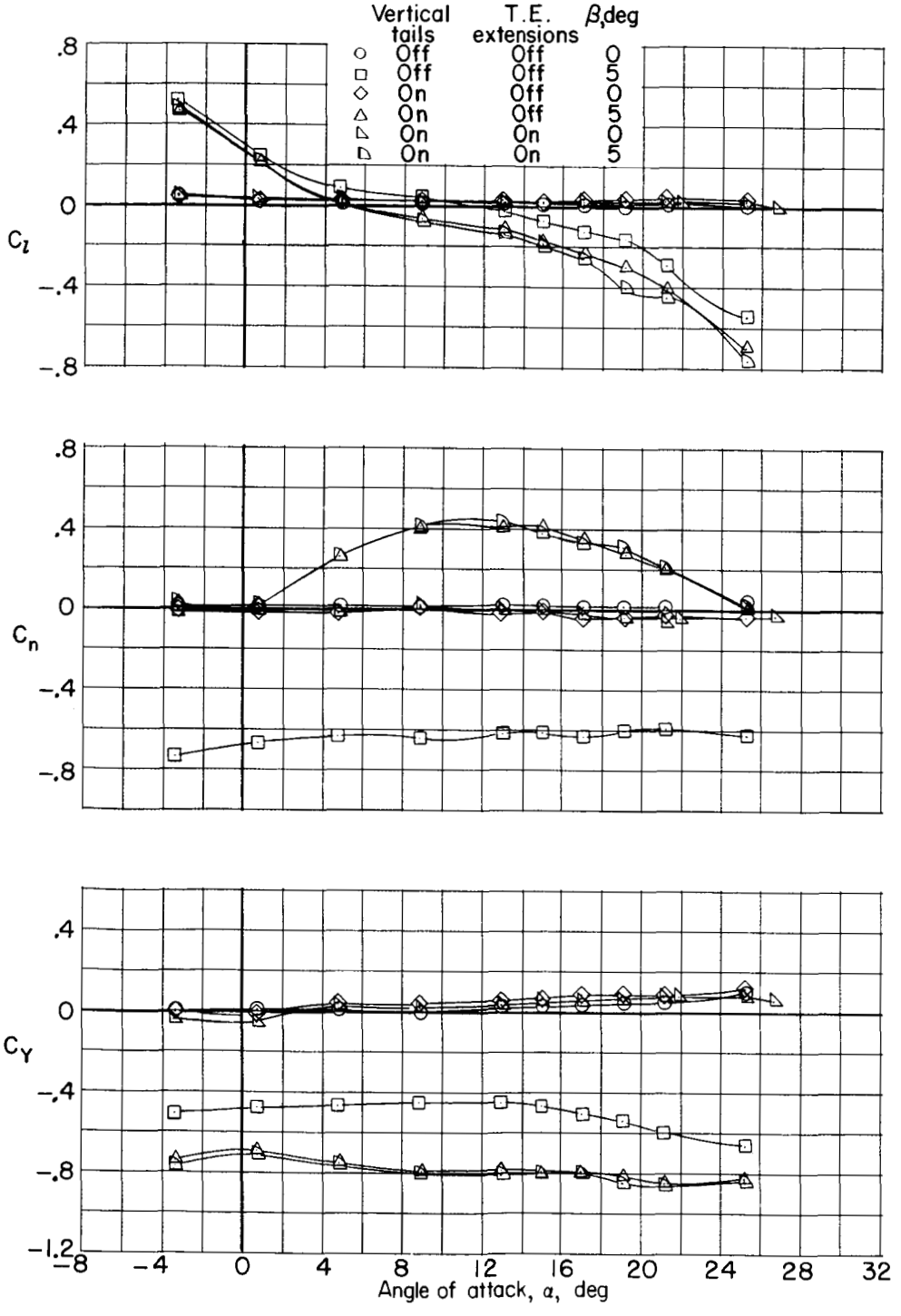

(c) M = 1.60.

Figure 22.- Concluded.

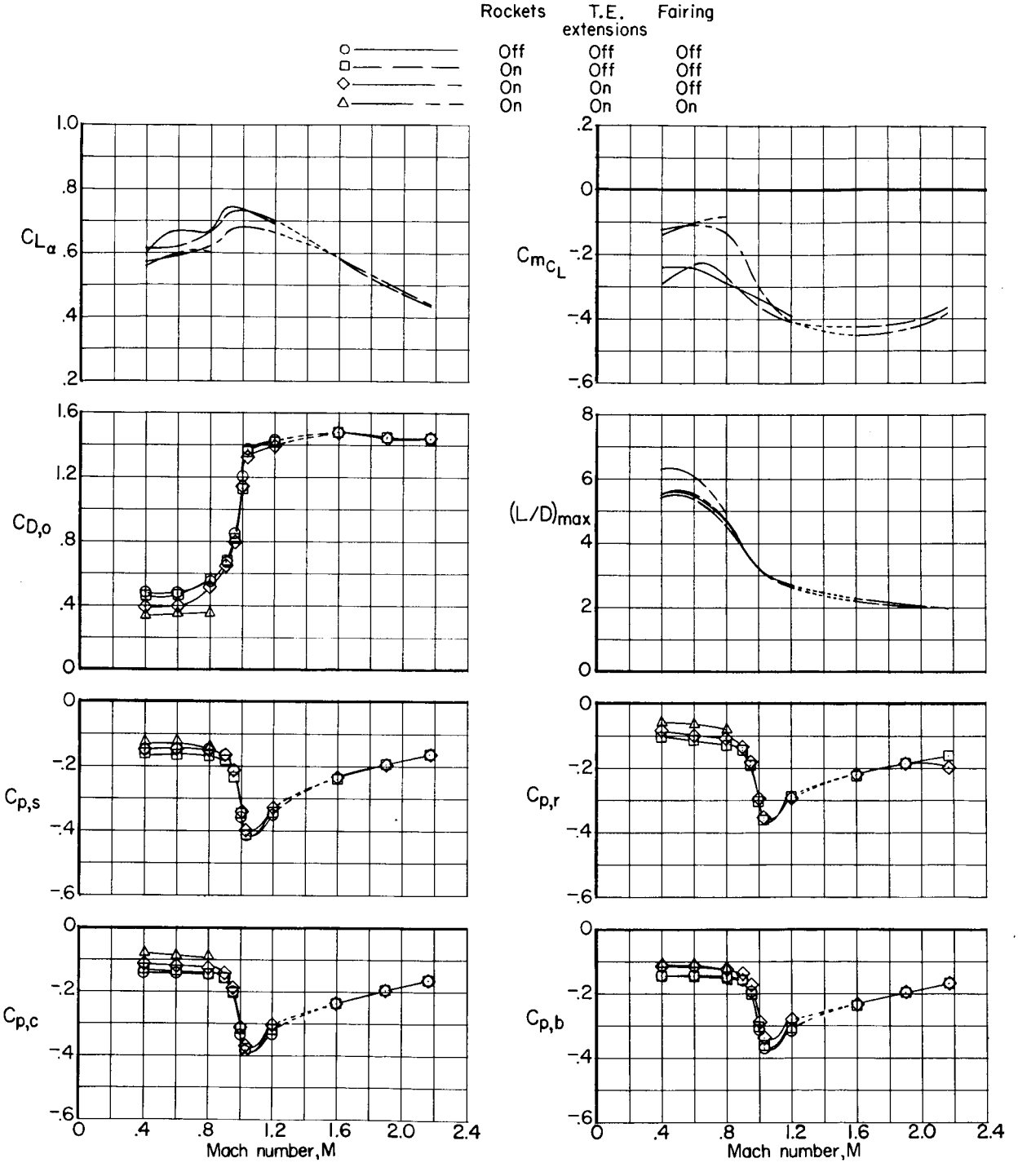

Figure 23.- Variation with Mach number of longitudinal stability and drag parameters for modified reusable booster including effects of rocket engines and trailing-edge extensions. Vertical tails on; $\beta = 0^o$.

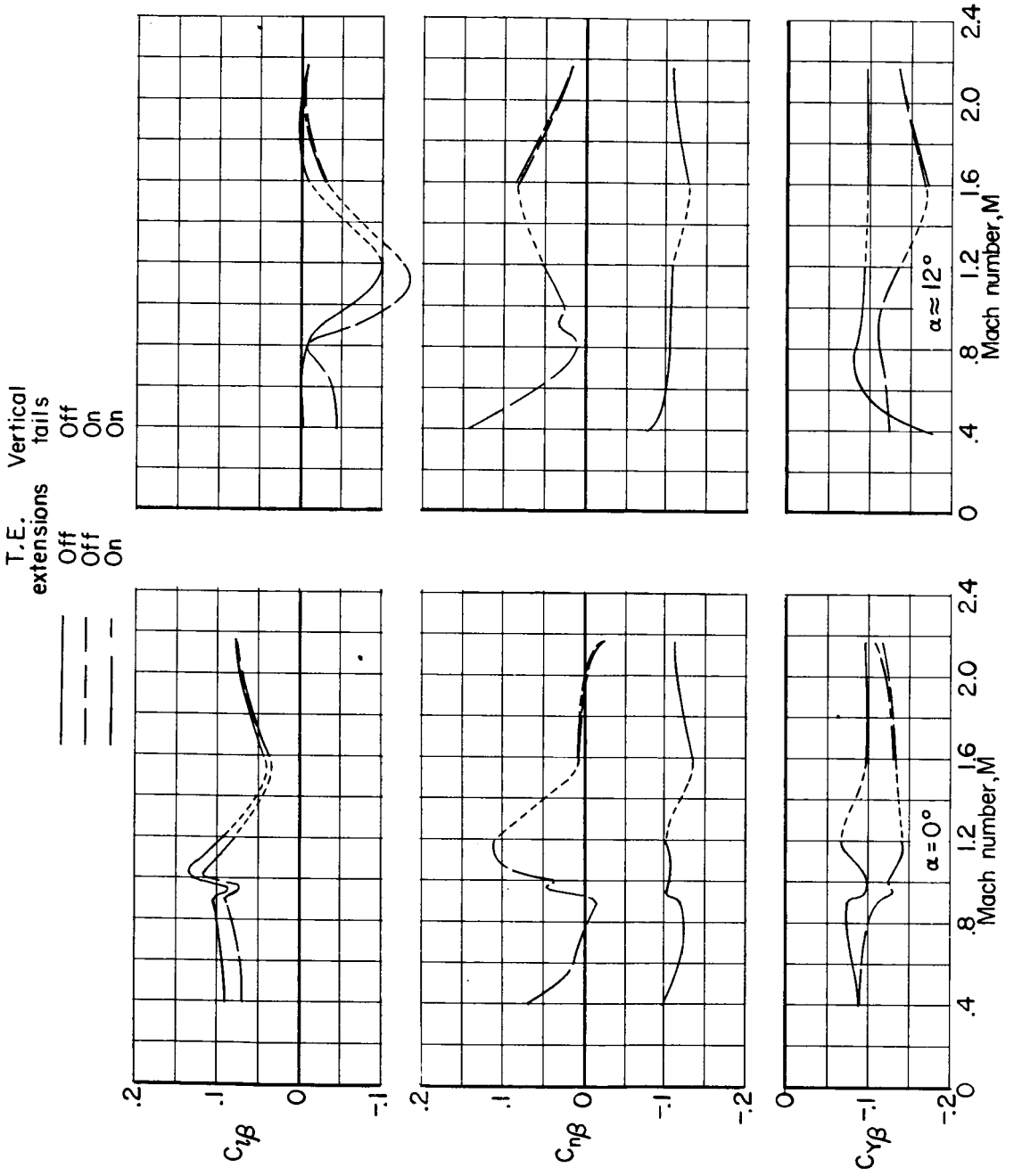

Figure 24.- Variation with Mach number of lateral-directional stability parameters for modified reusable booster including effects of rocket sizes, trailing-edge extensions, and vertical tails.

"The aeronautical and space activities of the United States shall be conducted so as to contribute . . . to the expansion of human knowledge of phenomena in the atmosphere and space. The Administration shall provide for the widest practicable and appropriate dissemination of information concerning its activities and the results thereof."

—NATIONAL AERONAUTICS AND SPACE ACT OF 1958

NASA S

TIONS

TEC
imp

TEC
of ir

TEC
buti

CON
nect

TEC
lang

TEC
and i

SPEC
NAS
NAS
proce
and s

ed

ss

i-
s.

s.

n

s

D

SCIENTIFIC AND TECHNICAL INFORMATION DIVISION

NATIONAL AERONAUTICS AND SPACE ADMINISTRATION

Washington, D.C. 20546